

1-1-2011

Synthesis Of N-Acetyl And C-Tert-Butyl Natural Amino Acid Substrates That Mimic Residues Of Polypeptides And Their Reactivity With $[\text{Fe}(\text{O})(\text{N}_4\text{py})]^{2+}$: Kinetic And Mechanistic Investigations

Ashley Ann Campanali
Wayne State University

Follow this and additional works at: http://digitalcommons.wayne.edu/oa_dissertations



Part of the [Inorganic Chemistry Commons](#), and the [Organic Chemistry Commons](#)

Recommended Citation

Campanali, Ashley Ann, "Synthesis Of N-Acetyl And C-Tert-Butyl Natural Amino Acid Substrates That Mimic Residues Of Polypeptides And Their Reactivity With $[\text{Fe}(\text{O})(\text{N}_4\text{py})]^{2+}$: Kinetic And Mechanistic Investigations" (2011). *Wayne State University Dissertations*. Paper 194.

**SYNTHESIS OF N-ACETYL AND C-TERT-BUTYL NATURAL AMINO ACID
SUBSTRATES THAT MIMIC RESIDUES OF POLYPEPTIDES AND THEIR
REACTIVITY WITH $[\text{Fe}^{\text{IV}}(\text{O})(\text{N4PY})]^{2+}$: KINETIC AND MECHANISTIC
INVESTIGATIONS
&
OXIDATION OF GLUTATHIONE BY METAL-BASED OXIDANTS**

by

ASHLEY ANN CAMPANALI

DISSERTATION

Submitted to the Graduate School

of Wayne State University,

Detroit, Michigan

in partial fulfillment of the requirements

for the degree of

DOCTOR OF PHILOSOPHY

2011

MAJOR: CHEMISTRY

Approved by:

Advisor

Date

DEDICATION

For the woman who guided me throughout life, who made many sacrifices to give me the things she did not have and who did everything in her power to help me realize my dreams. To this woman, the one who made me who I am, I owe everything. Mom I dedicate this in your honor – thank you for all you have done for me, I will be forever grateful and indebted to God to have you as my mother.

ACKNOWLEDGEMENTS

First I would like to thank God, through whom all things are possible. Through God's love and strength we are guided to do his work and make the world a better place. Next I would like to thank all those who have touched my life, contributed to my development and who have inspired me to achieve anything I could imagine. These people are my family: Karen Campanali, my mother, Sean Kuczarski, my husband, Nicole Campanali, my sister, my grandparents, aunts, uncles and cousins. These people are my best friends, whom I have been blessed to know. You are truly lucky to have one great friend in life, God has showered me with his love by having these people in my life, I am lucky to know them: Manuella Eppelboym, Amanda Meeker, Peter Stasko, Paul Stasko, Jennifer Woodward, Alan Ertle, Luis Labrador and Marcin Ksiazek.

I would like to take this opportunity to honor an excellent man, who recently left this world, Dr. Richard Mancuso, better known to the students and staff that loved him as Doc. He was the chair of the physics department at SUNY Brockport. He left behind students that have been touched by his kindness, care, love and intelligence. He taught us to seek the answers to great questions, to live life with curiosity and to never forget to treat others with respect and kindness. Doc, I will never forget all our conversations, especially all your help with String theory for my seminar. You will always be with me and I aspire to look at life with your curiosity. I will never forget you and the lessons you taught me.

I would like to thank all my friends I met at Wayne State University, especially those from the Kodanko Lab. When I joined the Kodanko Lab, Ahmed Abboulatta and Nitin Jabre joined with me. I would like to thank them for all their help and for sharing

their knowledge and experience with me. I am truly grateful to have such wonderful coworkers and friends. I would like to thank all my past and present coworkers in the Kodanko Lab and I wish all of them the best life has to offer.

I would like to thank all the professors I have taught under as a teaching assistant: Dr. Zibuck, Dr. Chow, Dr. Winter and Dr. Barber. I thank you for being the great teachers you are and for inspiring me through your care and concern for your students. I have learned many important lessons from you that I will carry with me in my future teaching experiences.

I would like to thank Wayne State University for giving me the opportunity to earn my Ph.D. at an institute with inspiring professors that conduct cutting-edge research. I would like to thank my committee members Dr. Winter, Dr. Guo and Dr. Cavallo-Medved, for all their time and help.

I would like to thank all the staff in the chemistry department for truly making the department a friendly place. I would like to especially thank the staff in the business office for all their help during the Graduate Research Symposium each year. We are truly lucky to have such wonderful people working in the department.

Last, but not least, I would like to thank my advisor Professor Jeremy J. Kodanko for everything he has done for his group members. I could not imagine going through the Ph.D. Program without him as my advisor. It is not difficult to see that his students' education is his number one priority and I would like to thank him for his support, guidance and never giving up on any of us (I would especially like to thank him for never giving up on me). I have been blessed to be one of Jeremy's students and pray that I will make him proud in my future endeavors. Thank you for everything Jeremy.

TABLE OF CONTENTS

Dedication.....	ii
Acknowledgements.....	iii
List of figures.....	viii
List of schemes.....	ix
List of graphs.....	xi
List of tables.....	xiii
CHAPTER 1 Synthesis of N-Acetyl and N-Tert-Butyl Amino Acid Substrates that Mimic Residues of Polypeptides and their Reactivity with $[\text{Fe}^{\text{IV}}(\text{O})(\text{N4Py})]^{2+}$: Kinetic and Mechanistic Investigations.....	1
1.1 Introduction.....	1
1.1.1 Reactive Oxygen Species: Implications and Sources.....	3
1.1.2 Reactivity of ROS with Proteins, Peptides and Amino Acids.....	5
1.1.3 Metal-based Oxidants.....	12
1.1.3.1 Heme and Non-Heme Fe^{IV} -Oxo Enzymes.....	12
1.1.3.2 Non-Heme Fe^{IV} -Oxo Complexes.....	17
1.1.4 Project Goals.....	22
1.2 Results and Discussion.....	23
1.2.1 Synthesis of Substrates to Mimic Amino Acid Residues of Polypeptides: Ac-AA-NHtBu.....	23
1.2.1.1 Synthesis of Ac-Gln-NHtBu.....	24
1.2.1.2 Synthesis of Ac-Ile-NHtBu.....	25
1.2.1.3 Synthesis of Ac-Asn-NHtBu.....	28
1.2.1.4 Optimized Synthesis of Ac-Cys-NHtBu.....	30
1.2.1.5 Synthesis of Ac-Tyr-NHtBu Derivatives: Ac-Tyr(OAc)-NHtBu and Ac-Tyr(OMe)-NHtBu.....	31

1.2.2	Kinetic & Mechanistic Studies of Ac-AA-NHtBu with $[\text{Fe}^{\text{IV}}(\text{O})(\text{N4Py})]^{2+}$	32
1.2.2.1	Kinetics and Mechanism of $[\text{Fe}^{\text{IV}}(\text{O})(\text{N4Py})]^{2+}$ with Ac-Cys-NHtBu...	35
1.2.2.2	Kinetics and Mechanism of $[\text{Fe}^{\text{IV}}(\text{O})(\text{N4Py})]^{2+}$ with Ac-Tyr-NHtBu...	39
1.2.2.3	Kinetics and Mechanism of $[\text{Fe}^{\text{IV}}(\text{O})(\text{N4Py})]^{2+}$ with Ac-Phe-NHtBu...	44
1.3	Conclusions and Future Directions	46
1.4	Experimental	47
1.5	References	58
CHAPTER 2 Oxidation of Glutathione by Metal-Based Oxidants		66
2.1	Introduction	66
2.1.1	Glutathione: Importance in Biology	68
2.1.2	Superoxide Dismutase and Catalase: ROS Scavengers	76
2.1.3	Copper-catalyzed Oxidation of Glutathione	79
2.1.4	Project Goals	84
2.2	Results and Discussion	85
2.2.1	GSH Oxidation by Ferryl $[\text{Fe}^{\text{IV}}(\text{O})(\text{N4Py})]^{2+}$ and Characterization of the Intermediate $[\text{Fe}^{\text{III}}(\text{SG})(\text{N4Py})]^{2+}$	85
2.2.1.1	General Reaction and UV-vis Spectroscopy for the Oxidation of GSH by $[\text{Fe}^{\text{IV}}(\text{O})(\text{N4Py})]^{2+}$	86
2.2.1.2	Control Experiments	88
2.2.1.3	Mass Spectrometry Data	89
2.2.1.4	Electron paramagnetic Resonance Spectroscopy Data	91
2.2.1.5	Kinetic Modeling	93
2.2.2	Catalytic Oxidation of GSH by $[\text{Fe}^{\text{II}}(\text{N4Py})(\text{MeCN})](\text{ClO}_4)_2$	100
2.2.2.1	Dioxygen Consumption Studies	102
2.2.2.2	Antioxidant Enzyme Inhibition Study	103
2.2.2.3	pH Dependence Study and Proposed Mechanism	105

2.3	Conclusions and Future Directions	107
2.4	Experimental	109
2.4.1	Single Turnover Experiments.....	109
2.4.2	Catalytic Oxidation Experiments.....	112
2.5	References.....	113
	Abstract	118
	Autobiographical statement.....	120

LIST OF FIGURES

Figure 1.1 Ligand used for site selective cleavage of streptavidin.....	10
Figure 1.2 CALI reagent constructed from $[\text{Ru}(\text{bipy})_3]^{2+}$ attached to peptoid GU40C....	11
Figure 1.3 Structure of 2-oxoglutarate.....	15
Figure 1.4 Structure of ferryl derived from TMC, $[\text{Fe}^{\text{IV}}(\text{O})(\text{TMC})(\text{NCCH}_3)]^{2+}$	18
Figure 1.5 Examples of ligands used in ferryl complexes	19
Figure 1.6 Model of $[\text{Fe}^{\text{IV}}(\text{O})(\text{N4Py})]^{2+}$	19
Figure 1.7 Substrate to mimic amino acid residues of polypeptides	23
Figure 1.8 Substrates synthesized.....	23
Figure 1.9 UV-vis spectrum over time for the decomposition of $[\text{Fe}^{\text{IV}}(\text{O})(\text{N4Py})]^{2+}$ (1 mM) at 680 nm upon treatment Ac-Ile-NHtBu (10 mM) with concomitant regeneration of the Fe^{II} species at 450 nm.....	32
Figure 1.10 X-band EPR spectrum of $[\text{Fe}^{\text{IV}}(\text{O})(\text{N4Py})]^{2+}$ (1 mM) upon treatment with substrate Ac-Tyr-NHtBu (10 equiv) in 1:1 $\text{H}_2\text{O}:\text{MeCN}$ at 0 °C; frozen in liquid N_2 after less than 15 seconds. Experimental Conditions: temperature, 125 K; microwaves, 10 mW at 9.34 GHz; modulation, 0.55 G; receiver gain, 100.	42
Figure 1.11 X-band EPR spectrum of $[\text{Fe}^{\text{IV}}(\text{O})(\text{N4Py})]^{2+}$ (1 mM) upon treatment with 2,4,6-tri- <i>tert</i> -butyl phenol (10 equiv) in 1:1 $\text{H}_2\text{O}:\text{MeCN}$ at 0 °C; frozen in liquid N_2 after less than 15 seconds. Experimental Conditions: temperature, 125 K; microwaves, 1.1 mW at 9.34 GHz; modulation, 0.55 G; receiver gain, 100.	43
Figure 2.1 Synthesis and redox cycling in GSH homeostasis	71
Figure 2.2 Cellular ROS and the role of antioxidant enzymes.....	78
Figure 2.3 High-resolution TOF-MS for $[\text{Fe}^{\text{III}}(\text{SG})(\text{N4Py})]^{2+}$ with m/z 364.5944 (left) and calculated fit (right)	90
Figure 2.4 High-resolution TOF-MS for $[\text{Fe}^{\text{II}}(\text{SG})(\text{N4Py})]^+$ with m/z 728.1829 (top) and calculated fit (bottom).....	90
Figure 2.5 Possible structures of $[\text{Fe}^{\text{III}}(\text{SG})(\text{N4Py})]^{2+}$	99

LIST OF SCHEMES

Scheme 1.1 The Fenton Reaction	3
Scheme 1.2 The Haber-Weiss Reaction.....	3
Scheme 1.3 Pathways for carbonyl product formation by reaction of ROS with peptides through oxidative cleavage of the backbone via the diamide pathway or the α -amidation pathway	7
Scheme 1.4 Proposed catalytic cycle for oxygen atom transfer by heme Cyt P450 to substrate R-H	14
Scheme 1.5 Reaction catalyzed by TauD and 2-oxoglutarate to yield sulfonates as an energy source for E.coli.....	15
Scheme 1.6 Mechanism of TauD and 2-oxoglutarate for oxidation of taurine	16
Scheme 1.7 Oxidation of cyclohexane by pregenerated ferryl species of polypyridyl ligands.....	20
Scheme 1.8 Transformations observed by non-heme ferryls	21
Scheme 1.9 Synthesis of Ac-Gln-NHtBu.....	24
Scheme 1.10 Synthetic trials to obtain a single diastereomer of Ac-Ile-NHtBu and final synthesis of a single diastereomer	26
Scheme 1.11 Oxazolone formation from the activated ester of Ac-Ile-OH.....	27
Scheme 1.12 Potential ring formation and dehydration of Asn side chain	28
Scheme 1.13 Synthesis of Ac-Asn-NHtBu via N-Fmoc and trityl protection	29
Scheme 1.14 Synthesis of Ac-Cys-NHtBu.....	30
Scheme 1.15 Synthesis of Ac-Tyr(OMe)-NHtBu and Ac-Tyr(OAc)-NHtBu.....	31
Scheme 1.16 Proposed ET-PT mechanism for the reaction of the Ac-Cys-NHtBu with $[\text{Fe}^{\text{IV}}(\text{O})(\text{N4Py})]^{2+}$	38
Scheme 1.17 Stabilizing properties of 2,4,6-tri- <i>tert</i> -butylphenol.....	42
Scheme 1.18 Orthoquinone product from the oxidation of Ac-Phe-NHtBu by $[\text{Fe}^{\text{IV}}(\text{O})(\text{N4Py})]^{2+}$	44
Scheme 2.1 Glutathione is composed of the amino acids glutamate, cysteine and glycine	68

Scheme 2.2 Thiol-transferase reaction.....	70
Scheme 2.3 Mercapturic pathway: detoxification of electrophiles (E) by GSH	73
Scheme 2.4 Structure of Cystine.....	74
Scheme 2.5 Dismutation of superoxide anions by superoxide dismutase.....	76
Scheme 2.6 Reaction catalyzed by the antioxidant enzyme catalase.....	77
Scheme 2.7 Stoichiometry for the oxidation of GSH in the 1 st phase	80
Scheme 2.8 Oxidation of 3-CCA by hydroxyl radical to yield fluorescent 7-OHCAA ...	81
Scheme 2.9 Copper –catalyzed mechanism for autoxidation of GSH.....	83
Scheme 2.10 Theoretical models 1 – 5 considered for <i>Dynafit</i>	94
Scheme 2.11 Proposed mechanism for the reaction of $[\text{Fe}^{\text{IV}}(\text{O})(\text{N4Py})]^{2+}$ with GSH	97
Scheme 2.12 Possible catalytic cycle for GSH oxidation	101
Scheme 2.13 Reactions of GSH and GS^- with O_2 to yield hydrogen peroxide and superoxide	104
Scheme 2.14 Proposed mechanism for the catalytic oxidation of GSH	106

LIST OF GRAPHS

Graph 1.1 Time course decay of $[\text{Fe}^{\text{IV}}(\text{O})(\text{N4Py})]^{2+}$ (1 mM) at 680 nm upon treatment of Ac-Ile-NHtBu (10 mM)	33
Graph 1.2 Decomposition of the ferryl (1 mM) at 680 nm upon treatment with 10 equiv Ac-Cys-NHtBu in $\text{CH}_3\text{CN}/\text{H}_2\text{O}$	35
Graph 1.3 Second-order plot for Ac-Cys-NHtBu (5 to 25 mM) with the ferryl (1 mM)..	36
Graph 1.4 Decomposition of the ferryl (1 mM) at 680 nm upon treatment with 10 equiv Ac-Cys-NHtBu in $\text{CD}_3\text{CN}/\text{D}_2\text{O}$	37
Graph 1.5 Decomposition of the ferryl (1 mM) at 680 nm upon treatment with 10 equiv Ac-Tyr-NHtBu in $\text{CH}_3\text{CN}/\text{H}_2\text{O}$	39
Graph 1.6 Second-order plot for Ac-Tyr-NHtBu (5 to 25 mM) with the ferryl (1 mM)..	40
Graph 1.7 Decomposition of the ferryl (1 mM) at 680 nm upon treatment with 10 equiv Ac-Tyr-NHtBu in $\text{CD}_3\text{CN}/\text{D}_2\text{O}$	41
Graph 1.8 Hammett-like plot for the reaction of Ac-Phe-NHtBu, Ac-Tyr(OMe)-NHtBu and Ac-Tyr(OMe)-NHtBu with $[\text{Fe}^{\text{IV}}(\text{O})(\text{N4Py})]^{2+}$ indicating electrophilic aromatic substitution.....	45
Graph 2.1 Comparison of $[\text{Fe}^{\text{IV}}(\text{O})(\text{N4Py})]^{2+}$ vs $[\text{Fe}^{\text{III}}(\text{SG})(\text{N4Py})]^{2+}$ for reaction of 1 mM ferryl with 5 mM GSH.....	87
Graph 2.2 Decay of $[\text{Fe}^{\text{IV}}(\text{O})(\text{N4Py})]^{2+}$ (650 nm) and regeneration of $[\text{Fe}^{\text{II}}(\text{OH}_2)(\text{N4Py})]^{2+}$ (450 nm).....	87
Graph 2.3 EPR spectra over time for the reaction of $[\text{Fe}^{\text{IV}}(\text{O})(\text{N4Py})]^{2+}$ with GSH	92
Graph 2.4 X-band EPR spectra from reaction of $[\text{Fe}^{\text{IV}}(\text{O})(\text{N4Py})]^{2+}$ (1 mM) with GSH (5 mM)	92
Graph 2.5 Best-calculated fit for kinetic model 5 for the reaction of $[\text{Fe}^{\text{IV}}(\text{O})(\text{N4Py})]^{2+}$ with varying concentrations of glutathione.....	96
Graph 2.6 Expansion of the first 10 minutes of absorbance vs. time for data used in the kinetic modeling	97
Graph 2.7 Plot for molar absorptivity at 650 nm.....	98
Graph 2.8 Consumption of GSH by $[\text{Fe}^{\text{II}}(\text{MeCN})(\text{N4Py})](\text{ClO}_4)_2$ under Ar (red), ambient O_2 (blue, 21%) and 100% O_2 (black).....	102

Graph 2.9 Inhibition study with SOD and catalase for the reactions of GSH with the iron complexes derived from EDTA and N4Py 104

Graph 2.10 pH study for the reaction of GSH with the complexes derived from N4Py and TPA in the presence and absence of SOD and catalase 106

LIST OF TABLES

Table 1.1 Examples of oxidation products for selected amino acids with ROS (OH [•])	8
Table 1.2 Pseudo-first order rate constants and k_{rel} for substrates Ac-AA-NHtBu (k_{rel} is with respect to the decomposition of the ferryl alone with no substrate added)	34
Table 2.1 Catalyst screen for oxidation of GSH.....	101

CHAPTER 1

SYNTHESIS OF *N*-ACETYL AND *C-TERT*-BUTYL NATURAL AMINO ACID SUBSTRATES THAT MIMIC RESIDUES OF POLYPEPTIDES AND THEIR REACTIVITY WITH $[\text{Fe}^{\text{IV}}(\text{O})(\text{N4PY})]^{2+}$: KINETIC AND MECHANISTIC INVESTIGATIONS

1.1 Introduction

Reactive oxygen species (ROS) such as singlet oxygen ($^1\text{O}_2$), superoxide ($\text{O}_2^{\bullet-}$) and hydroxyl radical (OH^{\bullet}) can accumulate in the body's oxygen rich environment,^{1, 2} this process is known as oxidative stress and is well understood, especially using redox-active metals and radiolysis for their generation.¹⁻⁵ Oxidative stress can lead to physiological pathologies such as arteriosclerosis, ischemia/reperfusion injury, Alzheimer's and neurodegenerative diseases as well as other age related diseases.^{6, 7}

The reactivity of proteins with metal-based oxidants, however, is an uninvestigated field. Metal-based oxidants, where the reactive oxygen is doubly bound to the metal center, represent another pathway to the oxidation of proteins. Metal-based oxidants offer an important advantage over ROS, such as the ability to tune their stability and selectivity with a substrate by alteration of either the metal center or the ligand structure.⁸ In tuning the stability and selectivity of the metal-based oxidant, the oxidation of proteins could be limited to a select few amino acid residues (where as ROS such as hydroxyl radical are non-discriminant). While metal-based oxidants have not been used to investigate protein oxidation, they are well known in nature.⁹⁻¹²

Metal-based oxidants where the reactive metal center is iron are known as ferryls and are widely accepted as intermediates in heme and non-heme proteins that activate

dioxygen, such as cytochrome P450 and TauD, respectively.^{12, 13} Biomimetic non-heme ferryls have been shown to oxidize strong C-H bonds.⁸ The ferryl $[\text{Fe}^{\text{IV}}(\text{O})(\text{N4Py})]^{2+}$ has been shown to be stable at room temperature for several days yet reacts to oxidize substrates upon addition. For example, $[\text{Fe}^{\text{IV}}(\text{O})(\text{N4Py})]^{2+}$ affords cyclohexanol, via a hydroxylation, upon addition of cyclohexane.⁸ Due to this literature report and the fact that it has been well characterized, $[\text{Fe}^{\text{IV}}(\text{O})(\text{N4Py})]^{2+}$ was chosen as the ferryl of interest for investigating the reactivity of metal-based oxidants with proteins.

The first subsection introduces ROS and their implications in the oxidation of proteins and highlights some examples of their practical applications. The next subsection discusses metal-based oxidants as a means to oxidize substrates selectively with strong C-H bonds as observed in heme and non-heme proteins as well as artificial enzyme systems. The last subsection introduces the goals of the research presented in section two, where our results in the field of oxidation of amino acids by a metal-based oxidant will be discussed. We have synthesized amino acid substrates and conducted kinetic and mechanistic investigations for their reactions with $[\text{Fe}^{\text{IV}}(\text{O})(\text{N4Py})]^{2+}$.

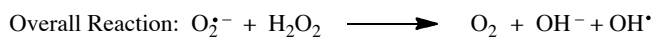
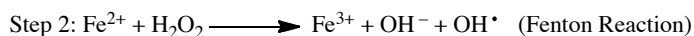
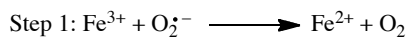
1.1.1 Reactive Oxygen Species: Implications and Sources

Reactions of ROS with proteins, free amino acids and polypeptides have been studied for decades due to their involvement in aging^{1, 2, 4, 5, 14-17} Sources of ROS are known, such as the respiratory chain, and can accumulate in the body, which can lead to physiological implications.^{5, 6, 18-20} ROS can be generated through pro-oxidants from environmental pollutants or in the body from processes such as lipid peroxidation or arginine nitric oxide synthetase.⁶ Generation of ROS by metal-ion catalyzed processes such as Fenton or Haber-Weiss type mechanisms are known.^{4, 6} In the Fenton reaction (Scheme 1.1), Fe^{2+} reacts with hydrogen peroxide to form hydroxyl radical,²¹ whereas the Haber-Weiss mechanism (Scheme 1.2) involves the reaction of Fe^{3+} with superoxide to form Fe^{2+} and O_2 .^{22, 23} The second step of the Haber-Weiss mechanism (Scheme 1.2) is the Fenton reaction, therefore either pathway may generate ROS by metal-ion catalyzed processes.

Scheme 1.1 The Fenton Reaction



Scheme 1.2 The Haber-Weiss Reaction



Hydroxyl radical and superoxide are not the only ROS. Others include hydrogen peroxide (H_2O_2), hydroperoxyl radical (HOO^\bullet), alkoxyl radical (RO^\bullet) and singlet oxygen

($^1\text{O}_2$). Nitric oxide (NO^\bullet , formed by nitric acid synthetase), is an example of Reactive Nitrogen Species (RNS) and is also known to oxidize biomolecules.^{5, 6} NO^\bullet can react with superoxide or carbon dioxide to form other RNS, peroxynitrite (ONOO^-) and nitrosoperoxocarbonate (ONOOCO_2^-), respectively.⁵ Although there are other ROS and RNS capable of oxidizing proteins, the following subsection will focus on examples of the reactivity of hydroxyl radical, a potent ROS.

1.1.2 Reactivity of ROS with Proteins, Peptides and Amino Acids

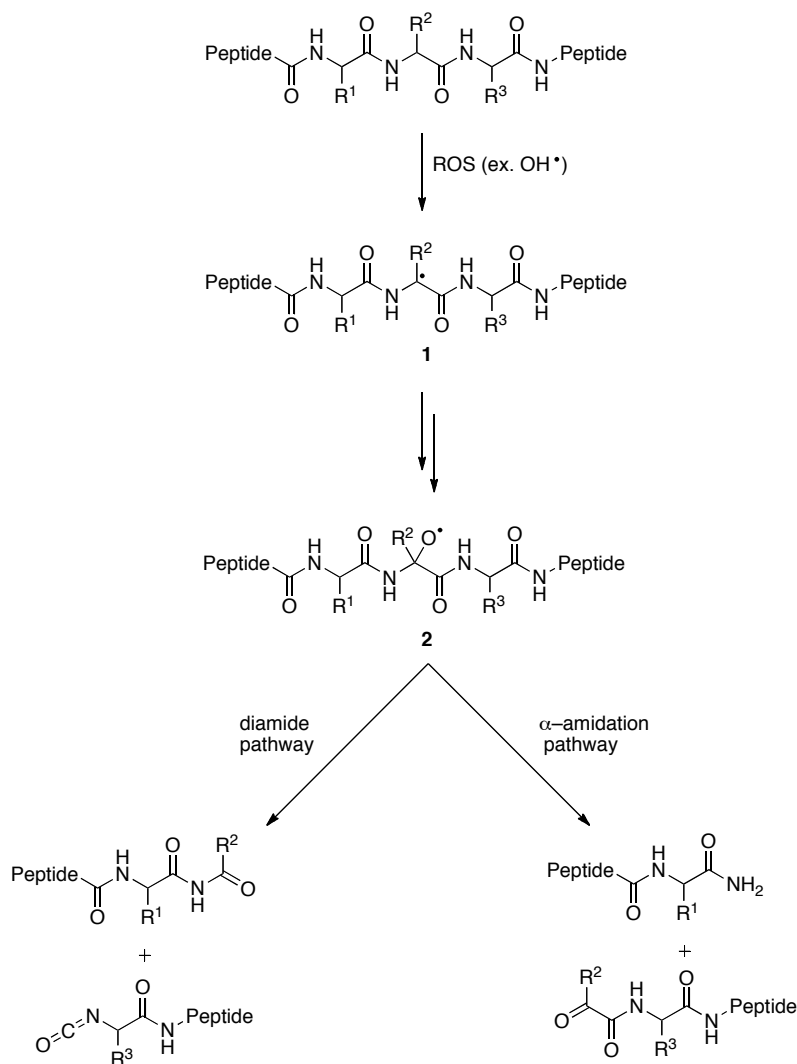
The reactivity and selectivity of ROS vary by species. For example, hydroxyl radical is highly reactive and therefore shows little discrimination in its residue specificity during oxidation of proteins. However, unlike hydroxyl radical, singlet oxygen and hydrogen peroxide display selectivity and oxidize single amino acid residues in proteins.^{24, 25} The rates of reaction between singlet oxygen and the amino acid residues of Trp, Tyr, Met, Cys and His on proteins are kinetically significant compared to the rate of reaction with other residues. For example, the rate of reaction of singlet oxygen with the amino acid residue Met was found to be $1.6 \times 10^7 \text{ dm}^3 \text{ sec}^{-1}$ at physiological pH.²⁴ While some ROS show selectivity, the following section will focus on the description of the more potent hydroxyl radical.

Accumulation of oxidized amino acid residues of proteins and peptides, also known as oxidative stress, has been linked to aging as well as other pathological conditions such as arteriosclerosis and Alzheimer's disease.^{5, 6, 18-20} Supporting studies have illustrated that cell death can occur through the oxidation of proteins by hydroxyl radical generated from ionizing radiation.²⁶ Experiments conducted over the last several decades have established the reactivity of ROS with amino acids and proteins^{1, 5, 6, 18-20, 26} and pioneering work identified oxidation products for these reactions.^{1, 14, 27-31} These studies mainly involve generation of ROS by radiolysis (using γ -radiation)¹ or metal-catalyzed processes.

Identification of oxidation products and determination of the mode of action for the reactions of ROS with proteins is of great importance. ROS can be generated in the body as metabolites, enter the body through environmental pollutants or be generated

upon exposure to X-ray, γ -ray and UV-radiation.⁵ In radiolysis studies, hydroxyl radical or a mixture of superoxide and hydroxyl radical can form.¹ H-atom abstraction via hydroxyl radical either at the α -C–H (**1**) or on the amino acid side chain has been established (Scheme 1.3). Trapping of carbon-centered radicals by O₂ (**2**) leads to fragmentation of the backbone (diamide pathway or the α -amidation pathway) of the amino acid or peptide via a peroxy and alkoxy radical. Hydroxyl radical may trap the carbon- or heteroatom-centered radical resulting in hydroxylation. Cross-link formation via side chain radical dimerization, such as with cysteine or tyrosine, is another known pathway.^{1, 5, 6} These mechanisms have also been implicated during metal-catalyzed oxidation processes.⁵ As the length and steric hindrance of the side chain of an amino acid increases, chemoselectivity shifts such that reaction at the side chain dominates rather than at the α -C–H position.^{14, 32, 33} For example, glycine and alanine residues are mainly oxidized at the α -C–H position leading to backbone cleavage and result in the formation of amides and keto acid products.^{1, 14, 34} On the other hand, side chain oxidation dominates amino acids such as tyrosine forming the products 3,4-dihydroxyphenylalanine (DOPA) and dityrosine through cross-linkages.³⁵ The following describes the oxidation of amino acid residues with ROS during radiolysis or by metal-catalyzed processes.

Scheme 1.3 Pathways for carbonyl product formation by reaction of ROS with peptides through oxidative cleavage of the backbone via the diamide pathway or the α -amidation pathway



As mentioned above, glycine and alanine oxidation by ROS is initiated by H-atom abstraction at the α -C-H bond that leads to backbone cleavage, but other amino acid residues have either solely side chain oxidation or a mixture of side chain oxidation and backbone cleavage. Backbone cleavage tends to proceed to a lesser extent.^{1, 5} For example, oxidation of the side chains of glutamic and aspartic acid at the γ - and β -C-H

positions respectively represent the dominant pathway for their reaction with ROS, however, backbone oxidation of N-acetyl-glutamic acid has been observed as a minor product.³⁶ Competition between side chain and backbone oxidation is also prevalent in amino acids such as arginine, threonine, serine and lysine.¹ A summary of oxidation products can be found in Table 1.1 for selected amino acids. Side chains of leucine and valine are hydroxylated to give 3-hydroxyleucine and 4- or 3-hydroxyvaline as oxidation products^{1, 32} and phenylalanine is oxidized to *ortho/meta*-tyrosine. The phenol side chain of tyrosine is oxidized to 3,4-dihydroxyphenylalanine (DOPA) and dityrosine through cross-linkages.^{5, 6, 35, 37} Other aromatics such as tryptophan are converted to various derivatives such as 2-, 4-, 5-, 6- and 7-hydroxytryptophan as well as other decomposition products that have not been identified.^{1, 3, 6}

Table 1.1 Examples of oxidation products for selected amino acids with ROS (OH[•])

Amino Acid	Oxidation Product(s)	Ref.
Histidine	2-oxo-histidine, aspartic acid, asparagine	5, 38
Phenylalanine	2-, 3-, and 4-hydroxyphenylalanine and 2,3- dihydroxyphenylalanine	5
Tyrosine	dityrosine and 3,4-dihydroxyphenylalanine	35
Tryptophan	formylkynurinine, 2-,4-,5-,6-, and 7-hydroxytryptophan + others	3, 5
Cysteine	sulfenic acid and disulfides	1, 27
Methionine	methionine sulfoxide/sulfone	5
Arginine	glutamic semialdehyde	29
Lysine	α -amino adipic semialdehyde	29, 30
Proline	glutamic semialdehyde, 2-pyrrolidone + others	29, 31
Threonine	2-amino-3-ketobutyric acid	39
Glutamic Acid	oxalic acid	5

Although damaging to proteins and biological substrates, ROS have found practicalities in the field of protein structure determination. Hydroxyl radical has been used in protein footprinting,^{40, 41} a type of structural determination for mapping surface

residues of proteins. These hydroxyl radicals may be generated by radiolysis or by metal-catalysts, such as $\text{Fe}^{\text{II}}\text{EDTA}$.⁴² Hydroxyl radical footprinting with $\text{Fe}^{\text{II}}\text{EDTA}$ has been used to explore protein-protein interactions of 16S rRNA and 30S ribosomal subunit of *Escherichia coli*.⁴³ Fe^{II} was incorporated into this subunit by complexation with 1-(*p*-bromoacetamidobenzyl)-EDTA, which was attached to the ribosomal protein S4 via a cysteine residue, Cys-31. Hydroxyl radical generation from a single Fe^{II} atom results in backbone cleavage of the rRNA near the Cys-31 residue. In footprinting, the same reaction is carried out using an unbound protein and through gel electrophoresis, a “footprint” of bands is obtained that can be compared to determine where the protein-protein interactions are located. There will be a missing band where there are protein-protein interactions because the bound protein eliminates cleavage at the site of interaction.^{43, 44} Another area where ROS have practical applications is in site selective protein cleavage and inactivation.

By anchoring EDTA to a protein affinity group, site selective cleavage reagents have been identified. For example, EDTA has been attached to biotin (Figure 1.1) to deliver redox-active metals, such as Fe^{3+} or Cu^{2+} , to the biotin binding site of streptavidin. Hydroxyl radical formation is directed at the biotin binding site and affords site selective cleavage of the protein backbone.⁴⁵

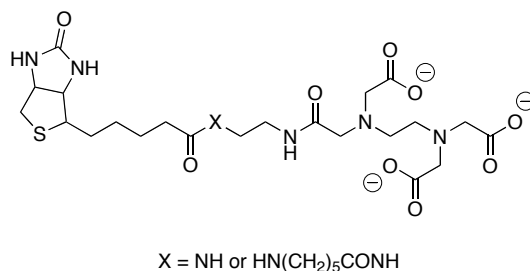


Figure 1.1 Ligand used for site selective cleavage of streptavidin

Photosensitizers that generate ROS inactivate proteins by delivery of ROS upon exposure to light. The chromophore $[\text{Ru}(\text{bipy})_3]^{2+}$, which is a highly efficient generator of the ROS species singlet oxygen $^1\text{O}_2$ upon exposure to light,⁴⁶ was attached to GU40C, a highly selective protein binding peptoid (Figure 1.2). This conjugate has been used in chromophore-assisted light inactivation (CALI) for the disruption of tyrosine kinase receptor VEGFR2. This kinase receptor is important for signaling in angiogenesis. The peptoid-conjugate, RuGU40C, inhibits endothelial growth factor (VEGF) mediated autophosphorylation of VEGFR2, thereby disrupting the receptor. Lee, Lim and Kodadek have shown that in the presence of light, this inhibitor is transformed from a 49 μM inhibitor (without light) to a 59 nM inhibitor (in the presence of light). While this conversion is a drastic improvement, the scope of these types of reagents is limited by the need for exposure to light,⁴⁷ which cannot penetrate deeper than 1 cm under the skin.⁴⁸

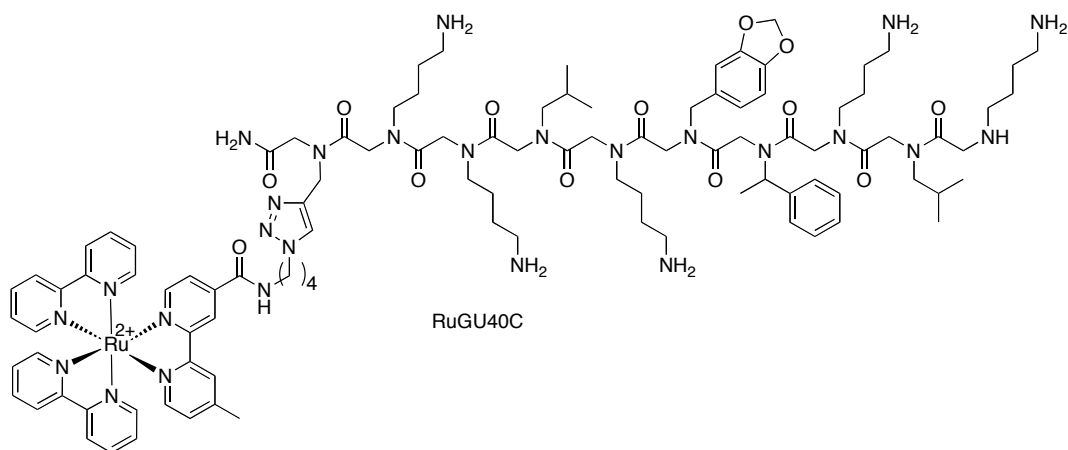


Figure 1.2 CALI reagent constructed from $[\text{Ru}(\text{bipy})_3]^{2+}$ attached to peptoid GU40C

As can be noted from this section, ROS, such as hydroxyl radical, are not selective for the oxidation of amino acid residues in peptides. However, they may be made into a type of selective reagent by use of a protein affinity group or ligand. CALI reagents are selective in their affinity group as well as their ROS, however, their scope is limited by access to light activation. The following section will discuss another type of oxidant where the reactive oxygen is not a ROS, but rather an oxygen atom bound to a metal center. These metal-based oxidants include heme and non-heme ferryls and while they are known in enzymes that activate dioxygen,¹² their oxidation of proteins is underexplored.

1.1.3 Metal-based Oxidants

1.1.3.1 Heme and Non-Heme Fe^{IV}-Oxo Enzymes

Activation of dioxygen is known for many heme and non-heme iron enzymes. These enzymes catalyze a variety of transformations that are critical in biological processes. An example is cytochrome P450 (Cyt P450), which catalyzes the oxidation of organic substrates such as lipids and xenobiotics.¹² Another example is taurine: α -ketoglutarate dioxygenase (TauD), which catalyzes the oxidative decarboxylation of 2-oxoglutarate, after which, taurine is hydroxylated and the liberated product serves as a source of sulfur for biological processes.⁴⁹ These two enzymes will be discussed in detail due to the wide acceptance of the involvement of Fe^{IV}-oxo intermediates.^{12, 13, 50-52}

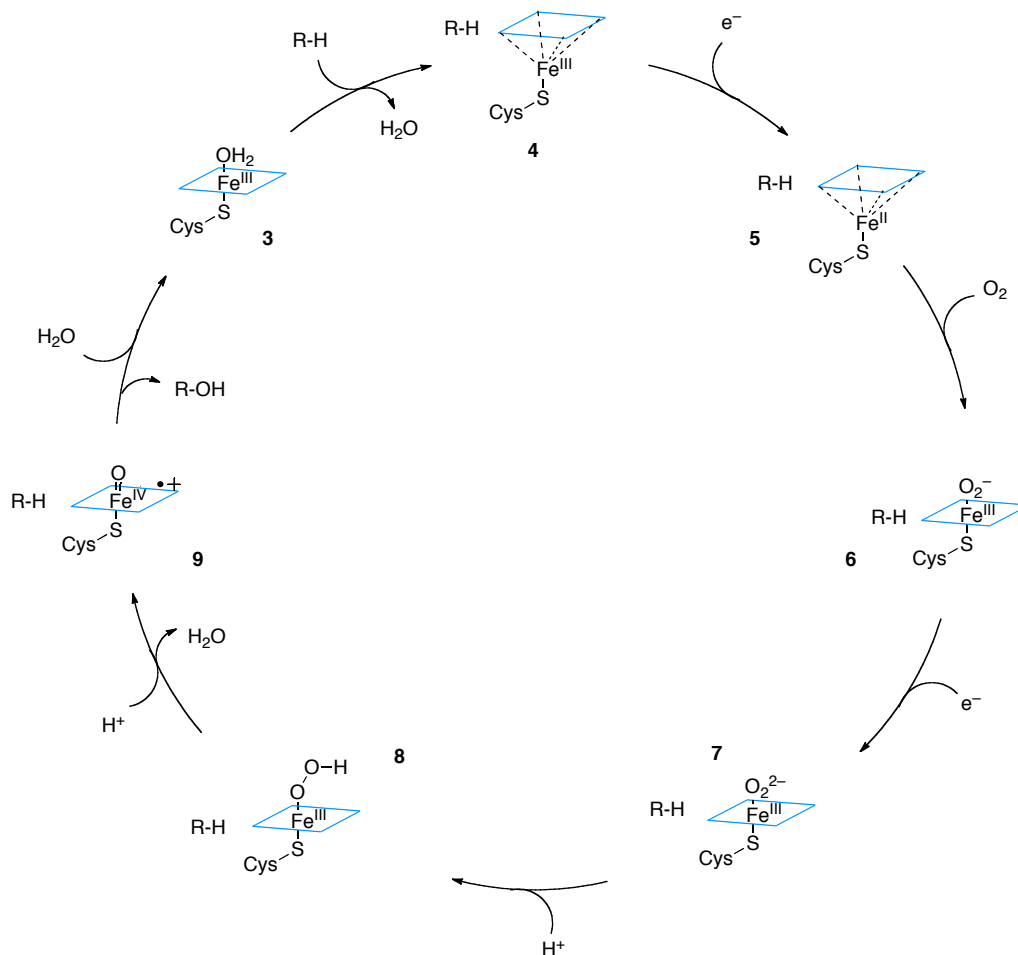
The terminal oxidase Cyt P450 is a microsomal enzyme that activates dioxygen and catalyzes oxygen atom transfer via a high-valent Fe^{IV}O porphyrin π -cation radical to organic substrates.⁵³ This oxygen incorporation into substrates makes the Cyt P450 family important in biological processes. This enzyme is not only involved in destroying the activity of certain environmental pollutants, but plays an important part in cell death (cellular toxicity).^{54, 55} Cyt P450 has a central role in the deactivation/activation of most carcinogens and can influence tumor development and progression in a negative or positive way. It can also metabolize anti-cancer drugs thereby affecting the response of tumors to the specific drug.⁵⁵ For these reasons the mechanism of Cyt P450 has been studied. It is now accepted that the catalytic cycle precedes through an Fe^{IV}-oxo intermediate.

Scheme 1.4 outlines the catalytic cycle of Cyt P450 for the oxygen atom transfer via a high-valent Fe^{IV}O porphyrin π -cation radical.⁵⁰ Once the substrate binds to the

enzyme, a conformational change takes place and water leaves the axial position of the heme (**3** to **4**). Single-electron reduction of Fe^{III} gives Fe^{II} (**4** to **5**) followed by binding of dioxygen to the axial position (**6**) which affords a second conformational change. Single-electron reduction of the bound O_2^- gives O_2^{2-} (**6** to **7**), which is subsequently protonated to give a Fe^{III} -hydroperoxo species (**8**). Protonation and loss of a water molecule result in the formation of a high-valent $\text{Fe}^{\text{IV}}\text{O}$ porphyrin π -cation radical (**9**) that reacts with R-H to transfer the oxygen atom. Biomimetic catalysts have been developed by many groups to afford oxygen atom transfer and hydroxylation of various substrates as described in this mechanism.⁵⁶⁻⁵⁹

Studies of biomimetic Fe^{III} -porphyrins have revealed that the reactivity of the complexes can be controlled by the axial ligand choice as well as the electronics of the porphyrin. These electronics can be modified by either increasing or decreasing the electron-density of the aryl substituents of the porphyrin ligand.⁵⁰

Scheme 1.4 Proposed catalytic cycle for oxygen atom transfer by heme Cyt P450 to substrate R-H



Taurine: α -ketoglutarate dioxygenase (TauD) is a non-heme enzyme whose active oxidant has been identified as a high spin ferryl species.^{51, 60, 61} This enzyme affords oxidative decarboxylation of the α -keto carboxylate substrate 2-oxoglutarate (Figure 1.3). The oxidation of the C-H bond of taurine occurs concomitantly with this oxidative cleavage. In *E.coli*, TauD along with 2-oxoglutarate helps provide the microbe with a source of sulfur, an alternative energy source, (Scheme 1.5). Sulfur is liberated from hydroxylated taurine is used by the microbe during sulfate starvation.^{13, 62-64}

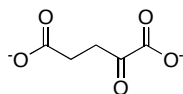
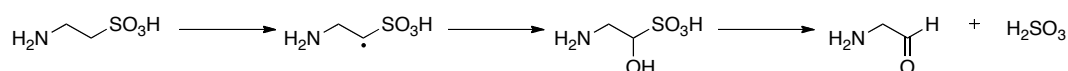


Figure 1.3 Structure of 2-oxoglutarate

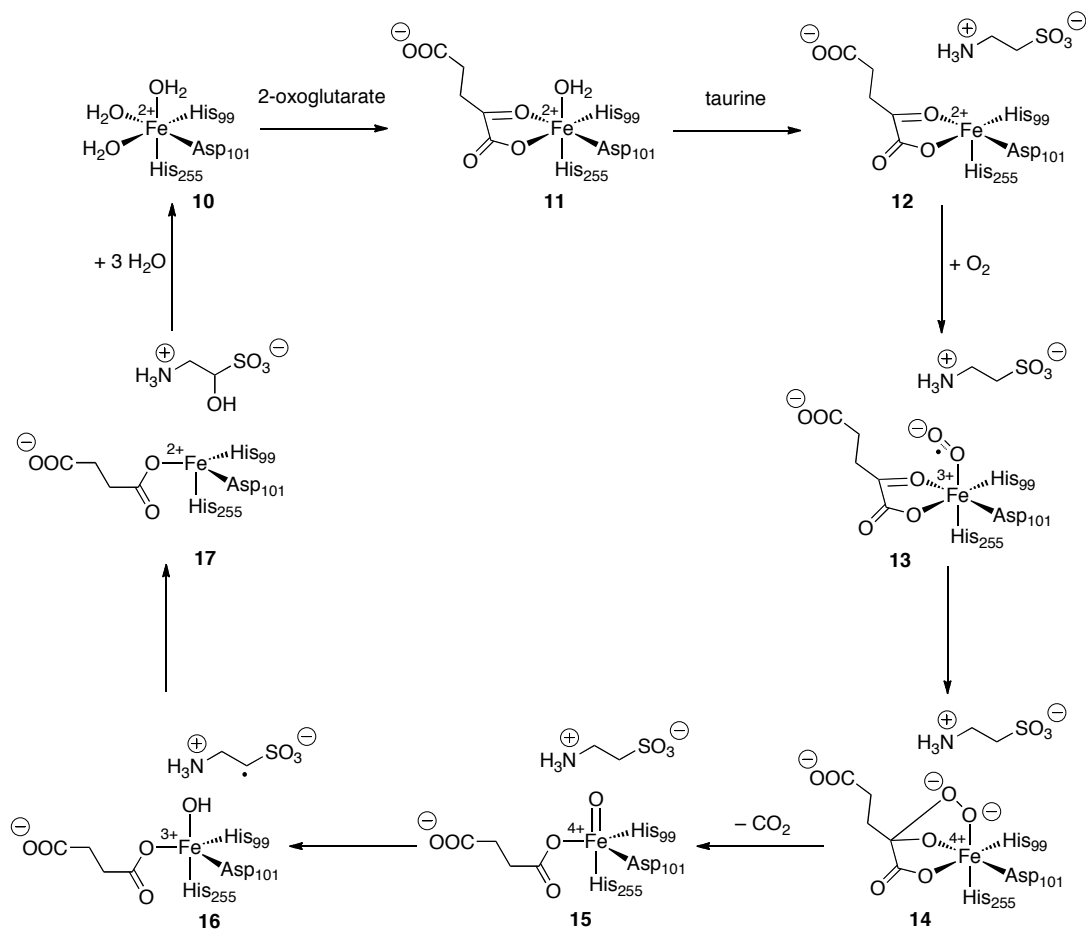
Scheme 1.5 Reaction catalyzed by TauD and 2-oxoglutarate to yield sulfonates as an energy source for *E. coli*



The mechanism of the α -ketoglutarate dioxygenase family of enzymes was proposed almost three decades ago,⁶⁴ but no evidence existed for the proposed ferryl species until recently.^{61, 63} The first evidence that a ferryl species is an intermediate was collected using stopped-flow absorbance along with Mössbauer spectroscopy (using a freeze-quench technique) on TauD (**15**, Scheme 1.6).⁶¹ Further evidence for **15** as an intermediate came from the observation of a large deuterium kinetic isotope effect (KIE = 35) for the C-1 position of taurine.^{51, 65} Finally, characterization data with EXAFS, X-ray crystallography and resonance Raman spectroscopy became available.^{66, 67} A mechanism is proposed where 2 equatorial bound water molecules on the Fe^{2+} center are displaced to allow for binding of 2-oxoglutarate (**10** to **11**). The substrate taurine is introduced and the axial water molecule is lost (**12**) to allow for activation of O_2 forming an Fe^{3+} center (**13**). Oxidation of 2-oxoglutarate (**14**) and subsequent release of CO_2 affords a ferryl (**15**) which abstracts a hydrogen atom from C-1 of taurine. This leads to the formation of an Fe^{III} -hydroxyl species (**16**) which rebounds to hydroxylate at the C-1 position of taurine. Hydroxylated taurine can serve as a source of sulfur in other biological processes by the

breaking of the S–C bond. The release of succinate is the rate-limiting step allowing the process to reoccur (**17** to **10**).^{63, 64}

Scheme 1.6 Mechanism of TauD and 2-oxoglutarate for oxidation of taurine



As this section has highlighted, ferryl species are biologically relevant oxidants found in both heme and non-heme enzymes that activate dioxygen. The following section introduces complexes designed to mimic these types of oxidants by generating ferryl species for the oxidation of substrates.

1.1.3.2 Non-Heme Fe^{IV}-Oxo Complexes

There has been much interest in the past 20 years to develop catalysts that mimic those of heme and non-heme iron active sites that activate dioxygen to effect oxidation of alkanes. These mimics are usually used in conjunction with oxidants such as peroxy acids, hydrogen peroxide, O₃ and KHSO₅^{8, 68, 69} to generate metal-based oxidants that can cleave C-H bonds of alkanes.⁵⁷ The first well-characterized non-heme high-valent ferryl complex was uncovered around the same time as evidence for the involvement of a ferryl intermediate in TauD was observed.^{68, 70, 71}

Wieghardt and coworkers reported the first spectroscopic evidence for a non-heme ferryl species in which they obtained Mössbauer and EPR data that supported a mononuclear, low-spin (S = 1) Fe^{IV}-oxo in biomimetic studies. The ferryl from the complex [Fe^{III}(cyclam-acetato)(CF₃SO₃)]¹⁺ was generated using O₃ in water/acetone at -80 °C.⁷² Three years later, the Fe^{IV}-oxo derived from a macrocyclic ligand, TMC, was the first ferryl to be isolated and a crystal structure was obtained. In the reaction of [Fe^{II}(TMC)(OTf)₂] with iodosyl benzene (PhIO) in acetonitrile at -40 °C, a pale green species was formed in 2 min with a yield greater than 90% (Figure 1.4). This species had a λ_{max} = 820 nm with an extinction coefficient of 400 M⁻¹cm⁻¹. It was also observed that hydrogen peroxide would afford the same species, however, 3 equiv of the oxidant and 3 h was needed to achieve the quantity generated in 2 min with PhIO. The species was shown to be stable at -40 °C for approximately one month and decayed at room temperature. Mass spectrometry data along with X-ray diffraction data were collected. The crystal structure of [Fe^{IV}(O)(TMC)(NCCH₃)](OTf)₂ was in good agreement with EXAFS data for synthetic Fe^{IV}-oxo porphyrin complexes.^{73, 74} The Fe-O bond length was found to be 1.646(3) Å

which is shorter than bond lengths observed in di-oxo-bridged species that have single Fe-O bonds.⁶⁸

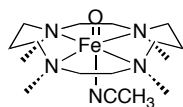


Figure 1.4 Structure of ferryl derived from TMC, $[\text{Fe}^{\text{IV}}(\text{O})(\text{TMC})(\text{NCCH}_3)]^{2+}$

Ferryls have been used in a variety of transformations including catalytic epoxidation of olefins,⁷⁵ hydroxylation reactions and oxygen atom transfer reactions.^{8, 76} Studies show that the structure of the ligand has an influence on the ferryl's stability and its reactivity with substrates.^{8, 68, 69} As was mentioned previously, the ferryl derived from the ligand TMC was more stable at lower temperatures and decayed upon exposure to ambient temperature. The ferryl derived from TPA is not thermally stable at room temperature. In contrast, the ferryls derived from the pentadentate ligands N4Py and Bn-TPEN (Figure 1.5) have been observed to be thermally stable at room temperature. In fact, the ferryl derived from N4Py, $[\text{Fe}^{\text{IV}}(\text{O})(\text{N4Py})]^{2+}$, is stable for several days at room temperature (Figure 1.6).⁸ The difference in denticity is most likely an important factor in the observed stability between TPA and N4Py or Bn-TPEN ferryls. While $[\text{Fe}^{\text{IV}}(\text{O})(\text{N4Py})]^{2+}$ is stable for several days at room temperature, pH appears to play a role in stability as well; this ferryl was reported to be stable between pH 5-6,^{69, 76, 77} however a recent report by Que and coworkers show this ferryl to be stable in water at neutral pH.⁷⁸ Discrepancy between the two reports may be due to the nature of the buffer utilized.

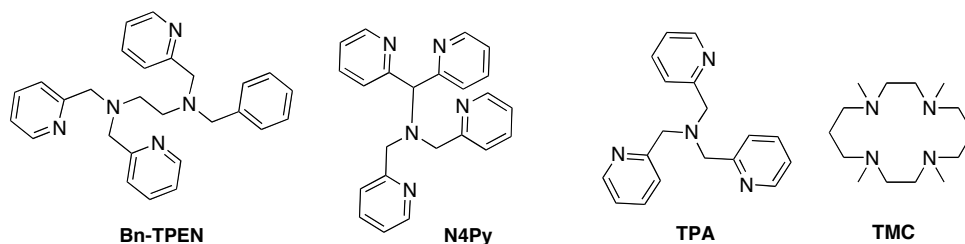


Figure 1.5 Examples of ligands used in ferryl complexes

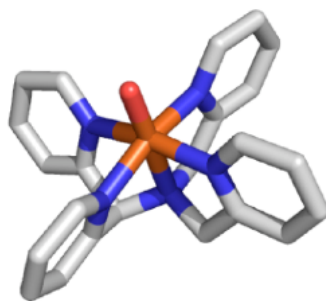
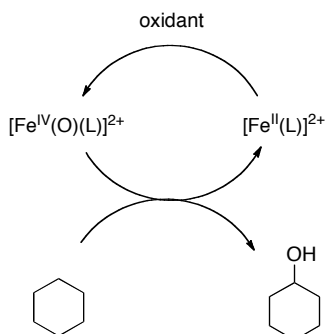


Figure 1.6 Model of $[\text{Fe}^{\text{IV}}(\text{O})(\text{N4Py})]^{2+}$

The ferryls derived from Bn-TPEN and N4Py oxidize strong C-H bonds, such as those present in cyclohexane, with a C-H bond dissociation energy of 99.3 kcal/mol (Scheme 1.7). These ferryls are well characterized by various spectroscopic techniques. While the ferryls derived from Bn-TPEN and N4Py are more stable than others at room temperature, they react with hydrocarbon substrates such as triphenylmethane to afford oxygen atom insertion products. The reaction of $[\text{Fe}^{\text{IV}}(\text{O})(\text{N4Py})]^{2+}$ with 25 equiv of triphenylmethane affords an oxygen atom insertion into the activated C-H bond of triphenylmethane to afford triphenylmethanol in 90% yield. Upon addition of the triphenylmethane at room temperature, the decomposition of the ferryl was observed by UV-vis spectroscopy with a concomitant generation of $[\text{Fe}^{\text{II}}(\text{N4Py})]^{2+}$ in a quantitative yield. Most importantly, a linear relationship was observed between the log of the second

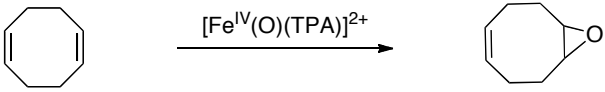
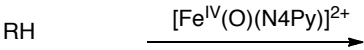
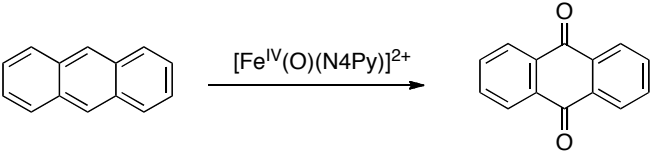
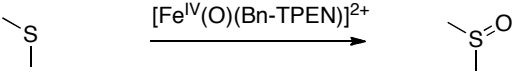
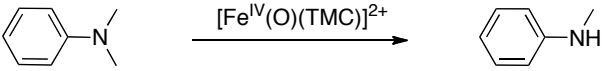
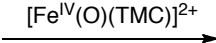
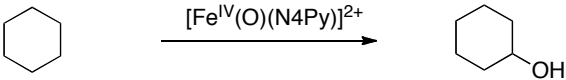
order rate constant vs bond dissociation energy for many substrates. These substrates include Ph_3CH , cumene, PhEt, PhMe and cyclohexane.⁸

Scheme 1.7 Oxidation of cyclohexane by pregenerated ferryl species of polypyridyl ligands



As was mentioned previously, ferryls can affect a wide variety of oxidation reactions such as aromatic hydroxylation,⁷⁹ sulfur/phosphorous oxidation,^{8, 76, 80} *N*-dealkylation,⁸¹ oxidation of alcohols,⁸² hydroxylation of hydrocarbons⁸ and epoxidation.⁸³ Scheme 1.8 illustrates the diverse versatility of non-heme ferryl species.

Scheme 1.8 Transformations observed by non-heme ferryls

Type of transformation	Example	Ref
epoxidation of alkenes:	 <chem>C1=CCCCC1</chem> $\xrightarrow{[\text{Fe}^{\text{IV}}(\text{O})(\text{TPA})]^{2+}}$ <chem>C12=CCCC1O2</chem>	80
oxidation of ROH:	 <chem>RH</chem> $\xrightarrow{[\text{Fe}^{\text{IV}}(\text{O})(\text{N4Py})]^{2+}}$ <chem>ROH</chem>	79
aromatic hydroxylation:	 <chem>C1=CC=C2C=CC=CC2=C1</chem> $\xrightarrow{[\text{Fe}^{\text{IV}}(\text{O})(\text{N4Py})]^{2+}}$ <chem>O=C1C=CC(=O)C=C1</chem>	76
sulfur oxidation:	 <chem>CS</chem> $\xrightarrow{[\text{Fe}^{\text{IV}}(\text{O})(\text{Bn-TPEN})]^{2+}}$ <chem>CS(=O)</chem>	7
N-dealkylation:	 <chem>CN(C)c1ccccc1</chem> $\xrightarrow{[\text{Fe}^{\text{IV}}(\text{O})(\text{TMC})]^{2+}}$ <chem>Nc1ccccc1</chem>	78
phosphorus oxidation:	 <chem>P(C)(C)C</chem> $\xrightarrow{[\text{Fe}^{\text{IV}}(\text{O})(\text{TMC})]^{2+}}$ <chem>OP(C)C</chem>	73, 77
hydroxylation of alkanes:	 <chem>C1CCCCC1</chem> $\xrightarrow{[\text{Fe}^{\text{IV}}(\text{O})(\text{N4Py})]^{2+}}$ <chem>OC1CCCCC1</chem>	7

1.1.4 Project Goals

The previous discussion involved the oxidation of various organic substrates with ferryls; however, none of these studies involved the oxidation of proteins. We have chosen to investigate the oxidation of proteins with the ferryl derived from the pentadentate ligand N4Py, $[\text{Fe}^{\text{IV}}(\text{O})(\text{N4Py})]^{2+}$. As described above, this ferryl has been well characterized. Iron was chosen as a cofactor instead of other metals such as Ru due to its bioavailability.^{84, 85} Recently, Jackson and Kodanko have shown that polypyridyl ligands, such as Bn-TPEN and N4Py, can strip iron from ferritin in the presence of a reductant and generate Fe^{II} -complexes.⁸⁶ This is an important result suggesting that Fe^{II} complexes could be formed in cells by reduction of iron from ferritin in the presence of ligands such as N4Py. In order to carry out this investigation, a series of goals were outlined.

The first goal was to synthesize substrates that mimic amino acid residues of polypeptides. These substrates would then be used in the second goal, which was to determine the order of reactivity for the reaction of the ferryl with each substrate. The third and final goal was to conduct mechanistic investigations for the most reactive amino acid substrates. The following sections describe the efforts made to achieve the goals of this project.

1.2 Results and Discussion

1.2.1 Synthesis of Substrates to Mimic Amino Acid Residues of Polypeptides: Ac-AA-NHtBu

A collaborative effort in the Kodanko Lab was made to design and synthesize substrates that mimic individual amino acid residues.⁸⁷ We have synthesized substrates for all 20 naturally occurring amino acids using solution phase methodology. These substrates have *C*-terminal and *N*-terminal amides installed to mimic individual residues, specifically *tert*-butyl and acetyl respectively (Figure 1.7). The substrate syntheses described in this section include those derived from glutamine (Gln), asparagine (Asn), isoleucine (Ile), tyrosine (Tyr) and cysteine (Cys) (Figure 1.8).⁸⁷⁻⁸⁹

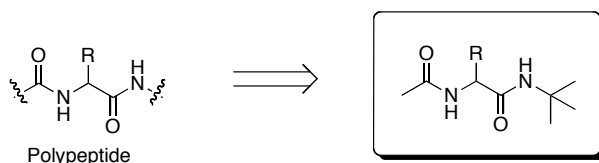


Figure 1.7 Substrate to mimic amino acid residues of polypeptides

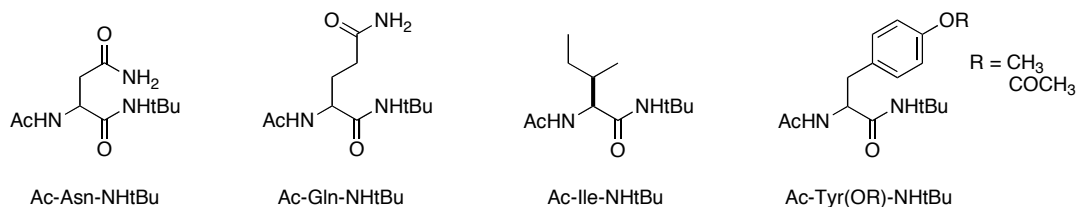
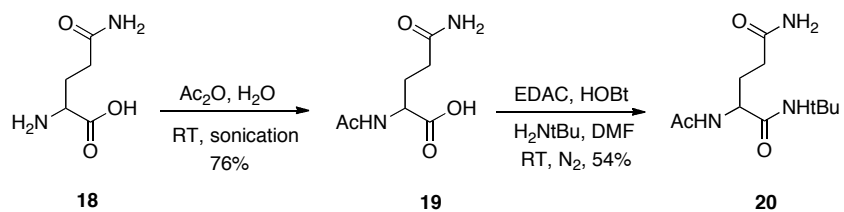


Figure 1.8 Substrates synthesized

1.2.1.1 Synthesis of Ac-Gln-NHtBu

Synthesis of the substrate derived from Gln required no protecting groups. N-acetyl-Gln-OH (**19**) was prepared by treatment of NH₂-Gln-OH (**18**) with 4 equiv of acetic anhydride (76%, Scheme 1.9). The free acid (**19**) was then coupled with *tert*-butylamine using 1 equiv of both HOBT and EDAC to produce Ac-Gln-NHtBu (**20**, 54%).

Scheme 1.9 Synthesis of Ac-Gln-NHtBu



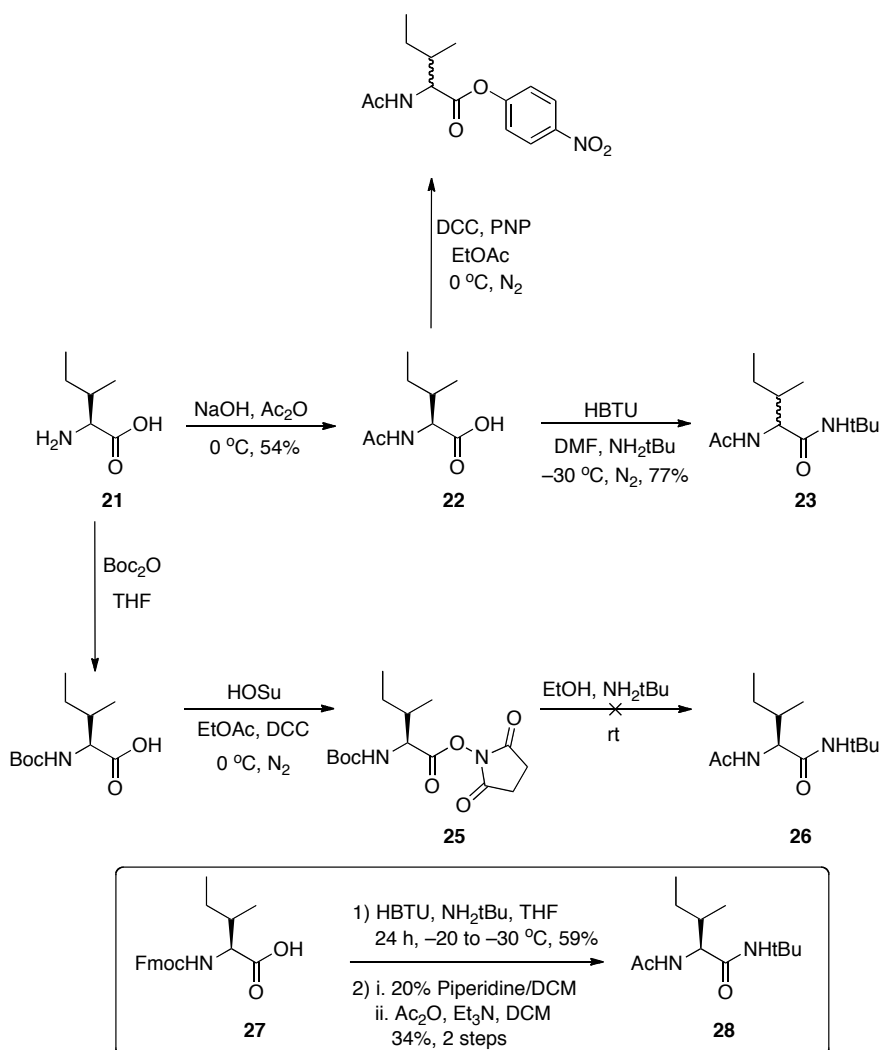
1.2.1.2 Synthesis of Ac-Ile-NHtBu

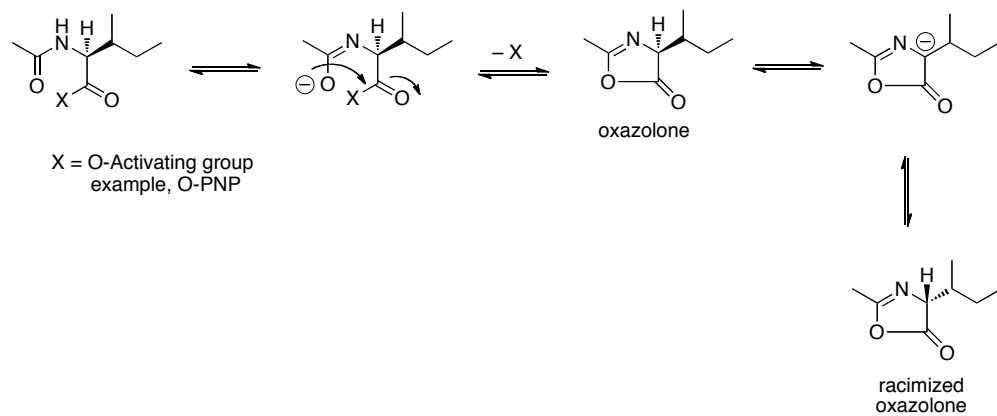
Unlike the synthesis of Ac-Gln-NHtBu, the substrate derived from Ile was not straightforward. While amide bond formation was facile, a diastereomeric mixture of the substrate was obtained during several synthesis attempts (Scheme 1.10) Epimerization at the α -stereocenter was difficult to suppress. A literature search uncovered that acetylation under basic conditions affords non-epimerized N-acetyl amino acids.⁹⁰ Therefore, this strategy was used in place of the initial acetylation conditions of acetic anhydride and acetic acid. Cold sodium hydroxide was added to a mixture of H₂N-Ile-OH and acetic anhydride to maintain an alkaline pH throughout the acetylation (**21** to **22**). Acetylation lead to formation of a single diastereomer Ac-Ile-OH (**22**), however, condensation with *tert*-butylamine did not (**23**). While many different reaction conditions and coupling reagents were screened, all resulted in the formation of diastereomeric mixtures. Examples of coupling reagents screened include HBTU, EDAC/HOBt and EDAC. Condensation with *tert*-butylamine was attempted with the succinimide ester Boc-Ile-OSu (**25**), however, no product was observed.⁹¹ Epimerization at the α -carbon most likely resulted from the formation of an oxazolone intermediate (Scheme 1.11) that is easily epimerized via deprotonation. This could be due to a slower condensation with the bulky nucleophile, *tert*-butylamine. While these reaction conditions failed to produce a single diastereomer, one condition was found to yield the product without epimerization.

Condensation of Fmoc-Ile-OH (**27**) with *tert*-butylamine using HBTU at $-20\text{ }^{\circ}\text{C}$ in THF afforded the single diastereomer Fmoc-Ile-NHtBu (59%). The solvent seems to play an important role in the formation of a single diastereomer as solvents such as DMF resulted in epimerization. The *N*-Fmoc group was removed using 20% piperidine/CH₂Cl₂

and the resulting primary amine, H₂N-Ile-NHtBu, was acetylated. Acetylation was carried out using acetic anhydride in the presence of triethylamine to give Ac-Ile-NHtBu as a single diastereomer (**28**, 34% over 2 steps).

Scheme 1.10 Synthetic trials to obtain a single diastereomer of Ac-Ile-NHtBu and final synthesis of a single diastereomer

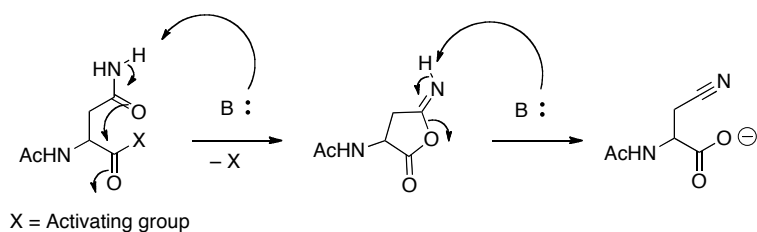


Scheme 1.11 Oxazolone formation from the activated ester of Ac-Ile-OH

1.2.1.3 Synthesis of Ac-Asn-NHtBu

The synthesis of the substrate derived from Asn, Ac-Asn-NHtBu (**30**), proved to be challenging after the initial pathway failed to produce the final product. Initial attempts followed the synthetic route of Ac-Gln-NHtBu (**20**), but condensation of Ac-Asn-OH and *tert*-butylamine using the coupling reagent EDAC did not yield the product in a significant quantity, presumably due to complications of ring formation or dehydration of the side chain (Scheme 1.12).⁹² Another route towards **30** was attempted using Ac-Asp(OBn)-NHtBu⁸⁷ as a starting material. Ac-Asp(OBn)-NHtBu is an intermediate in the synthesis the substrate Ac-Asp-NHtBu, which was previously synthesized in the Kodanko Lab.⁹³ Attempts to transform the benzyl ester into an amide using methanolic ammonia failed.^{94, 95} The benzyl ester never fully converted to the desired amide, but instead converted to a methyl ester in addition to the desired amide, even at higher reaction temperatures and longer reaction times. Isolation of the substrate from the methyl ester was unsuccessful, therefore a third and final route was attempted.

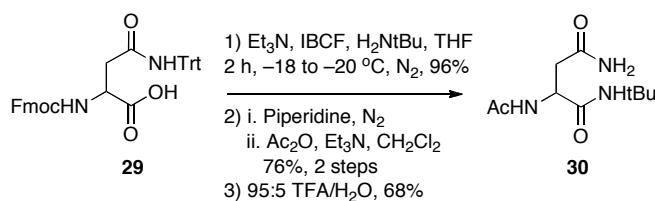
Scheme 1.12 Potential ring formation and dehydration of Asn side chain



Fmoc-Asn(Trt)-OH (**29**, Scheme 1.13) was utilized in the successful synthesis of **30**, and, after optimization, condensation with *tert*-butylamine using the coupling reagent isobutyl chloroformate and the base TEA at low temperature furnished Fmoc-Asn(Trt)-

NHtBu in excellent yield (96%). The base labile protecting group was removed with piperidine. The free amine, H₂N-Asn(Trt)-NHtBu, was acetylated to give the trityl protected product Ac-Asn(Trt)-NHtBu (76% over 2 steps). Finally, the acid labile trityl group was removed using 95:5 TFA/H₂O to furnish Ac-Asn-NHtBu (**30**, 68%). These deprotection conditions allowed for ease of product isolation as the triphenylmethanol byproduct could be removed easily by precipitation with H₂O.⁸⁷

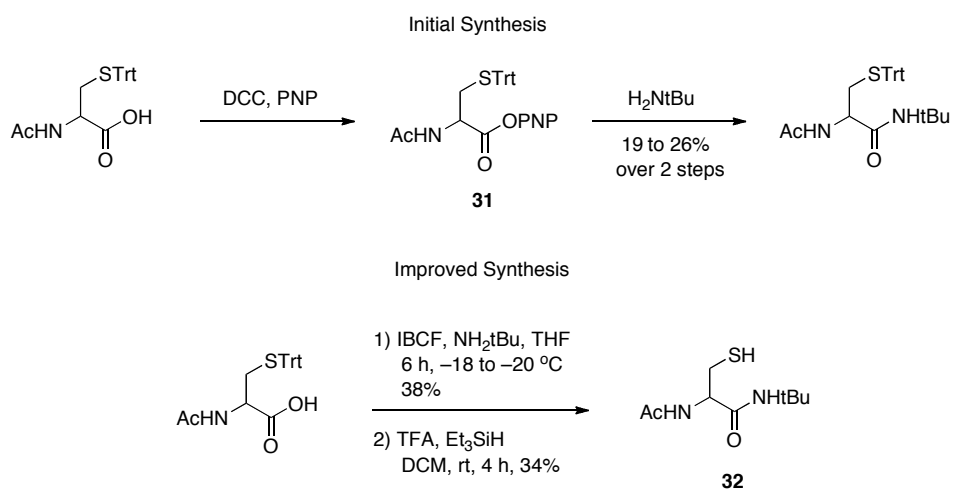
Scheme 1.13 Synthesis of Ac-Asn-NHtBu via N-Fmoc and trityl protection



1.2.1.4 Optimized Synthesis of Ac-Cys-NHtBu

Previously, Ac-Cys(Trt)-NHtBu was prepared in a 19 to 26% yield by making an activated *p*-nitrophenol-ester (**31**, PNP-ester) at the *C*-terminal before subsection to *tert*-butylamine for condensation (Scheme 1.14). Before condensation, the PNP-ester was purified by crystallization from the reaction mixture and filtered. The product was subsequently washed with ethyl acetate and finally subjected to *tert*-butylamine. Crystallization and isolation of the ester by filtration led to low yields because the PNP-ester was soluble in ethyl acetate. While the solvent and reaction mixture were cooled to $-20\text{ }^{\circ}\text{C}$, the product redissolved during filtration. Attempts were made to obtain a higher and more consistent yield in which several coupling reagents were tested. No reagent gave the desired product in high yield, however, a reproducible yield of 38% was obtained using IBCF and no further attempts were made to optimize the coupling further. The removal of the trityl protecting group remained the same as the original synthesis.

Scheme 1.14 Synthesis of Ac-Cys-NHtBu

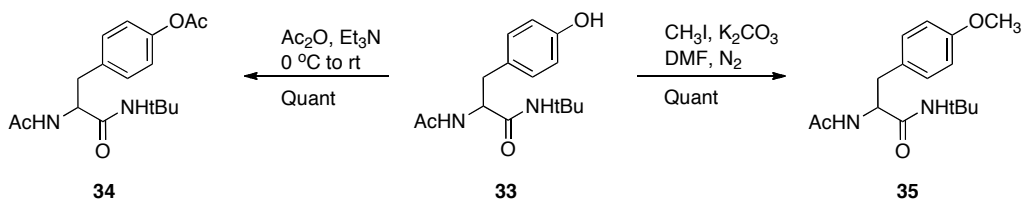


1.2.1.5 Synthesis of Ac-Tyr-NHtBu Derivatives: Ac-Tyr(OAc)-NHtBu and Ac-Tyr(OMe)-NHtBu

Substrates derived from Tyr (**34** and **35**) were synthesized in order to conduct experiments to provide support for the mechanisms of the ferryl with Ac-Tyr-NHtBu (**33**) and Ac-Phe-NHtBu (**36**, *vide infra*). These two unnatural amino acid derivatives, one with an electron-withdrawing group (EWG) and one with an electron-donating group (EDG), Ac-Tyr(OAc)-NHtBu (**34**) and Ac-Tyr(OMe)-NHtBu (**35**), respectively, were readily made from the previously synthesized **33**.⁹³

Triethylamine was added to **33**, followed by addition of acetic anhydride. This resulted in the facile acetylation of the alcohol group to yield **34** in a quantitative yield (Scheme 1.15). The base K_2CO_3 was added to **33** followed by iodomethane and resulted in the methylation of the alcohol group in a quantitative yield to provide **35**.

Scheme 1.15 Synthesis of Ac-Tyr(OMe)-NHtBu and Ac-Tyr(OAc)-NHtBu



1.2.2 Kinetic & Mechanistic Studies of Ac-AA-NHtBu with $[\text{Fe}^{\text{IV}}(\text{O})(\text{N4Py})]^{2+}$

After the preparation of substrates, kinetic studies were conducted using 10 mol% of $[\text{Fe}^{\text{II}}(\text{N4Py})(\text{MeCN})](\text{ClO}_4)_2$ and KHSO_5 along with 10 mM substrate. Reactions were carried out in a 1:1 $\text{H}_2\text{O}:\text{CH}_3\text{CN}$ mixture. The ferryl, $[\text{Fe}^{\text{IV}}(\text{O})(\text{N4Py})]^{2+}$, was preformed using $[\text{Fe}^{\text{II}}(\text{N4Py})(\text{MeCN})](\text{ClO}_4)_2$ and KHSO_5 for 10 min before the addition of the substrate. The decomposition of the ferryl species was monitored by UV-vis spectroscopy at 680 nm. Decomposition of $[\text{Fe}^{\text{IV}}(\text{O})(\text{N4Py})]^{2+}$ upon treatment with Ac-Ile-NHtBu can be found in Figure 1.9 and time course decay of $[\text{Fe}^{\text{IV}}(\text{O})(\text{N4Py})]^{2+}$ at 680 nm can be found in Graph 1.1. It should be noted that Ac-Ile-NHtBu caused the decomposition of the ferryl species within the same time frame of the ferryl decomposition alone and therefore its reactivity, from a kinetic standpoint, was considered insignificant.

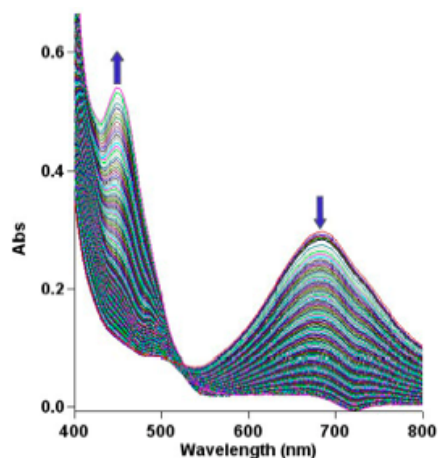
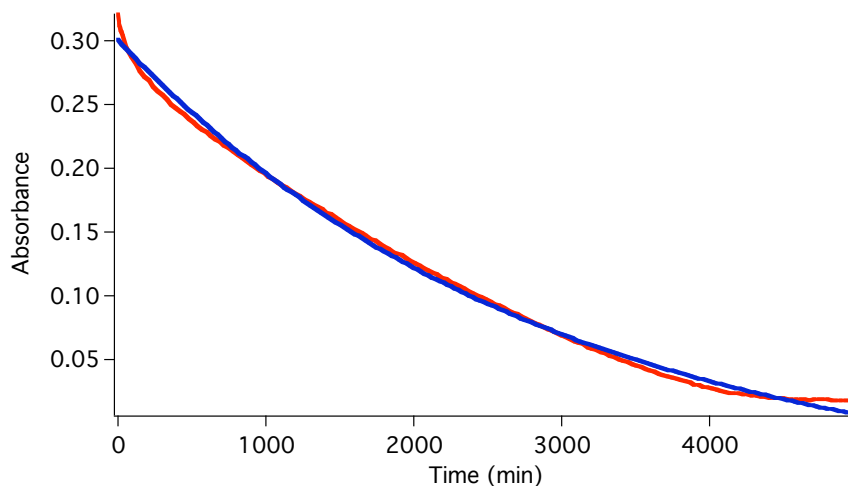


Figure 1.9 UV-vis spectrum over time for the decomposition of $[\text{Fe}^{\text{IV}}(\text{O})(\text{N4Py})]^{2+}$ (1 mM) at 680 nm upon treatment Ac-Ile-NHtBu (10 mM) with concomitant regeneration of the Fe^{II} species at 450 nm

Graph 1.1 Time course decay of $[\text{Fe}^{\text{IV}}(\text{O})(\text{N4Py})]^{2+}$ (1 mM) at 680 nm upon treatment of Ac-Ile-NHtBu (10 mM)



The pseudo-first order rate constants for the reaction of the ferryl with substrates synthesized in the previous section can be found in Table 1.2. (Conditions: $[\text{Fe}^{\text{IV}}(\text{O})(\text{N4Py})]^{2+} = 1 \text{ mM}$; Ac-AA-NHtBu = 10 mM) The following subsections will discuss the most reactive substrates derived from cysteine (**32**) and tyrosine (**33**), as well as experiments with the less reactive substrate derived from phenylalanine (**36**).⁸⁸

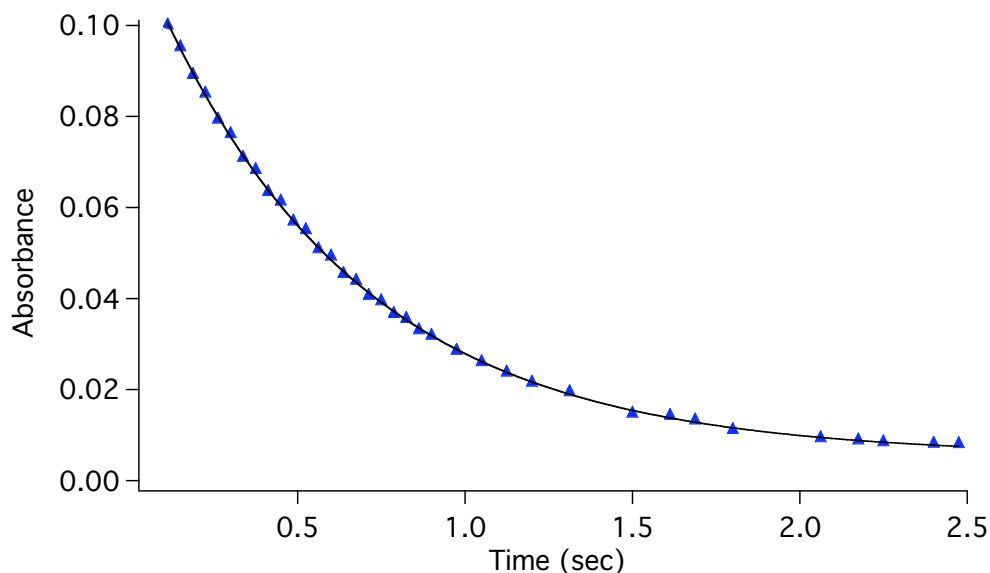
Table 1.2 Pseudo-first order rate constants and k_{rel} for substrates Ac-AA-NHtBu (k_{rel} is with respect to the decomposition of the ferryl alone with no substrate added)

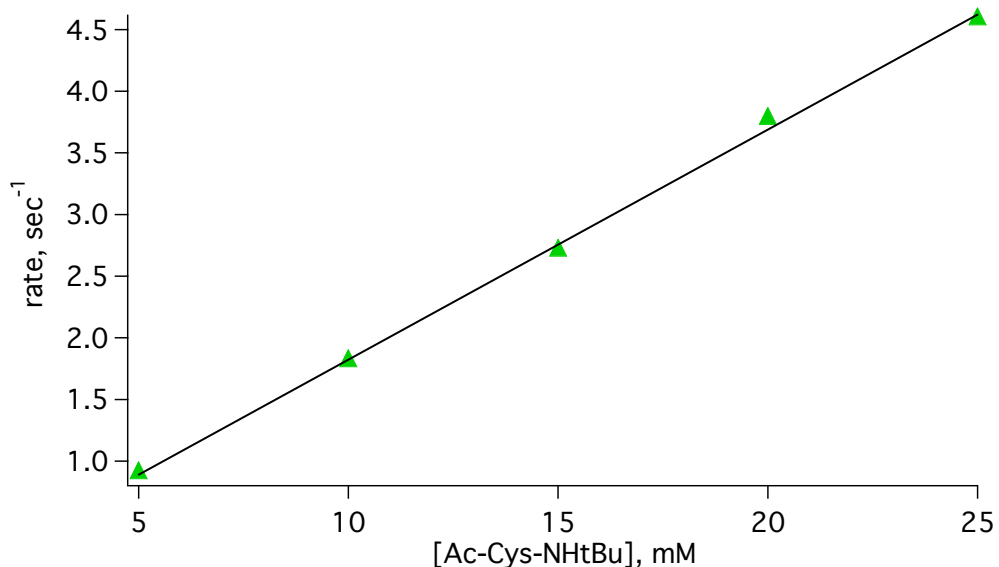
Ac-AA-NHtBu	k_{obs} , sec^{-1}	k_{rel}
Cys	1.7(1)	340,000
Tyr	$3.4(1) \times 10^{-1}$	68,000
Gly	$5.8(2) \times 10^{-5}$	12
Tyr(OMe)	$2.5(2) \times 10^{-5}$	5
Gln	$1.6(2) \times 10^{-5}$	3.2
Phe	$1.4(4) \times 10^{-5}$	2.8
Asn	$1.4(1) \times 10^{-5}$	2.8
Tyr(OAc)	$1.3(1) \times 10^{-5}$	2.6
Ile	$5.0(5) \times 10^{-6}$	1.0

1.2.2.1 Kinetics and Mechanism of $[\text{Fe}^{\text{IV}}(\text{O})(\text{N4Py})]^{2+}$ with Ac-Cys-NHtBu

From Table 1.2 in the previous section, it is noted that the substrate derived from Cys (**32**) caused the decay of the ferryl faster than any other substrate with a pseudo-first order rate constant of $1.7(1) \text{ s}^{-1}$. Due to this fast rate of reaction, a bench-top UV-visible spectrophotometer was equipped with a stopped-flow apparatus in order to observe the decay of the ferryl at 680 nm. The k_{rel} shows that the **32** caused the ferryl to decay 340,000 times faster than the ferryl decomposition alone with no substrate added. This decay is shown in Graph 1.2 for the reaction in 1:1 acetonitrile/water. A second-order rate constant of $1.9(3) \times 10^2 \text{ M}^{-1}\text{s}^{-1}$ was obtained from the slope of the line from Graph 1.3, where 5 concentrations of **32** were plotted against the rate and a linear relationship was observed.

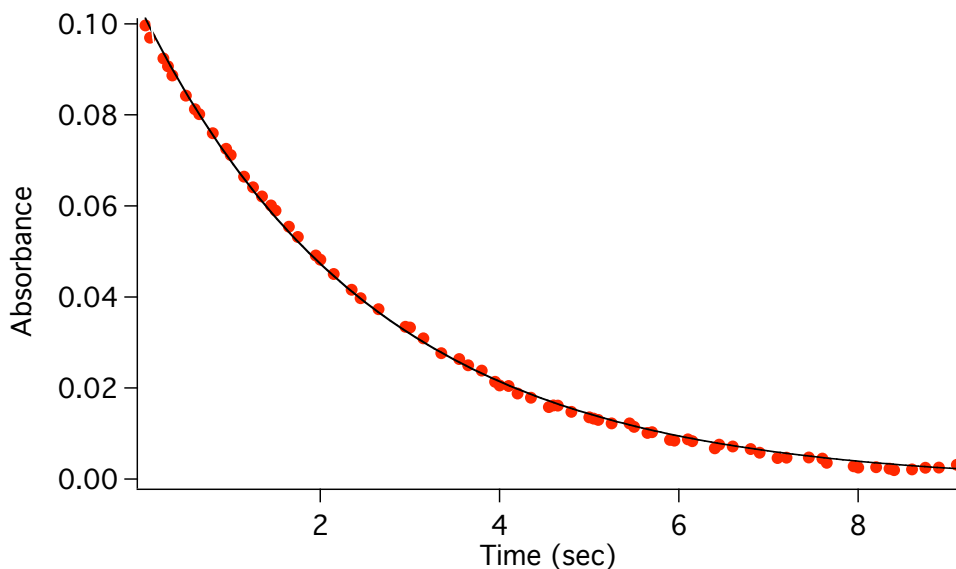
Graph 1.2 Decomposition of the ferryl (1 mM) at 680 nm upon treatment with 10 equiv Ac-Cys-NHtBu in $\text{CH}_3\text{CN}/\text{H}_2\text{O}$



Graph 1.3 Second-order plot for Ac-Cys-NHtBu (5 to 25 mM) with the ferryl (1 mM)

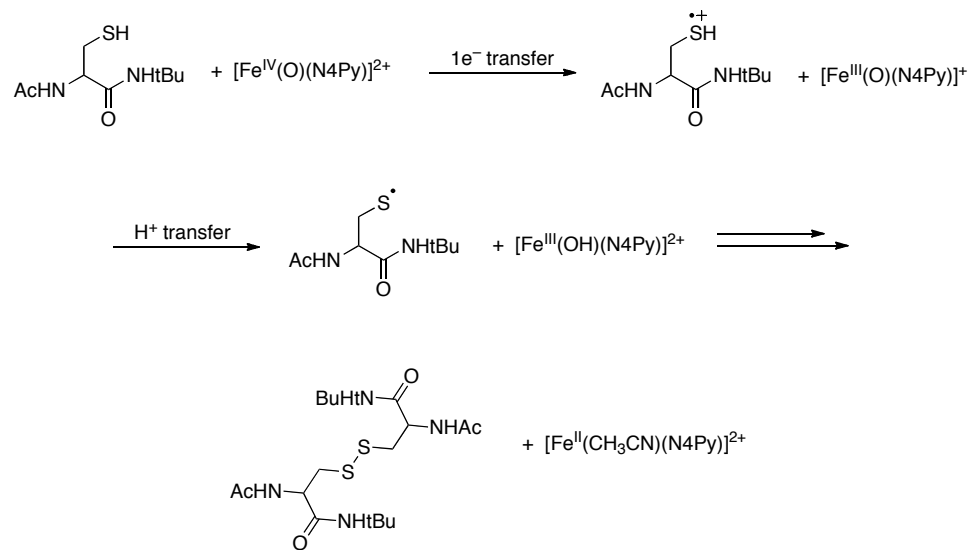
In order to study the mechanism for the reaction of $[\text{Fe}^{\text{IV}}(\text{O})(\text{N4Py})]^{2+}$ with **32**, a kinetic isotope effect (KIE) was determined by carrying out the reaction deuterated solvents (Graph 1.4). A slower pseudo-first order rate constant was observed in deuterated solvent, $3.7(1) \times 10^{-1} \text{s}^{-1}$, and a KIE of 4.3 was calculated using the rates obtained from the reactions carried out in $\text{CH}_3\text{CN}/\text{H}_2\text{O}$ and $\text{CD}_3\text{CN}/\text{D}_2\text{O}$. This KIE may suggest an electron transfer (ET) from the sulfur of the thiol functionality to the ferryl that is rate limiting, followed by a proton transfer (PT) to yield a thiyl radical. However, based on literature, an HAT mechanism cannot be ruled out on the basis of KIE alone.

Graph 1.4 Decomposition of the ferryl (1 mM) at 680 nm upon treatment with 10 equiv Ac-Cys-NHtBu in CD₃CN/D₂O



Support for the mechanism in Scheme 1.16 was observed in the UV-vis spectral data in which the regeneration of the water bound Fe^{II}(N4Py) was much slower than the decomposition of the ferryl, suggesting there is a lag due to the formation of a long-lived intermediate, in this case, an [Fe^{III}(OH)(N4Py)]²⁺. Further support comes from the fact that thiols are strong reducing agents and have a high redox potential of +0.9 mV, therefore, an ET to the ferryl should be facile. These observations support the proposed mechanism in Scheme 1.16 where the formation of a thiyl radical by ET followed by PT to the ferryl leads to the formation of a disulfide. This disulfide product was observed by ESI-MS and a yield of 61%, with respect to the ferryl, was determined by internal standard (cyclooctadiene) using ¹H-NMR spectroscopy. Interestingly, no oxidation of **32** was observed that lead to the addition of one or more oxygen atoms to the sulfur, such as sulfenic or sulfinic acid. The disulfide was the only oxidation product detected.

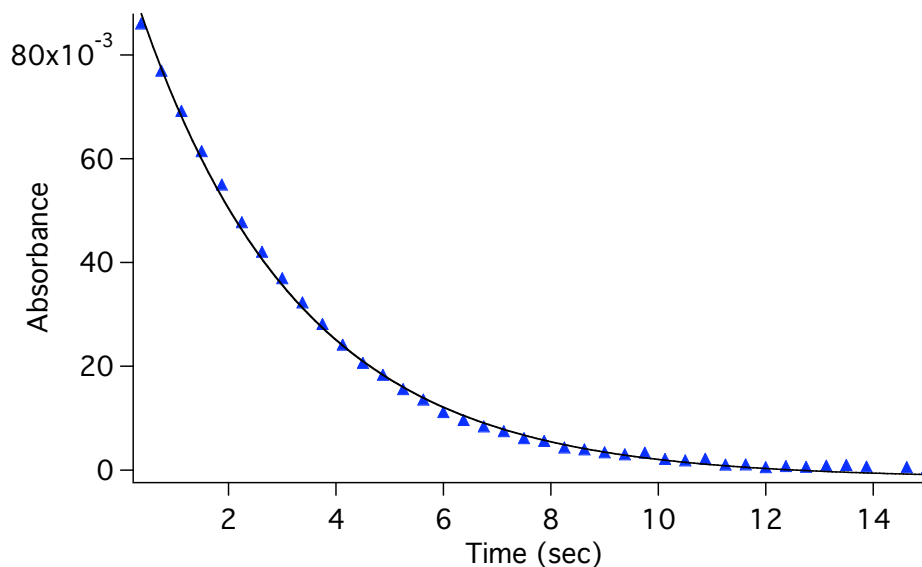
Scheme 1.16 Proposed ET-PT mechanism for the reaction of the Ac-Cys-NHtBu with $[\text{Fe}^{\text{IV}}(\text{O})(\text{N4Py})]^{2+}$

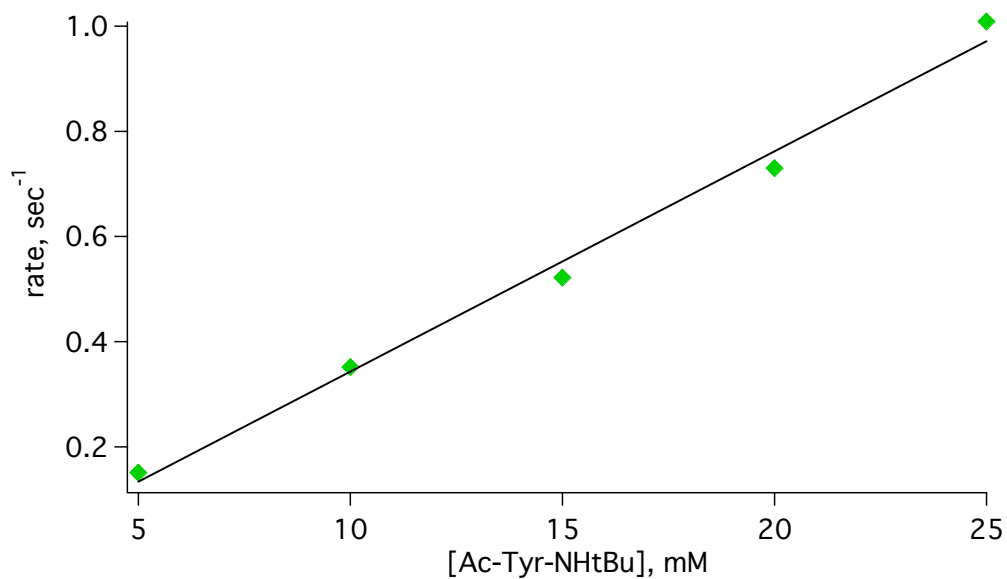


1.2.2.2 Kinetics and Mechanism of $[\text{Fe}^{\text{IV}}(\text{O})(\text{N4Py})]^{2+}$ with Ac-Tyr-NHtBu

Ac-Tyr-NHtBu (**33**) caused the decay of the ferryl faster than all other substrates, except **32**, with a pseudo-first order rate constant of $3.4(1) \times 10^{-1} \text{ s}^{-1}$. A stopped-flow apparatus was employed as in the case of **32**. Ac-Tyr-NHtBu caused the ferryl to decay 68,000 times faster than the decomposition of the ferryl alone with no substrate added (Graph 1.5). As was the case with the **32**, when a plot of five concentrations vs rate was plotted, a linear relationship was observed with the slope of the line giving a second order rate constant of $4.2(3) \times 10^1 \text{ M}^{-1} \text{ s}^{-1}$ (Graph 1.6). Due to the dissolution of a polymeric substance, most likely a tyrosine polymer, the identity of the product was not determined.

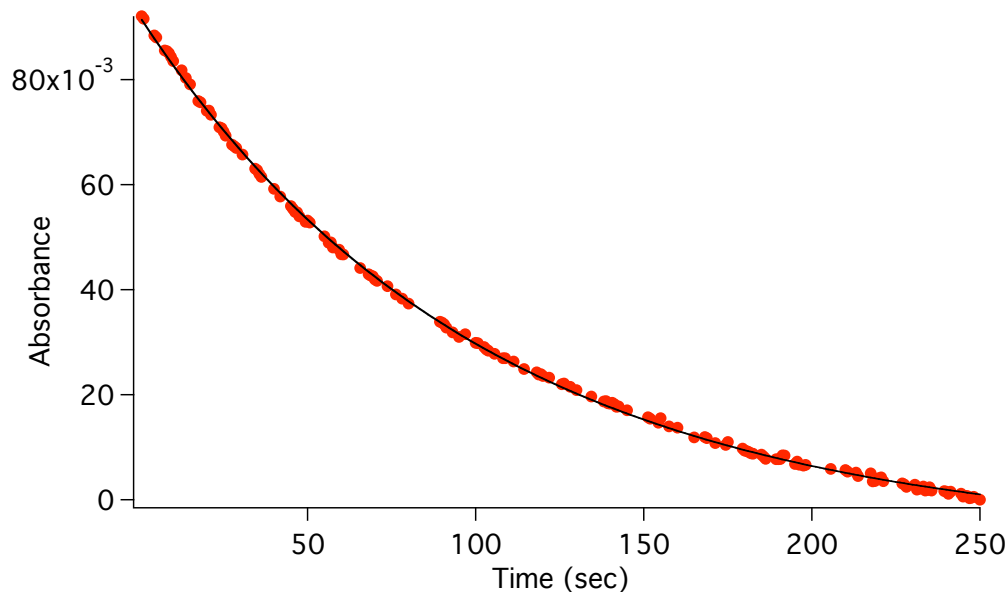
Graph 1.5 Decomposition of the ferryl (1 mM) at 680 nm upon treatment with 10 equiv Ac-Tyr-NHtBu in $\text{CH}_3\text{CN}/\text{H}_2\text{O}$



Graph 1.6 Second-order plot for Ac-Tyr-NHtBu (5 to 25 mM) with the ferryl (1 mM)

While the rate of reaction with the ferryl was only second to **32**, the rate changed significantly upon carrying out the reaction in CD₃CN/D₂O, $k_{\text{obs}} = 1.2(1) \times 10^{-2} \text{ s}^{-1}$, and a large KIE of 29 was obtained (Graph 1.7). Large KIEs have been observed in non-heme enzymes that activate dioxygen, such as TauD.^{49, 66} Such a large KIE suggests that the ferryl species reacts with Ac-Tyr-NHtBu via a HAT mechanism, however, further studies were conducted to support this hypothesis.

Graph 1.7 Decomposition of the ferryl (1 mM) at 680 nm upon treatment with 10 equiv Ac-Tyr-NHtBu in CD₃CN/D₂O



Since a HAT mechanism was hypothesized, the result would lead to a phenoxyl radical which would be observable by electron paramagnetic resonance spectroscopy (EPR). In an attempt to observe the phenoxyl radical, the reaction was freeze quenched in a quartz EPR tube, using liquid nitrogen immediately upon mixing, and subjected to EPR analysis. Only trace radical was observed, even when the reaction solutions were cooled in an ice bath before mixing (Figure 1.10). Due to the propensity of the tyrosyl radical to polymerize (it is an unstable, short-lived radical), the reaction was carried out using a substrate that has a more stable phenoxyl radical, 2,4,6-tri-*tert*-butylphenol. This phenol has stabilizing properties; the radical is stabilized by the electron-donating ability of the *tert*-butyl groups and by resonance delocalization to lead to three tertiary radicals within the aromatic ring (Scheme 1.17, only one resonance within the ring is shown). As was

expected, an intense resonance indicative of an organic radical was observed at $g = 2.0045$ (Figure 1.11).

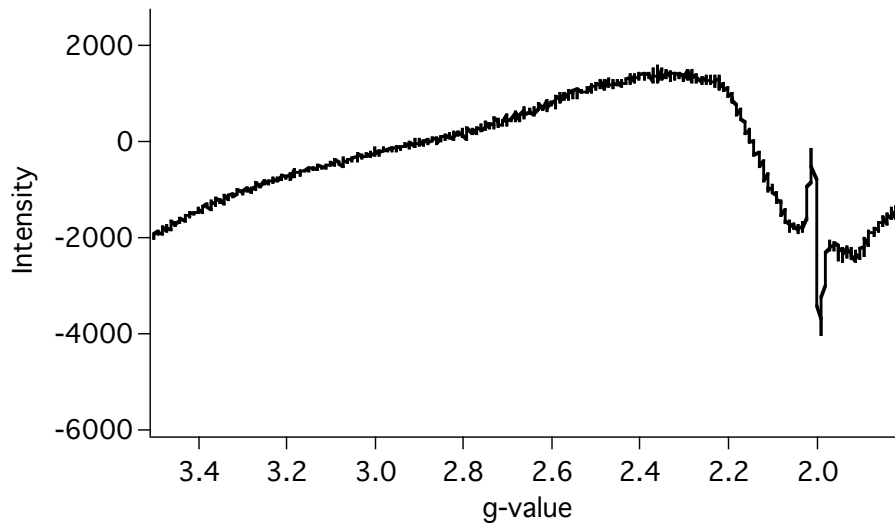
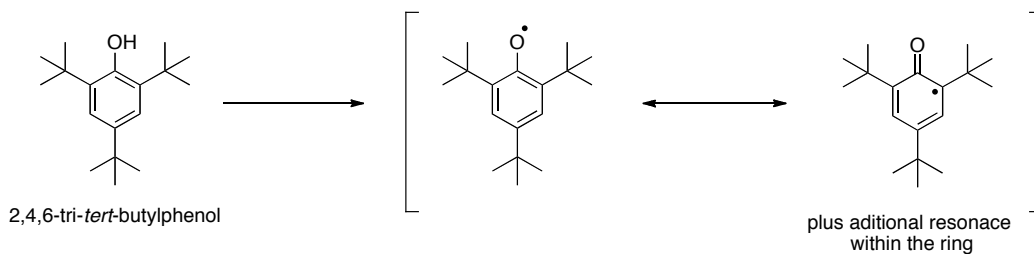


Figure 1.10 X-band EPR spectrum of $[\text{Fe}^{\text{IV}}(\text{O})(\text{N4Py})]^{2+}$ (1 mM) upon treatment with substrate Ac-Tyr-NHtBu (10 equiv) in 1:1 $\text{H}_2\text{O}:\text{MeCN}$ at 0°C ; frozen in liquid N_2 after less than 15 seconds. Experimental Conditions: temperature, 125 K; microwaves, 10 mW at 9.34 GHz; modulation, 0.55 G; receiver gain, 100.

Scheme 1.17 Stabilizing properties of 2,4,6-tri-*tert*-butylphenol



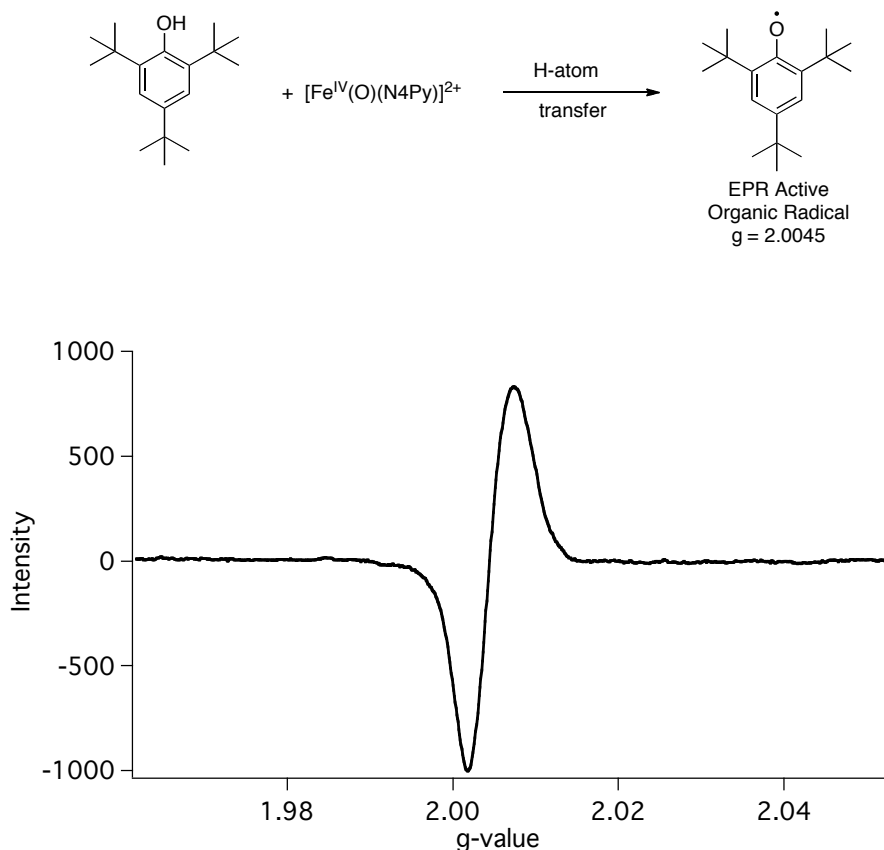


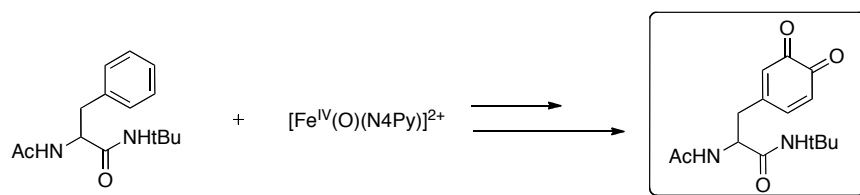
Figure 1.11 X-band EPR spectrum of $[\text{Fe}^{\text{IV}}(\text{O})(\text{N4Py})]^{2+}$ (1 mM) upon treatment with 2,4,6-tri-*tert*-butyl phenol (10 equiv) in 1:1 $\text{H}_2\text{O}:\text{MeCN}$ at 0°C ; frozen in liquid N_2 after less than 15 seconds. Experimental Conditions: temperature, 125 K; microwaves, 1.1 mW at 9.34 GHz; modulation, 0.55 G; receiver gain, 100.

Based on the EPR results, it is evident that the ferryl is reacting with the hydrogen atom of the phenol group. Additional support comes from the Tyr derivatives (**34** and **35**), where the phenolic oxygen has been acetylated or methylated thereby shutting down the possibility of a HAT. Both these derivatives are much slower to react with the ferryl, 26,000 and 16,000 times slower, respectively. The reactivity of these derivatives provides evidence that supports a mechanism in which the fast reaction of the ferryl with **33** is due to the presence of a hydrogen atom of the phenol functional group.

1.2.2.3 Kinetics and Mechanism of $[\text{Fe}^{\text{IV}}(\text{O})(\text{N4Py})]^{2+}$ with Ac-Phe-NHtBu

A former co-worker in the Kodanko Lab identified the product of the reaction between Ac-Phe-NHtBu (**36**) and $[\text{Fe}^{\text{IV}}(\text{O})(\text{N4Py})]^{2+}$ as an orthoquinone (Scheme 1.18).⁸⁹ Ac-Phe-NHtBu caused the decomposition of the ferryl with a pseudo-first order rate constant of $1.4(4) \times 10^{-5} \text{ s}^{-1}$. This rate was not considered significant from a kinetic standpoint since **36** only accelerated the decay of the ferryl by a factor of 2.8. Nevertheless, a comparison to the mechanism of the Tyr substrate was of interest.

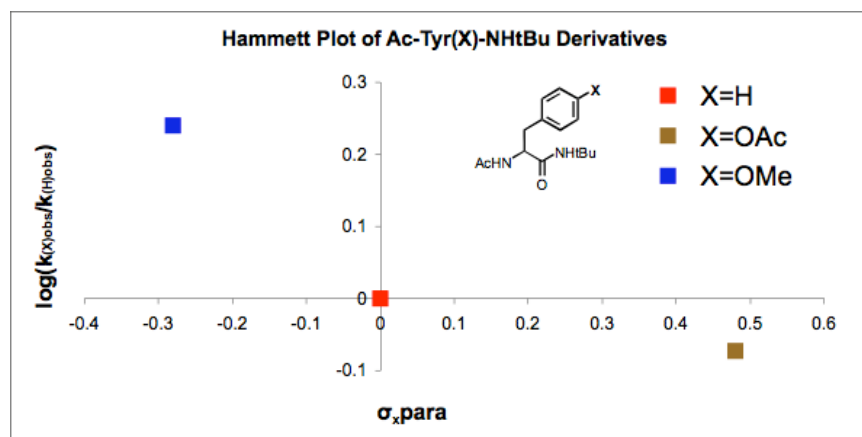
Scheme 1.18 Orthoquinone product from the oxidation of Ac-Phe-NHtBu by $[\text{Fe}^{\text{IV}}(\text{O})(\text{N4Py})]^{2+}$



By creating a Hammett-like plot, using the rates of Ac-Tyr(OMe)-NHtBu, Ac-Tyr(OAc)-NHtBu and Ac-Phe-NHtBu, a trend was noted. It was hypothesized that the reaction between the ferryl and **33** was an electrophilic aromatic substitution (EAS) through which two hydroxyl groups are added to the Phe ring and subsequent oxidation of the dihydroquinone product led to the diquinone that was observed by ^1H NMR.⁹⁶ If the mechanism was proceeding through an EAS, the substrate with the electron-donating group, Ac-Tyr(OMe)-NHtBu, should increase the rate of reaction compared to Ac-Phe-NHtBu. Likewise, the substrate with an electron-withdrawing group should slow down the rate of reaction. While the graph cannot be considered a true Hammett plot, due to the EDG/EWG not being para to the reactive center, a trend can still be noted (Graph 1.8).

As was expected, the rate of decomposition for the substrate with an electron-donating group **35** was faster than **36**, $2.5(2) \times 10^{-5} \text{ s}^{-1}$ and $1.4(4) \times 10^{-5} \text{ s}^{-1}$ respectively. Also, the substrate with an electron-withdrawing group **34** was $1.3(1) \times 10^{-5} \text{ s}^{-1}$. A negative value for ρ (the slope of a line on a Hammett plot) would be obtained from this graph if it were a true Hammett plot where a trendline with a negative slope would be indicative of a positive build up on the ring. This data supports EAS mechanism for the reaction of the ferryl with **36**.

Graph 1.8 Hammett-like plot for the reaction of Ac-Phe-NHtBu, Ac-Tyr(OMe)-NHtBu and Ac-Tyr(OAc)-NHtBu with $[\text{Fe}^{\text{IV}}(\text{O})(\text{N4Py})]^{2+}$ indicating electrophilic aromatic substitution



1.3 Conclusions and Future Directions

We have designed and synthesized amino acid substrates that mimic individual residues of amino acids of polypeptides. The substrates derived from Cys, Tyr, Phe, Gln, Asn and Ile were reacted with the $[\text{Fe}^{\text{IV}}(\text{O})(\text{N4Py})]^{2+}$ and their reactivity have been described. Ac-Cys-NHtBu and Ac-Tyr-NHtBu have been identified to cause the decay of the ferryl faster than any other of the 20 natural amino acid substrates and their mechanisms have been identified as ET-PT and HAT, respectively. Support for EAS with Ac-Phe-NHtBu was also observed through a Hammett-like plot. Reactive substrates can serve as guidelines for the testing of other metal-based oxidants to obtain the most reactive and selective oxidant toward the oxidation of specific amino acid residues.

Tuning of the ligand system or changing the metal center may improve selectivity and reactivity. We have identified that, unlike hydroxyl radical, there is greater selectivity with ferryls in reactions with amino acids. The ferryl $[\text{Fe}^{\text{IV}}(\text{O})(\text{N4Py})]^{2+}$ has shown reactivity that is kinetically significant with only 5 amino acid substrates and based on the results, a difference can clearly be distinguished between the reactivity of ROS vs metal-based oxidants with amino acids.⁸⁸ Future studies involve the alteration of the ligand environment and attachment of ligands to affinity groups as warheads to inactivate proteins. These warheads are the *apo* form of the catalyst (without iron) that will be directed to the target of interest by the affinity group. Presumably, these *apo* inhibitors can strip iron from ferritin to generate complexes that can oxidize amino acid residues and inactivate proteins.

1.4 Experimental

General Considerations: All reagents were purchased from commercial suppliers and used as received unless otherwise stated. ^1H and ^{13}C NMR spectra were recorded on a Varian FT-NMR Mercury-300, 400 or 500 MHz Spectrometer. Mass spectra were recorded on a Waters ZQ2000 single quadrupole mass spectrometer using an electrospray ionization source. IR spectra were recorded on a Nicolet FT-IR spectrophotometer. UV-vis spectra were recorded on a Varian Cary 50 spectrophotometer. $[\text{Fe}^{\text{II}}(\text{N4Py})(\text{CH}_3\text{CN})](\text{ClO}_4)_2$ was synthesized according to the literature procedures.⁹⁷ *N*-Acetyl-amino acids were synthesized from commercially available amino acids using standard literature procedures. All reactions were performed under ambient atmosphere unless otherwise noted.⁸⁸

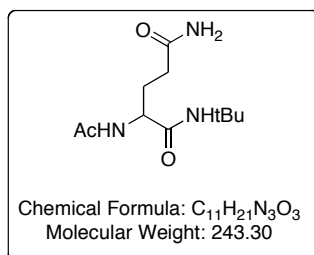
Caution: Perchlorate salts are potentially explosive and should be handled with care.

General Procedure for Kinetic Experiments. Reactions of $[\text{Fe}^{\text{IV}}(\text{O})(\text{N4Py})]^{2+}$ with amino acid substrates were conducted under pseudo-first-order conditions at ambient temperature. Rate constants correspond to an average of three runs. The reactions were monitored using a UV-vis spectrophotometer and solutions were prepared using the following procedure. $[\text{Fe}^{\text{II}}(\text{N4Py})(\text{MeCN})](\text{ClO}_4)_2$ (2 mM) in 3:1 $\text{H}_2\text{O}:\text{MeCN}$ (1.0 mL, 20 μmol) was treated with a solution Oxone[®] in H_2O (100 μL , 20 μmol , 1 equiv). Upon standing for 10 min, the solution color changed from orange-red to green. After 10 min, as judged by maximization of absorbance at 680 nm, the maximum generation of $[\text{Fe}^{\text{IV}}(\text{O})(\text{N4Py})]^{2+}$ species was reached. This solution was treated with 10 equiv of a particular amino acid substrate in 1:3 $\text{H}_2\text{O}:\text{MeCN}$ (900 μL , 200 μmol , 10 equiv). The

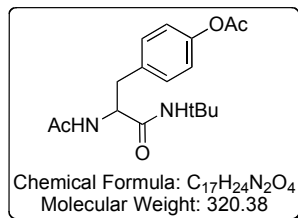
reaction was monitored by UV-vis spectroscopy after mixing for less than 10 sec. The decomposition absorbance traces of the ferryl ($\lambda = 680$ nm) showed first-order decay and fit well to the single exponential equation $[A = \Delta A(1 - e^{-kt}) + A_0]$ for substrates. Studies to determine KIE were conducted in the same manner as above except using the deuterated solvents CD_3CN and D_2O .⁸⁸

Experimental for Stopped-flow Kinetic Studies. Due to the high reactivity of *N*-Ac-Cys-NHtBu and *N*-Ac-Tyr-NHtBu, which cause the decomposition of $[Fe^{IV}(O)(N4Py)]^{2+}$ within a few seconds, a stopped-flow apparatus was employed. The procedure follows that of the general procedure for kinetic experiments, except the two solutions were loaded separately in syringes and were mixed using a KSHU stopped-flow apparatus. A Varian Cary 50 spectrophotometer was used to measure the absorbance at a single wavelength, 680 nm. Studies to determine KIE using stopped-flow conditions were conducted in the same manner as above except using the deuterated solvents CD_3CN and D_2O .⁸⁸

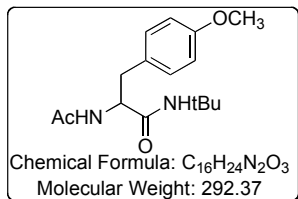
Experimental procedures and characterization data for new compounds:



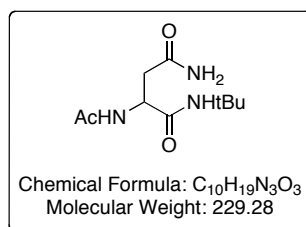
2-Acetamido-*N*-tert-butylpentanediamide. *Tert*-butylamine (2.70 mL, 36.4 mmol) was added to a mixture of EDAC (3.48 g, 18.2 mmol), HOBt (2.46 g, 18.2 mmol), *N*-Ac-Gln-OH (3.42 g, 18.2 mmol), and DMF (34 mL) in a dropwise fashion. After stirring at room temperature under an inert atmosphere for 14 h, the mixture was concentrated *in vacuo*. The resultant gummy liquid was titrated with DCM (35 mL). The solid that formed was filtered and washed with DCM. The white solid was dried in a vacuum desiccator over P₂O₅ with KOH to yield *N*-Ac-Gln-NHtBu, (2.48 g, 56%). m.p. = 204-206 °C; ¹H NMR (DMSO-d₆) δ 7.84 (d, *J* = 8.9 Hz, 1H), 7.48 (s, 1H), 7.26 (s, 1H), 6.72 (s, 1H), 4.17 (m, 1H), 2.03 (m, 2H), 1.82 (s, 3H), 1.64 (m, 2H), 1.23 (s, 9H); ¹³C NMR (DMSO-d₆) δ 178.1, 174.2, 172.5, 53.9, 51.7, 31.3, 27.8, 27.4, 21.8; IR (KBr) 3367, 3312, 3135, 2981, 2957, 2913, 2860, 2821, 1671, 1564, 1542, 1439, 1362, 1290 cm⁻¹; LRMS (ESMS) calc'd for C₁₁H₂₂N₃O₃ (M+H)⁺: 244, found: 244.⁹³



4-(2-acetamido-3-(tert-butylamino)-3-oxopropyl)phenyl acetate. At 0°C under an inert atmosphere, acetic anhydride (350 μ L, 3.59 mmol) was added to a mixture of triethylamine (750 μ L, 5.45 mmol), *N*-Ac-Tyr-NHtBu (500 mg, 1.79 mmol) and DMF (10 mL). The reaction mixture was allowed to warm to room temperature and was stirred for 12 h. The reaction mixture was concentrated *in vacuo* and the residue was dissolved in ethyl acetate (10 mL), washed with NH₄Cl (3 x 10 mL), NaHCO₃ (3 x 10 mL) and brine (3 x 10 mL). The organic layer was concentrated *in vacuo* after drying over anhydrous sodium sulfate. The solid was collected by vacuum filtration after stirred with ether (2 mL). Product was dissolved in CH₂Cl₂ (3 x 10 mL) and concentrated *in vacuo* to yield *N*-Ac-Tyr(OAc)-NHtBu (0.55 g, quantitative). m.p. = 225-227°C; ¹H NMR (DMSO-d₆) δ 8.03 (d, *J* = 8.9 Hz, 1H), 7.52 (s, 1H), 7.24 (d, *J* = 8.0 Hz, 2H), 6.98 (d, *J* = 8.1 Hz, 2H), 4.44 (m, 1H), 2.84 (dd, *J* = 13.8 Hz, 5.7 Hz 1H), 2.73 (dd, *J* = 12.4 Hz, 8.9 Hz 1H), 2.29 (s, 3H), 1.75 (s, 3H), 1.18 (s, 9H); ¹³C NMR (DMSO-d₆) δ 170.4, 169.2, 168.9, 148.9, 135.4, 130.2, 121.2, 54.1, 50.1, 37.6, 28.4, 22.5, 20.9; IR (KBr) 3282, 3074, 2967, 2917, 1765, 1643, 1555, 1508, 1451, 1366, 1216, 1196, 1166, 1018, 911 cm⁻¹; LRMS (ESMS) calc'd for C₁₇H₂₅N₂O₄ (M+H)⁺: 321, found: 321.⁸⁸

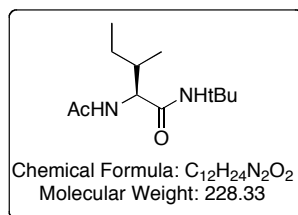


2-acetamido-N-tert-butyl-3-(4-methoxyphenyl)propanamide. Iodomethane (70 μ L, 0.97 mmol) was added to a yellow mixture of K₂CO₃ (220 mg, 1.50 mmol), *N*-Ac-Tyr-NHtBu (220 mg, 790 μ mol) and DMF (40 mL); the yellow color disappeared during the course of the reaction of the reaction and the reaction progress was monitored by TLC. Upon completion, the mixture was concentrated *in vacuo*. The residue was dissolved in CHCl₃ (20 mL) and NH₄Cl (20 mL) and the crude product was extracted with CHCl₃ (4 x 20 mL). The combined organic layer was washed with H₂O (1 x 10 mL) and concentrated *in vacuo* after drying over anhydrous sodium sulfate. The crude product was purified by silica gel flash column chromatography (gradient; 2-5% MeOH:CH₂Cl₂) to yield *N*-Ac-Tyr(OCH₃)-NHtBu (0.24 g, quantitative). m.p.= 225-227°C; ¹H NMR (DMSO-d₆) δ 7.90 (d, *J* = 8.5 Hz, 1H), 7.47 (s, 1H), 7.12 (d, *J* = 8.24 Hz, 2H), 6.79 (d, *J* = 8.2 Hz, 2H), 4.39 (m, 1H), 3.69 (s, 3H), 2.78 (dd, *J* = 14.0 Hz, 5.5 Hz, 1H), 2.64 (dd, *J* = 13.4 Hz, 9.2 Hz, 1H), 1.74 (s, 3H), 1.19 (s, 9H); ¹³C NMR (DMSO-d₆) δ 170.6, 168.8, 157.7, 130.2, 129.8, 113.3, 54.9, 54.3, 50.0, 37.5, 28.4, 22.5; IR (KBr) 3268, 3082, 2965, 2826, 1637, 1559, 1515, 1451, 1391, 1363, 1289, 1252, 1227, 1178, 1041 cm⁻¹; LRMS (ESMS) calc'd for C₁₆H₂₅N₂O₃ (M+H)⁺: 293, found: 293.⁸⁸



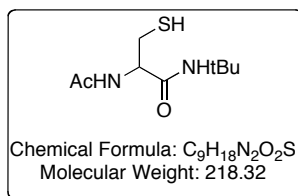
2-Acetamido-*N*¹-*tert*-butylsuccinamide. Isobutylchloroformate (IBCF) (1.0 mL, 7.4 mmol) was added, dropwise over 15 min under an inert atmosphere at -20 to -18 °C, to a mixture of *N*-Fmoc-Asn(Trt)-OH (4.00 g, 6.69 mmol), triethylamine (1.0 mL, 7.4 mmol) and THF (80 mL). After stirring 15 min, *tert*-butylamine (0.60 mL, 7.4 mmol) was added to the mixture over 10 min. Upon completion of the reaction, as judged by TLC analysis, 2.3 h, the reaction mixture was concentrated *in vacuo*. The crude product was purified by silica gel flash column chromatography (EtOAc:Hexane) to yield *N*-Fmoc-Asn(Trt)-NHtBu (4.24 g, 96%). Under an inert atmosphere at rt, *N*-Fmoc-Asn(Trt)-NHtBu (1.5 g, 2.3 mmol) was dissolved in piperidine (20 mL) and the reaction was monitored by TLC analysis until complete consumption of the starting material was observed. The reaction mixture was concentrated *in vacuo* and the residue was dissolved in DCM (4 mL). Triethylamine (1.60 mL, 11.5 mmol) and acetic anhydride (0.22 mL, 2.3 mmol) were added consecutively and upon complete consumption of starting material, as judged by TLC analysis, the reaction mixture was concentrated *in vacuo*. The crude product was purified by silica gel flash column chromatography (EtOAc:Hexane) to yield *N*-Ac-Asn(Trt)-NHtBu, (821 mg, 76% over 2 steps). *N*-Ac-Asn(Trt)-NHtBu (300 mg, 0.637 mmol) was dissolved in 95:5 TFA:H₂O (4 mL) and stirred for 2.5 h under an inert atmosphere. H₂O was added (2 mL) and the precipitate was filtered. The filtrate was concentrated *in vacuo*, ether was added to the concentrate and the resulting white

precipitate, *N*-Ac-Asn-NHtBu, was collected by filtration. The product was dried *in vacuo* (98 mg, 68%). m.p. = decomposition; ^1H NMR (D_2O) δ 4.41 (t, $J = 7.3$ Hz, 2H), 2.59 (dd, $J = 15.4, 6.5$ Hz, 1H), 2.51 (dd, $J = 14.7, 7.3$ Hz, 1H), 1.89 (s, 3H), 1.85 (s, 9H); ^{13}C NMR (D_2O) δ 174.8, 174.2, 171.6, 51.8, 51.6, 37.2, 27.9, 21.9; IR (KBr) 3285, 2916, 2848, 1656, 1551, 1366 cm^{-1} ; LRMS (ESMS) calc'd for $\text{C}_{10}\text{H}_{19}\text{N}_3\text{O}_3\text{Na}$ ($\text{M}+\text{Na}$) $^+$: 252, found: 252.⁹³



2-Acetamido-*N*-tert-butyl-3-methylpentanamide. HBTU (3.21 g, 8.49 mmol) was added to *N*-Fmoc-Ile-OH (3.00 g, 8.49 mmol) and were allowed to react for 15 min in THF (300 mL) under an inert atmosphere at -20 to -30 °C. *Tert*-butylamine (0.71 mL, 9.35 mmol) was added dropwise over 10 min and the reaction mixture was stirred for 24 h. The mixture was concentrated to 40 mL *in vacuo* and the white precipitate was filtered after the addition of EtOAc (100 mL). The filtrate was washed with a saturated aqueous NH₄Cl (3 × 50 mL), 5% NaHCO₃ (2 × 50 mL) and saturated NaCl solution (1 × 10 mL). The organic layer was dried over anhydrous sodium sulfate, concentrated *in vacuo* and the resulting crude product was purified by silica gel flash column chromatography (EtOAc:Hexane). The product was recrystallized from hot EtOAc/Hexane to yield *N*-Fmoc-Ile-NHtBu (2.04 g, 59%). *N*-Fmoc-Ile-NHtBu (0.33 g, 0.81 mmol) was dissolved in 20% piperidine/DCM (16 mL) and the reaction was stirred until complete consumption of the starting material was observed by TLC. The reaction mixture was concentrated *in vacuo* and CH₂Cl₂ (6 mL) was added. Acetic anhydride was added (0.36 mL, 3.2 mmol) and the reaction was stirred until complete consumption of the starting material was observed by TLC. The reaction mixture was concentrated *in vacuo* and the crude product was purified by silica gel flash column chromatography (Acetone:CH₂Cl₂) and recrystallized from hot EtOAc/Hexane to yield, *N*-Ac-Ile-NHtBu, (187 mg, 34% over 2 steps) m.p. = 202-203 °C; ¹H NMR (CD₃OD) δ 7.55 (s, 1H), 4.06 (d, *J* = 8.9, 1H), 1.97 (s, 3H), 1.75 (m, 1H), 1.55 (m, 1H), 1.27 (s, 9H), 1.08 (m, 1H), 0.92 (m, 6H); IR (KBr)

3275, 3078, 2963, 2874, 1727, 1644, 1557, 1454, 1363, 1267, 1225 cm^{-1} ; ^{13}C NMR (D_2O) δ 171.9, 171.8, 59.7, 59.6, 38.1, 28.8, 26.0, 22.4, 15.8, 11.3; LRMS (ESMS) calc'd for $\text{C}_{12}\text{H}_{25}\text{N}_2\text{O}_2$ ($\text{M}+\text{H}$) $^+$: 229, found: 229.⁹³



2-Acetamido-*N*-*tert*-butyl-3-mercaptopropanamide. Isobutylchloroformate (0.55 mL, 4.22 mmol) was added dropwise over 5 min, under an inert atmosphere while the temperature was maintained between -18 and -20°C , to a mixture of triethylamine (0.60 mL, 4.22 mmol), *N*-Ac-Cys(Trt)-OH (1.55 g, 3.83 mmol) and THF (100 mL). The reaction mixture was allowed to warm to room temperature after the dropwise addition of *tert*-butylamine (0.32 mL, 4.22 mmol), over 10 min and the mixture was stirred for 6 h. The mixture was concentrated *in vacuo* and the crude product was purified by silica gel flash column chromatography (EtOAc:Hexane) to yield a white solid, *N*-Ac-Cys(Trt)-NHtBu, (0.640 g, 38%). ^1H NMR (CDCl_3) δ 7.32 (m, 15 H), 6.90 (brd, $J = 6.4$ Hz, 1H), 6.88 (s, 1H), 3.93 (m, 1H), 2.68 (dd, $J = 12.9, 7.3$ Hz, 1H), 2.46 (dd, $J = 12.9, 6.4$ Hz, 1H), 1.89 (s, 3H), 1.28 (s, 9H).

A mixture of *N*-Ac-Cys(Trt)-NHtBu (0.400 g, 0.870 mmol), TFA (2.5 mL), and CH_2Cl_2 (2.5 mL) was stirred under an inert atmosphere for 1 h. Triethylsilane (0.21 mL, 1.30 mmol) was added and the mixture was allowed to stir at rt for 3 h. The reaction mixture was concentrated *in vacuo* and the residue was titrated with CH_2Cl_2 /Hexane to yield a crude white solid that was purified by silica gel flash column chromatography (EtOAc:Hexane) to yield the white solid *N*-Ac-Cys-NHtBu (0.120 g, 63%). m.p. = 172 – 174°C ; ^1H NMR (CD_3OD) δ 4.35 (m, 1H), 2.75 (m, 2H), 1.98 (s, 3H), 1.32 (s, 9H); ^{13}C NMR (CD_3OD) δ 162.1, 161.1, 48.4, 43.3, 19.8, 18.0, 13.4; IR (thin film) 3267, 3093,

2964, 1631, 1569, 1447, 1386, 1363, 1259, 1225; cm^{-1} ; LRMS (ESMS) calc'd for $\text{C}_9\text{H}_{19}\text{N}_2\text{O}_2\text{S} (\text{M}+\text{H})^+$: 219, found: 219.⁹³

1.5 References

- (1) Garrison, W. M., *Chem. Rev.* **1987**, *87*, 381-98.
- (2) Stadtman, E. R., *Annu. Rev. Biochem.* **1993**, *62*, 797-821.
- (3) Armstrong, R. C.; Swallow, A. J., *Radiat. Res.* **1969**, *40*, 563-79.
- (4) Stadtman, E. R., *Free Radic. Biol. Med.* **1990**, *9*, 315-325.
- (5) Stadtman, E. R.; Levine, R., *Amino Acids* **2003**, *25*, 207-218.
- (6) Berlett, B. S.; Stadtman, E. R., *J. Biol. Chem.* **1997**, *272*, 20313-20316.
- (7) Matés, J.; Pérez-Gómez, C.; Núñez de Castro, I., *Clin. Biochem.* **1999**, *32*, 595-603.
- (8) Kaizer, J.; Klinker, E. J.; Oh, N. Y.; Rohde, J.-U.; Song, W. J.; Stubna, A.; Kim, J.; Münck, E.; Nam, W.; Que, L., Jr., *J. Am. Chem. Soc.* **2004**, *126*, 472-473.
- (9) Hoffart, L. M.; Barr, E. W.; Guyer, R. B.; Bollinger, J. M., Jr.; Krebs, C., *Proc. Natl. Acad. Sci. U. S. A.* **2006**, *103*, 14738-14743.
- (10) De Visser, S. P., *J. Am. Chem. Soc.* **2006**, *128*, 9813-9824.
- (11) Behan, R. K.; Hoffart, L. M.; Stone, K. L.; Krebs, C.; Green, M. T., *J. Am. Chem. Soc.* **2006**, *128*, 11471-11474.
- (12) Denisov Ilia, G.; Makris Thomas, M.; Sligar Stephen, G.; Schlichting, I., *Chem. Rev.* **2005**, *105*, 2253.
- (13) Costas, M.; Mehn, M. P.; Jensen, M. P.; Que, L., Jr., *Chem. Rev.* **2004**, *104*, 939-986.
- (14) Garrison, W. M.; Jayko, M. E.; Bennett, W., *Radiat. Res.* **1962**, *16*, 483.
- (15) Davies, M. J., *Biochim. Biophys. Acta* **2005**, *1703*, 93.

- (16) Starke-Reed, P. E.; Oliver, C. N., *Arch. Biochem. Biophys.* **1989**, *275*, 559-67.
- (17) Agarwal, S.; Sohal, R. S., *Biochem. Biophys. Res. Commun.* **1993**, *194*, 1203-6.
- (18) Smith, M. A.; Harris, P. L. R.; Sayre, L. M.; Perry, G., *Proc. Natl. Acad. Sci. U. S. A.* **1997**, *94*, 9866-9868.
- (19) Smith, C. D.; Carney, J. M.; Starke-Reed, P. E.; Oliver, C. N.; Stadtman, E. R.; Floyd, R. A.; Markesbery, W. R., *Proc. Natl. Acad. Sci. U. S. A.* **1991**, *88*, 10540-3.
- (20) Levine, R. L., *Free Radic. Biol. Med.* **2002**, *32*, 790-796.
- (21) Fenton, H. J. H., *J. Chem. Soc., Trans.* **1894**, *65*, 899.
- (22) Kehrer, J. P., *Toxicology* **2000**, *149*, 43-50.
- (23) Koppenol, W. H., *Redox Rep.* **2001**, *6*, 229-234.
- (24) Davies, M. J., *Biochem. Biophys. Res. Commun.* **2003**, *305*, 761-770.
- (25) Shechter, Y.; Burstein, Y.; Patchornik, A., *Biochemistry* **1975**, *14*, 4497-4503.
- (26) Schuessler, H.; Schilling, K., *Int. J. Radiat. Biol.* **1984**, *45*, 267.
- (27) Swallow, A. J., *Radiation Chemistry of Organic Compounds*. 1960.
- (28) Schuessler, H.; Schilling, K., *Int. J. Radiat. Biol. Relat. Stud. Phys. Chem. Med.* **1984**, *45*, 267-81.
- (29) Amici, A.; Levine, R. L.; Tsai, L.; Stadtman, E. R., *J. Biol. Chem.* **1989**, *264*, 3341-6.

- (30) Requena, J. R.; Chao, C.-C.; Levine, R. L.; Stadtman, E. R., *Proc. Natl. Acad. Sci. U. S. A.* **2001**, *98*, 69-74.
- (31) Uchida, K.; Kato, Y.; Kawakishi, S., *Biochem. Biophys. Res. Commun.* **1990**, *169*, 265-71.
- (32) Liebster, J.; Kopoldova, J., *Radiat. Res.* **1966**, *27*, 162-73.
- (33) Joshi, A.; Rustgi, S.; Moss, H.; Riesz, P., *Int. J. Radiat. Biol. Relat. Stud. Phys. Chem. Med.* **1978**, *33*, 205-29.
- (34) Garrison, W. M.; Kland-English, M. J.; Sokol, H. A.; Jayko, M. E., *J. Phys. Chem.* **1970**, *74*, 4506-9.
- (35) Davies, K. J. A.; Delsignore, M. E.; Lin, S. W., *J. Biol. Chem.* **1987**, *262*, 9902-7.
- (36) Sokol, H. A.; Bennett-Corniea, W.; Garrison, W. M., *J. Am. Chem. Soc.* **1965**, *87*, 1391-2.
- (37) Giulivi, C.; Davies, K. J. A., *J. Biol. Chem.* **1993**, *268*, 8752-9.
- (38) Uchida, K.; Kawakishi, S., *FEBS Lett.* **1993**, *332*, 208-10.
- (39) Taborsky, G.; McCollum, K., *Biochemistry* **1973**, *12*, 1341-8.
- (40) Jay, D. G., *J. Biol. Chem.* **1984**, *259*, 15572-8.
- (41) Jue, R. A.; Doolittle, R. F., *Biochemistry* **1985**, *24*, 162-70.
- (42) Zhong, M.; Lin, L.; Kallenbach, N. R., *Proc. Natl. Acad. Sci. U. S. A.* **1995**, *92*, 2111.
- (43) Heilek, G. M.; Marusak, R.; Meares, C. F.; Noller, H. F., *Proc. Natl. Acad. Sci. U. S. A.* **1995**, *92*, 1113-1116.

- (44) Zaychikov, E.; Schickor, P.; Denissova, L.; Heumann, H., *Methods Mol. Biol.* **2001**, *148*, 49-61.
- (45) Hoyer, D.; Cho, H.; Schultz, P. G., *J. Am. Chem. Soc.* **1990**, *112*, 3249-50.
- (46) DeRosa, M. C.; Crutchley, R. J., *Coord. Chem. Rev.* **2002**, *233-234*, 351-371.
- (47) Lee, J.; Udugamasooriya, D. G.; Lim, H.; Kodadek, T., *Nat. Chem. Biol.* **2010**, *6*, 258-260.
- (48) Vrouenraets, M. B.; Visser, G. W. M.; Snow, G. B., *Anticancer Res.* **2003**, *23*, 505-522.
- (49) de Visser, S. P., *Angew. Chem., Int. Ed.* **2006**, *45*, 1790-1793.
- (50) Nam, W., *Acc. Chem. Res.* **2007**, *40*, 522-531.
- (51) Price, J. C.; Barr, E. W.; Glass, T. E.; Krebs, C.; Bollinger, J. M., *J. Am. Chem. Soc.* **2003**, *125*, 13008-13009.
- (52) Ryle, M. J.; Liu, A.; Muthukumaran, R. B.; Ho, R. Y. N.; Koehntop, K. D.; McCracken, J.; Que, L.; Hausinger, R. P., *Biochemistry* **2003**, *42*, 1854-1862.
- (53) Markris, T. M.; von Koenig, K.; Schlichting, I.; Sligar, S. G., *J. Inorg. Biochem.* **2006**, *100*, 507-518.
- (54) Gonzalez, F. J.; Gelboin, H. V., *Drug Metab. Rev.* **1994**, *26*, 165-183.
- (55) Murray, G. I., *Am. J. Pathol.* **2000**, *192*, 419-426.
- (56) Mueller, J., *Iron Catal. Org. Chem.* **2008**, 29-47.
- (57) Costas, M.; Chen, K.; Que, L., *Coord. Chem. Rev.* **2000**, *200-202*, 517-544.

- (58) Oldenburg, P. D.; Mas-Balleste, R.; Que, L., Jr., *Prepr. - Am. Chem. Soc., Div. Pet. Chem.* **2007**, *52*, 175-178.
- (59) Tanase, S.; Bouwman, E., *Adv. Inorg. Chem.* **2006**, *58*, 29-75.
- (60) Sastri, C. V.; Oh, K.; Lee, Y. J.; Seo, M. S.; Shin, W.; Nam, W., *Angew. Chem., Int. Ed.* **2006**, *45*, 3992-3995.
- (61) Price, J. C.; Barr, E. W.; Tirupati, B.; Bollinger, J. M.; Krebs, C., *Biochemistry* **2003**, *42*, 7497-7508.
- (62) van der Ploeg, J. R.; Weiss, M. A.; Saller, E.; Nashimoto, H.; Saito, N.; Kertesz, M.; Leisinger, T., **1996**, *J. Bacteriol.*
- (63) Price, J. C.; Barr, E. W.; Hoffart, L. M.; Krebs, C.; Bollinger, J. M., *Biochemistry* **2005**, *44*, 8138-8147.
- (64) Hanauske-Abel, H. M.; Günzler, V., *J. Theor. Biol.* **1982**, *94*, 421-455.
- (65) Abu-Omar, M. M.; Loaiza, A.; Hontzeas, N., *Chem. Rev.* **2005**, *105*, 2227-2252.
- (66) Proshlyakov, D. A.; Henshaw, T. F.; Monterosso, G. R.; Ryle, M. J.; Hausinger, R. P., *J. Am. Chem. Soc.* **2004**, *126*, 1022-1023.
- (67) Riggs-Gelasco, P. J.; Price, J. C.; Guyer, R. B.; Brehm, J. H.; Barr, E. W.; Bollinger, J. M.; Krebs, C., *J. Am. Chem. Soc.* **2004**, *126*, 8108-8109.
- (68) Rohde, J.-U.; In, J.-H.; Lim, M. H.; Brennessel, W. W.; Bukowski, M. R.; Stubna, A.; Münck, E.; Nam, W.; Que, L., Jr., *Science* **2003**, *299*, 1037-1039.
- (69) Sastri, C. V.; Seo, M. S.; Park, M. J.; Kim, K. M.; Nam, W., *Chem. Commun.* **2005**, 1405-1407.

- (70) Lim, M. H.; Rohde, J. U.; Stubna, A.; Bukowski, M. R.; Costas, M.; Ho, R. Y. N.; Munck, E.; Nam, W.; Que, L., *Proc. Natl. Acad. Sci. U. S. A.* **2003**, *100*, 3665-3670.
- (71) Kaizer, J.; Costas, M.; Que, L., Jr., *Angew. Chem., Int. Ed.* **2003**, *42*, 3671-3673.
- (72) Grapperhaus, C. A.; Mienert, B.; Bill, E.; Weyhermueller, T.; Wieghardt, K., *Inorg. Chem.* **2000**, *39*, 5306-5317.
- (73) Penner-Hahn, J. E., *J. Am. Chem. Soc.* **1986**, *108*, 7819.
- (74) Wolter, T., *J. Inorg. Biochem.* **2000**, *78*, 117.
- (75) Groves, J. T.; Nemo, T. E.; Myers, R. S., *J. Am. Chem. Soc.* **1979**, *101*, 1032-1033.
- (76) Nam, W., *Acc. Chem. Res.* **2007**, *40*, 522-531.
- (77) Bautz, J.; Bukowski, M. R.; Kerscher, M.; Stubna, A.; Comba, P.; Lienke, A.; Munck, E.; Que, L., Jr., *Angew. Chem., Int. Ed.* **2006**, *45*, 5681-5684.
- (78) Wang, D.; Zhang, M.; Buñahmann, P.; Que, L., *J. Am. Chem. Soc.* **2010**, *132*, 7638-7644.
- (79) de Visser, S. P.; Oh, K.; Han, A.-R.; Nam, W., *Inorg. Chem.* **2007**, *46*, 4632-4641.
- (80) Kim, S. O.; Sastri, C. V.; Seo, M. S.; Kim, J.; Nam, W., *J. Am. Chem. Soc.* **2005**, *127*, 4178-4179.
- (81) Nehru, K.; Seo, M. S.; Kim, J.; Nam, W., *Inorg. Chem.* **2007**, *46*, 293-298.
- (82) Oh, N. Y.; Suh, Y.; Park, M. J.; Seo, M. S.; Kim, J.; Nam, W., *Angew. Chem., Int. Ed.* **2005**, *44*, 4235-4239.

- (83) Balland, V.; Charlot, M. F.; Banse, F.; Girerd, J. J.; Mattioli, T.; Bill, E.; Bartoli, J. F.; Battioni, P.; Mansuy, D., *Eur. J. Inorg. Chem.* **2004**, *2004*, 301-308.
- (84) Petrat, F.; De Groot, H.; Sustmann, R.; Rauen, U., *Biol. Chem.* **2002**, *383*, 489-502.
- (85) Esposito, B. P.; Epsztejn, S.; Breuer, W.; Cabantchik, Z. I., *Anal. Biochem.* **2002**, *304*, 1-18.
- (86) Jackson, C.; Kodanko, J. J., *Metallomics* **2010**, *2*, 407-411.
- (87) Ekkati, A. R.; Campanali, A. A.; Abouelatta, A. I.; Shamoun, M.; Kalapugama, S.; Kelley, M.; Kodanko, J. J., *Amino Acids* **2010**, *38*, 747-751.
- (88) Abouelatta, A. I.; Campanali, A. A.; Ekkati, A. R.; Shamoun, M.; Kalapugama, S.; Kodanko, J. J., *Inorg. Chem.* **2009**, *48*, 7729-7739.
- (89) Ekkati, A. R.; Kodanko, J. J., *J. Am. Chem. Soc.* **2007**, *129*, 12390-12391.
- (90) Reddy, A. V.; Ravindranath, B., *Synth. Commun.* **1992**, *22*, 257-64.
- (91) Ray, S.; Drew, M. G. B.; Das, A. K.; Banerjee, A., *Tetrahedron* **2006**, *62*, 7274-7283.
- (92) Jones, J., *Amino Acid and Peptide Synthesis*. Oxford University Press: New York, 2002.
- (93) Ekkati, A. R.; Campanali, A. A.; Abouelatta, A. I.; Shamoun, M.; Kalapugama, S.; Kelley, M.; Kodanko, J. J., *Amino Acids* **2010**, *38*, 747-751.
- (94) Swayze, E. E.; Townsend, L. B., *J. Org. Chem.* **1995**, *60*, 6309-17.
- (95) Ramasamy, K.; Kini, G. D.; Robins, R. K.; Revankar, G. R., *Nucleos. Nucleot.* **1987**, *6*, 901-11.
- (96) Ekkati, A. R.

(97) Roelfes, G.; Lubben, M.; W. Leppard, S.; Schudde, E. P.; Hermant, R. M.; Hage, R.; Wilkinson, E. C.; Que, L., Jr.; Feringa, B. L., *J. Mol. Catal. A: Chem.* **1997**, *117*, 223-227.

CHAPTER 2

OXIDATION OF GLUTATHIONE BY METAL-BASED OXIDANTS

2.1 Introduction

Glutathione (GSH) is a ubiquitous tripeptide that is involved in various cellular functions, including cell proliferation. It is important in the detoxification of ROS such as hydroxyl radical and works with other antioxidants to protect cells from oxidative stress.¹ While the role of GSH with ROS is well understood, reactions with metal-based oxidants have received less attention.² Therefore the reaction of GSH with metal-based oxidants is worth investigating, because GSH is known to detoxify ferryls such as ferryl myoglobin in cells.³

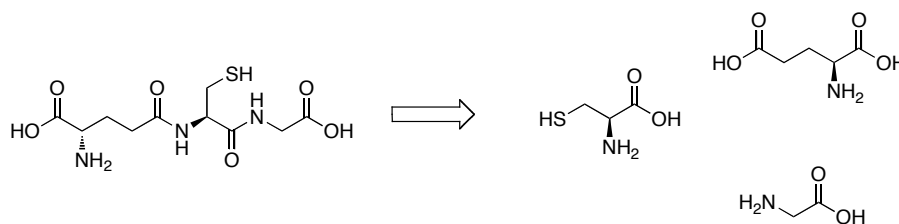
The work presented in this chapter is an extension of a result observed in the experiments from Chapter 1. Upon mixing of Ac-Cys-NHtBu with the ferryl $[\text{Fe}^{\text{IV}}(\text{O})(\text{N4Py})]^{2+}$ in 1:1 $\text{H}_2\text{O}/\text{MeCN}$, rapid decomposition of the ferryl at $\lambda_{\text{max}} = 680 \text{ nm}$ was observed by stopped-flow UV-vis spectroscopy and a disulfide product was identified.⁴ When the reaction was monitored, after the initial decomposition at 680 nm, a new green species developed that displayed a band at $\lambda_{\text{max}} = 658 \text{ nm}$. In order to identify the species responsible for this new absorption band, experiments were conducted with Ac-Cys-NHtBu, however only trace amounts of the green species were observed and its formation suffered from low reproducibility. We decided to choose another thiol based on the hypothesis that an $\text{S} \rightarrow \text{Fe}$ ligand-to-metal-charge-transfer (LMCT) was responsible for $\lambda_{\text{max}} = 658 \text{ nm}$, based on literature.⁵ Glutathione was chosen as a likely candidate to substitute for the cysteine derived substrate. Besides containing a thiol group, glutathione

was chosen because of its immense importance in biology, which will be further explained in the following sections.

2.1.1 Glutathione: Importance in Biology

Glutathione (L- γ -glutamyl-L-cysteine-glycine, GSH) is a multifunctional tripeptide composed of glutamate, cysteine and glycine (Scheme 2.1). It is responsible for modulation of various cellular functions, including but not limited to cell proliferation, storage of cysteine, detoxification (as an antioxidant), maintaining cell thiol status and regulation of nitric oxide homeostasis.^{1, 6-9} It is present in all mammalian tissues in concentrations up to 10 mM with the highest concentrations present in the liver. Approximately 90% of total GSH is located in the cytosol and 10% in the mitochondria. While these two areas contain a higher abundance of GSH, a small percentage can be found in the endoplasmic reticulum.¹ GSH typically exists in a 100 to 1 ratio with its oxidized form (GSSG), however, during oxidative stress, the ratio of GSH to GSSG can decrease significantly (4 to 1).¹⁰ As mentioned above, GSH is important in various cellular functions, several of which are described below.

Scheme 2.1 Glutathione is composed of the amino acids glutamate, cysteine and glycine



GSH is considered essential for mammalian cell survival¹¹ and is known to play an important role in cell proliferation and cell death, however its comprehensive role in nucleated cells remains unclear.¹² There have been conflicting reports in the past two decades concerning the concentration of GSH in the nucleus and its regulation is not

understood.¹³⁻¹⁷ These results are most likely due to a limit of current methodologies to measure GSH in the nucleus because most studies involve confluent cells even though the nucleus dramatically changes during each phase of the cell cycle. Cells in preparation of cellular division have a higher GSH content in the nucleus. While it has been shown that GSH concentrations increase prior to proliferation, the exact mechanism for this increase is under debate.¹² Recently, new methods have become available to determine redox status of the nucleus such as redox blot,¹⁸ however, there are no present methods for the determination of nuclear GSSG. Further developments in this field are needed to understand the compartmentalization of GSH and its role in cell proliferation.

While the mechanism of GSH transport into the nucleus is unresolved, passive diffusion through nuclear pores from the cytosol has been invoked.¹⁹ The redox status of the nucleus plays an important role in various functions. Nuclear GSH protects DNA from ionizing- and oxidant-induced damage²⁰ and maintains a reducing environment conducive to cell cycle progression, specifically gene transcription.²¹ GSH is also involved in DNA synthesis; it is a hydrogen donor in the reduction of ribonucleotides to produce deoxyribonucleotides. This reduction is catalyzed by the enzyme ribonucleotide reductase.^{22, 23} As was mentioned previously, exact determination of the GSH to GSSG ratio has not been achieved due to the changing levels during the cell cycle.¹⁰ A correlation between levels of GSH in the nucleus and the anti-apoptotic protein Bcl-2 has been realized, but is not fully understood. It is thought that Bcl-2 maintains high nuclear levels of GSH and in doing so evades apoptosis.¹⁷

While the redox status of the nucleus is still under investigation, overall GSH maintains intracellular redox and thiol homeostasis and the mechanisms are known. For

example, thiol-transferase catalyzes a reversible thiol-disulfide exchange between oxidized proteins and GSH. The redox status (GSH to GSSG ratio) of the cell determines the equilibrium direction (Scheme 2.2).^{1, 24} In order to limit the reverse of this reaction, where proteins contain mixed disulfides, the GSSG concentration is generally extremely low. This equilibrium regulates a variety of cellular processes including, but not limited to, signal transduction, enzyme activity, gene expression and transport activity.¹ An important example where signal transduction plays a key role in the fate of the cell is apoptosis.¹⁰

Scheme 2.2 Thiol-transferase reaction



Redox status (GSH to GSSG ratio) change within the cell is an important signaling mechanism. A shift to favor GSSG can signal the onset of apoptosis, or programmed cell death. GSH homeostasis is maintained by three known mechanisms, reduction of GSSG by glutathione reductase, *de novo* synthesis and uptake of GSH across the plasma membrane from exogenous sources.^{10, 25} *De novo* synthesis is catalyzed by GSH synthetase and glutamate cysteine ligase (GCL). It occurs in the cytosolic compartment in two steps that are ATP dependent (Figure 2.1), with the availability of cysteine, from the breakdown of extracellular GSH by GGT¹⁰ or the cystathionine pathway,²⁶ being rate limiting. Intracellular GSH is then transported to various compartments of the cell: the nucleus, the endoplasmic reticulum (ER) and the mitochondria. This is carried out by the help of transporters such as the carriers oxoglutarate and dicarboxylate which are located on the inner mitochondrial membrane and

aid in the transit of GSH into the mitochondria. Since synthesis takes place in the cytoplasm and not the mitochondria, matrix homeostasis is dependant on GSH transit.²⁷

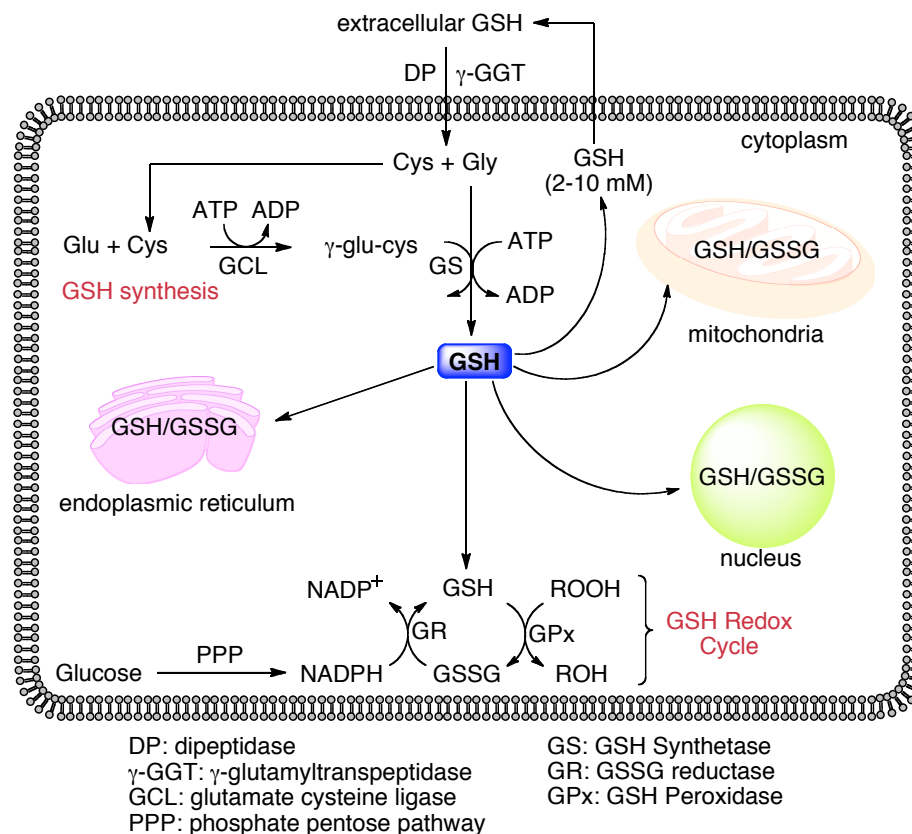


Figure 2.1 Synthesis and redox cycling in GSH homeostasis

Each of these compartments constitutes individual redox pools that are different from the cytoplasm. The mitochondria displays concentrations of GSH ranging from 5 to 10 mM and this GSH pool is separated from the cytosolic pool, metabolically, with respect to GSH turnover, the rate of GSH synthesis and susceptibility to oxidative stress.¹⁶ As was mentioned previously, GSH synthesis does not take place in the mitochondria because it does not contain GSH synthetase or glutamate cysteine ligase.

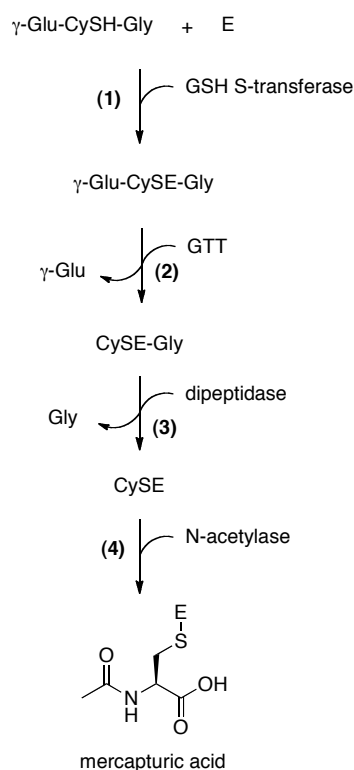
Therefore homeostasis of GSH is dependent on the transport of GSH from the cytoplasm compartment to the mitochondrial compartment¹⁰ via previously mentioned carriers.²⁷

The endoplasmic reticulum usually exhibits the same concentration of GSH as the cytoplasm (2 to 10 mM), however its redox equilibrium differs in that oxidized glutathione is favored and the majority of GSH is in the form of protein mixed disulfides.²⁸ In the endoplasmic reticulum, GSH maintains the catalytic function of oxidoreductase and reacts with ROS generated within the ER.^{29, 30} Changes in the redox state can lead to disruptions in the function of the endoplasmic reticulum, causing the activation of unfolding response and even trigger cell apoptosis.^{10, 31}

One of GSH's most significant roles is as an antioxidant that combats oxidative stress from ROS. In the previous chapter (1.1.1) generation of ROS was covered, especially important concerning GSH are those generated by the mitochondrial electron transport chain (M-ETC), including hydrogen peroxide (H_2O_2) and superoxide ($O_2^{\bullet-}$), which result in lipid peroxidation. The M-ETC represents the majority of oxygen consumption in cells, approximately 85% to 90%.³² In order to prevent damage to the cell, GSH reduces hydrogen peroxide with the help of GSH peroxidase resulting in the reversible formation of GSSG. Oxidized GSSG may be converted back to GSH by the action of glutathione reductase at the expense of NADPH. In the mitochondria, this redox cycle is of particular importance due to the fact that no catalase is present. In the peroxisome, however, catalase can aid in the detoxification of hydrogen peroxide.^{32, 33} Severe oxidative stress in the cell can lead to the depletion of GSH by active transport of GSSG out of the cell in an attempt to maintain redox equilibrium.²⁴ Not only does GSH detoxify ROS by antioxidant action, it also detoxifies xenobiotics and their metabolites.

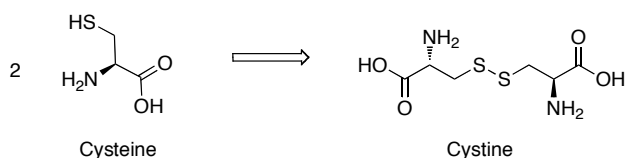
GSH detoxifies electrophiles such as xenobiotics and their metabolites by forming a conjugate with these compounds that irreversibly consumes GSH. This may either happen with the help of the enzyme glutathione S-transferase (GSH S-transferase) or spontaneously **(1)** (Scheme 2.3).³⁴ Once conjoined, the conjugate is typically released from the cell where the extracellular enzyme γ -glutamyltranspeptidase (GGT) catalyzes the transfer of the γ -glutamyl moiety **(2)**, leaving the conjugated cysteinyl-glycine. A cysteine-conjugate is formed by cleavage of the cysteinyl-glycine bond by dipeptidase **(3)**, an enzyme that cleaves dipeptides into their constituent amino acids, which then becomes enzymatically acetylated by N-acetylase **(4)** to form a mercapturic acid.¹

Scheme 2.3 Mercapturic pathway: detoxification of electrophiles (E) by GSH



GSH is a storage and transport vehicle for the extremely reactive amino acid cysteine. Due to the fact that cysteine may generate ROS during its auto-oxidation to cystine (Scheme 2.4) in extracellular regions, it is stored in the form of GSH until it is needed in biological processes. When required, GSH can be broken down into its constituent amino acids for incorporation into proteins.³⁴ The process by which cysteine is made available through the breakdown of GSH is known as the γ -glutamyl cycle. Once released from the cell, the γ -glutamyl moiety is transferred by GGT to produce cysteinyl-glycine and γ -glutamyl amino acid. From there γ -glutamyl amino acid may be directed back into the cell where it is converted to glutamate for reincorporation into GSH.¹

Scheme 2.4 Structure of Cystine



GSH has been shown to protect cells from apoptosis induced by damage from ferryl myoglobin. Ferryl myoglobin is known to oxidize biomolecules such as membrane lipids through single electron-transfer mechanisms³ and the mechanism is thought to involve a tyrosine residue, although the exact mechanism is not fully understood.³⁵ In these studies, ferryl myoglobin generation was shown to correlate with the induction of apoptosis. In cells that had been depleted of GSH, this apoptosis was enhanced suggesting a role for cell protection by GSH when ferryl myoglobin is formed.³

As can be noted from this section, GSH plays a vital role in the survival of mammalian cells. It contributes to many aspects of cell growth, function and death. The

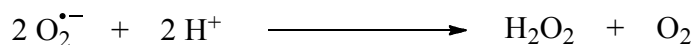
following sections will discuss two important enzymes that are scavengers of ROS, superoxide dismutase and catalase. These two enzymes work in conjunction with GSH as antioxidants to prevent oxidative damage.

2.1.2 Superoxide Dismutase and Catalase: ROS Scavengers

ROS are necessary for many biological processes, such as signal transduction. They are also involved in enzyme regulation, activating cytokine production, elimination of pathogens and cell growth.³⁶ However, there exists a delicate balance between their generation and their destruction by scavengers such as GSH, glutathione peroxidase (GPX), glutaredoxin, thioredoxin, peroxiredoxins, superoxide dismutase (SOD) and catalase. Any disruption in this homeostasis, by either over-production of ROS or by reduction in the quantity of antioxidant enzymes, leads to oxidative stress.^{36, 37} This section will focus on SOD and catalase activity in preventing oxidative stress.

The antioxidant enzyme superoxide dismutase catalyzes the dismutation of superoxide to dioxygen and hydrogen peroxide (Scheme 2.5). While hydrogen peroxide is still an ROS, it is less reactive than superoxide. Hydrogen peroxide can diffuse and be destroyed by catalase or glutathione peroxidase.^{38, 39} There are three different forms of superoxide dismutase, cytosolic, mitochondrial and extracellular.⁴⁰ Cytosolic SOD (Cu/Zn-SOD) contains two identical subunits (32 kDa), each containing a copper and zinc metal cluster that is bridged by a His residue.⁴⁰⁻⁴³ Mitochondrial SOD (Mn-SOD) is a 96 kDa homotetramer that has one manganese per subunit which cycles between Mn^{III} and Mn^{II}.⁴⁴

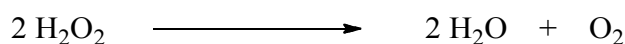
Scheme 2.5 Dismutation of superoxide anions by superoxide dismutase



The antioxidant enzyme catalase efficiently catalyzes the formation of water and dioxygen from two molecules of hydrogen peroxide (Scheme 2.6).⁴⁰ It consists of four

identical subunits. Each subunit (60 kDa) has a heme porphyrin moiety that is responsible for the catalytic function.⁴⁰ While catalase is not essential for certain types of cells, it plays a key role in the tolerance of cells to oxidative stress.⁴⁵ As catalase is not available in the mitochondria, GSH and GPX are relied upon heavily for destruction of hydrogen peroxide.

Scheme 2.6 Reaction catalyzed by the antioxidant enzyme catalase



These two enzymes work together along with several other key antioxidants to combat ROS generated in the cell. Figure 2.2 illustrates the importance of antioxidant enzymes in cells.⁴⁰ Electrons can leak from the endoplasmic reticulum (ER) from NADPH-cytochrome P450 and FADH₂ oxidases or from cytochrome b5 causing generation of superoxide. Xanthine and NADPH oxidases can generate superoxide in the cytoplasm and superoxide may leak from the mitochondrial electron-transport chain (M-ETC). These superoxide molecules may then be destroyed by SOD to form hydrogen peroxide. Hydrogen peroxide may be generated in the cell by the peroxisome or may be released from the mitochondria. The hydrogen peroxide in turn can be destroyed by catalase or glutathione peroxidase (GPX). In the presence of Fe²⁺ or Cu⁺, hydrogen peroxide may be converted to hydroxyl radical via the Fenton reaction which may in turn react with glutathione.⁴⁰

2.1.3 Copper-catalyzed Oxidation of Glutathione

The mechanisms of oxidation of glutathione by metal complexes is lacking in the literature, however there are a few reports on oxidation by complexes and metal ions in the past five decades.⁴⁶⁻⁵¹ The following section will discuss one report in particular, which illustrates the complex nature of the oxidation mechanisms. The authors elucidated the mechanism of copper-catalyzed oxidation of GSH, which was unclear in the literature.

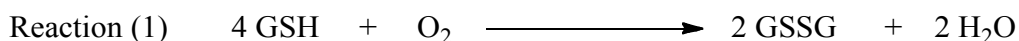
It is known that the glutathione thiol may react with dioxygen in the cell in the presence of copper or iron to form ROS. While it is understood that superoxide, hydrogen peroxide and hydroxyl radical can form, the mechanism and stoichiometry remained unclear. Low valent-metal reduction of dioxygen,⁵² as well as oxidation by a glutathione anion radical⁵³ are likely pathways that have been suggested for the generation of superoxide during copper-mediated GSH oxidation. GSH has been suggested to reduce superoxide to hydrogen peroxide⁵² and, as was mentioned previously, hydroxyl radical may be formed by the Fenton or Haber-Weiss reactions using hydrogen peroxide in the presence of iron or copper.^{52, 54, 55} The role of GSH is vastly contradictory depending on the account. Reported roles of GSH range from a simple reductant for the copper redox cycle to formation of Cu^+ -GSH complexes^{56, 57} that have been shown to display SOD activity.⁵⁸

Kachur, Koch and Biaglow have used dioxygen consumption studies and fluorescence and absorption spectroscopy to investigate both the involvement of ROS during the copper-mediated oxidation of GSH as well as the mechanism of oxidation. To

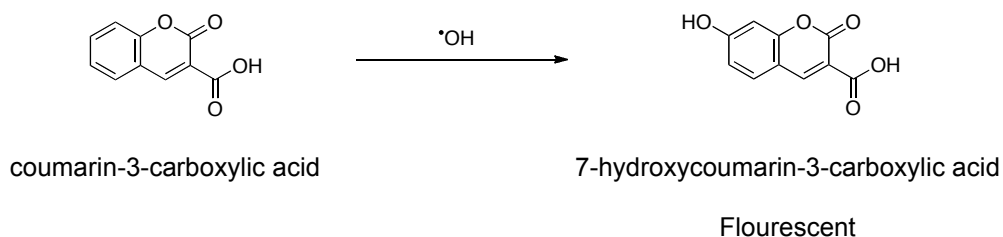
study the role of hydrogen peroxide and superoxide, catalase and SOD were employed, respectively.⁴⁸

They have determined the oxidation of GSH by copper to be biphasic according to the kinetics of dioxygen consumption and hydroxyl radical production. The 1st phase involves dioxygen consumption according to the stoichiometry of reaction (1) (Scheme 2.7), where 10 μM Cu^{2+} reacts with 0.1 mM GSH. The addition of SOD and catalase resulted in a 20% and 30% decrease, respectively, in the rate of dioxygen consumption during the 1st phase. However, while SOD did not alter the total amount of dioxygen consumed, catalase decreased the total amount consumed. It was concluded from these data that hydrogen peroxide and superoxide were produced during the oxidation reaction due to their effect on the rate of consumption of dioxygen.⁴⁸

Scheme 2.7 Stoichiometry for the oxidation of GSH in the 1st phase



Hydroxyl radical production was monitored by the addition of coumarin-3-carboxylic acid (3-CCA), which is converted to 7-hydroxycoumarin-3-carboxylic acid (7-OHCCA) upon reaction with one hydroxyl radical molecule (Scheme 2.8), and a dramatic increase in production was observed towards the end of the 1st phase. This increase corresponded to an increase (2-fold) in dioxygen consumption. Minor hydroxyl radical production was noted before the end of the 1st phase. This sudden change suggests the appearance of a different mechanism, the 2nd phase of oxidation. During the 2nd phase, excess dioxygen is consumed when compared to the predictions from the stoichiometry of reaction (1).⁴⁸

Scheme 2.8 Oxidation of 3-CCA by hydroxyl radical to yield fluorescent 7-OHCAA

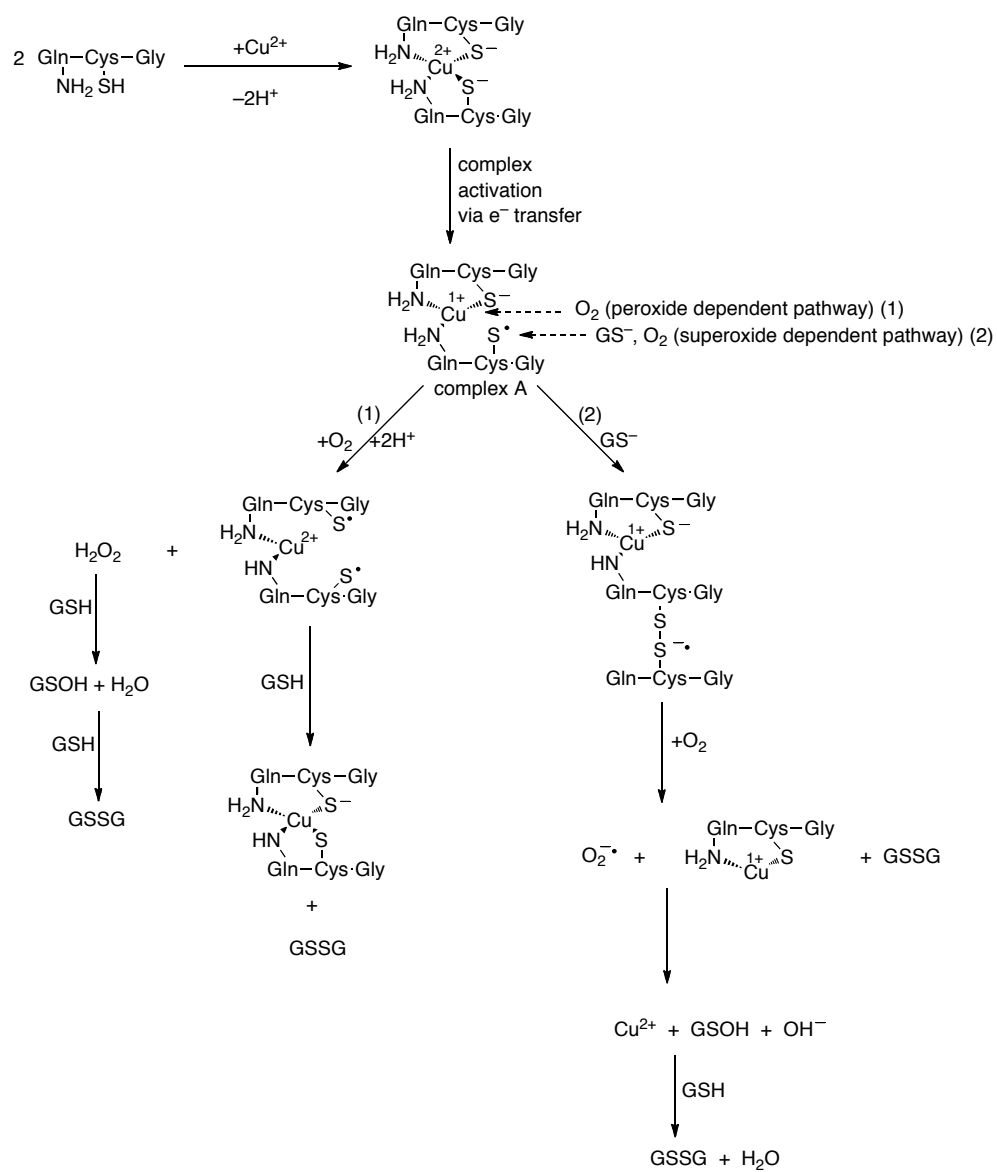
Ellman's reagent (DTNB) was used to determine the $[\text{GSH}]_{\text{free}}$ during the 1st phase. By varying the copper concentration that was mixed with GSH, they were able to correlate the absorbance at 412 nm (corresponding to amount of free thiol) directly to the copper concentration. As the concentration of copper was increased, the absorbance at 412 nm decreased. This suggested to the authors that a 1:1 $\text{Cu}^{2+}:\text{GSH}$ complex was being formed as the initial reaction between copper and GSH was slow. A $\text{Cu}^{2+}\text{-GSH}$ complex was also suggested by spectroscopic evidence, the appearance of absorption bands at 635 nm and 810 nm upon mixing of Cu^{2+} and GSH.⁴⁸

While they found the $[\text{Cu}^{2+}]$ to be directly associated with the rate of dioxygen consumption, it did not alter the overall quantity of dioxygen consumed. However, the production of hydroxyl radical during the 2nd phase was dependent on the $[\text{Cu}^{2+}]$. At $[\text{Cu}^{2+}]$ greater than half the $[\text{GSH}]$, a significant increase was noted in hydroxyl radical production. These data, unlike the data collected with DTNB, indicated that a 1:2 $\text{Cu}^{2+}:\text{GSH}$ complex was at play.⁴⁸

These data, taken together, suggest two independent and parallel pathways that are discussed by the authors. The formation of 1:1 and 1:2 $\text{Cu}^{2+}:\text{GSH}$ complexes are suggested and both are involved in the production of hydroxyl radical in the presence of hydrogen peroxide, but not superoxide. Scheme 2.9 shows the proposed mechanism, as

suggested by the authors, that supports observations when a large excess of GSH over Cu^{2+} is used, resulting in the formation of a 1:2 complex.⁴⁸ Once the 1:2 complex is activated by electron-transfer (complex A), the reaction can follow two pathways. The first pathway is peroxide-dependent (1), where the generation of hydrogen peroxide leads to the formation of GSSG. The second pathway is superoxide-dependent (2), where formation of superoxide leads to the generation of GSSG.

This discussion was meant to illustrate the complex nature of such metal-catalyzed oxidations and the difficulties faced in elucidating the mechanism. The following sections will discuss my work conducted in the Kodanko lab focusing on elucidating the mechanism of GSH oxidation by metal-based oxidants, by both single turnover reactions, as well as catalytic oxidation.

Scheme 2.9 Copper –catalyzed mechanism for autoxidation of GSH

2.1.4 Project Goals

We were interested in understanding the reaction between Ac-Cys-NHtBu and the ferryl species $[\text{Fe}^{\text{IV}}(\text{O})(\text{N4Py})]^{2+}$, however due to the low reproducibility of an observed green intermediate, GSH was chosen as a substitute for its importance in biology. The first part of this project involves the characterization of an iron-GSH intermediate, $[\text{Fe}^{\text{III}}(\text{SG})(\text{N4Py})]^{2+}$, by UV-vis and EPR spectroscopy. This species was first observed by UV-vis spectroscopy and its formula was fit by high-resolution time-of-flight mass spectrometry. Kinetic and mechanistic studies were carried out for the reaction between the ferryl and GSH when the ferryl species was pregenerated before its reaction with GSH. A mechanism for the single turnover reaction has been proposed.

Once this part of this project was completed, new literature showing the generation of ferryls by pentadentate iron-complexes in the presence of O_2 and a reductant, inspired us to attempt the above experiments catalytically. This work involves the reaction of the complex $[\text{Fe}^{\text{II}}(\text{N4Py})(\text{MeCN})](\text{ClO}_4)_2$ with GSH. An initial catalyst screen was carried out by examining the consumption of GSH over time and key complexes were examined further. The reaction between GSH and the ferryl derived from N4Py was tested for oxygen and pH dependence. Experiments with antioxidant enzymes were conducted to determine whether hydrogen peroxide or superoxide were important in the rate-determining step of the mechanism. A plausible mechanism has been suggested that fits with the data.

2.2 Results and Discussion

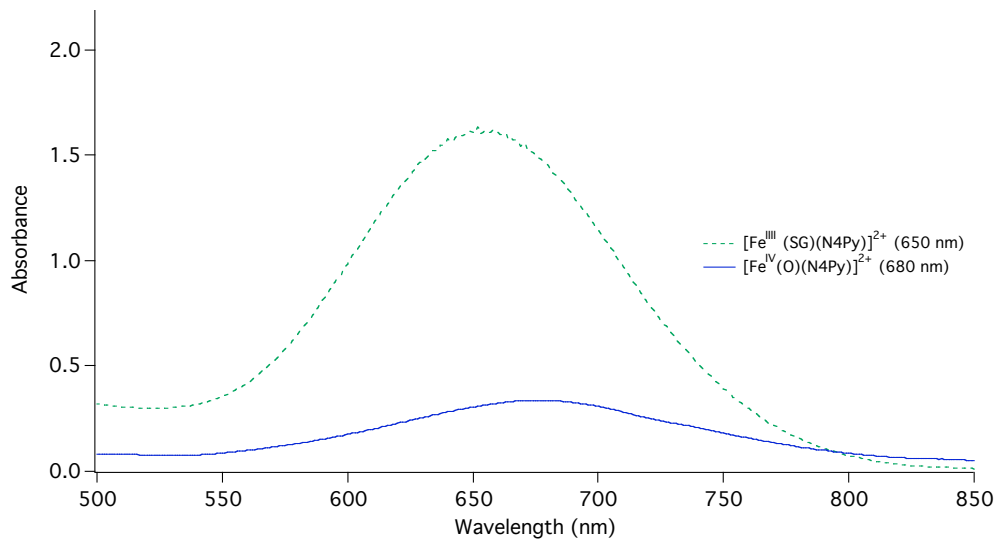
2.2.1 GSH Oxidation by Ferryl $[\text{Fe}^{\text{IV}}(\text{O})(\text{N4Py})]^{2+}$ and Characterization of the Intermediate $[\text{Fe}^{\text{III}}(\text{SG})(\text{N4Py})]^{2+}$

Glutathione (GSH) is involved in various cellular functions, including cell proliferation and apoptosis. It is important in the detoxification of ROS such as hydrogen peroxide and superoxide to protect cells from oxidative damage.¹ Reactions of GSH with metal-based oxidants have not been investigated,² therefore we have investigated the reaction of GSH with $[\text{Fe}^{\text{IV}}(\text{O})(\text{N4Py})]^{2+}$ in aqueous buffer. Acetonitrile was not necessary as with previous experiments involving Ac-Cys-NHtBu (1.2.2.1). The reaction of GSH (10 mM) with $[\text{Fe}^{\text{IV}}(\text{O})(\text{N4Py})]^{2+}$ (1 mM) leads to the formation of a green intermediate with $\lambda_{\text{max}} = 650$ nm. This green species, according to literature spectral data, is consistent with an S \rightarrow Fe ligand-to-metal-charge-transfer (LMCT).² Due to this observed result, the reaction was investigated in detail and $[\text{Fe}^{\text{III}}(\text{SG})(\text{N4Py})]^{2+}$ intermediate was characterized. Kinetic analysis was carried out to determine the mechanism of the reaction.

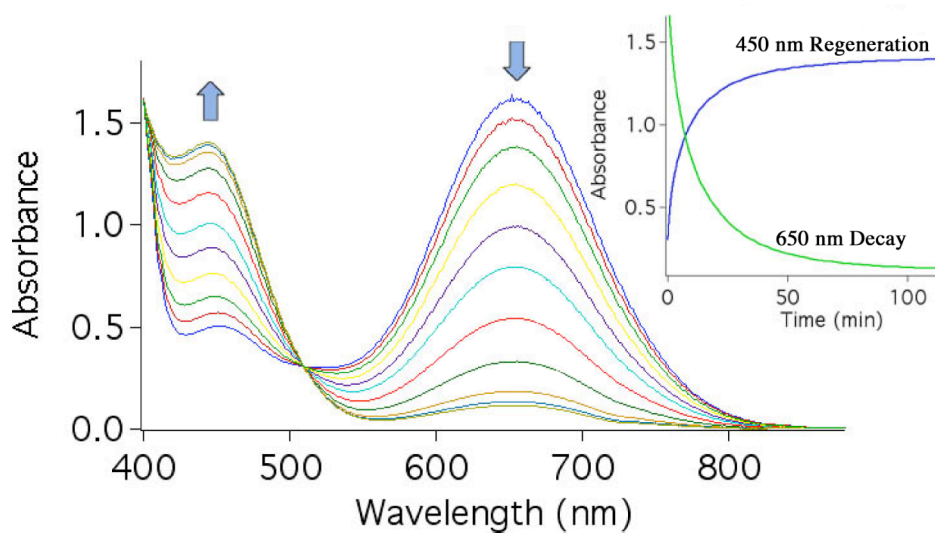
2.2.1.1 General Reaction and UV-vis Spectroscopy for the Oxidation of GSH by $[\text{Fe}^{\text{IV}}(\text{O})(\text{N4Py})]^{2+}$

The ferryl species $[\text{Fe}^{\text{IV}}(\text{O})(\text{N4Py})]^{2+}$ was pregenerated in acetate buffer (100 mM, pH = 6.02) by treating the complex $[\text{Fe}^{\text{II}}(\text{N4Py})(\text{MeCN})](\text{ClO}_4)_2$ with 2 equiv of peracetic acid. Upon maximum generation of the ferryl species, as judged by UV-vis spectroscopy (680 nm), a buffer solution of GSH was added and rapid formation of a green intermediate with absorbance maxima at 650 nm was observed. This new band was distinguishable from the ferryl species, which displays $\lambda_{\text{max}} = 680$ nm (Graph 2.1). As the green species at 650 nm decayed, a concurrent regeneration of $[\text{Fe}^{\text{II}}(\text{OH}_2)(\text{N4Py})]^{2+}$ at $\lambda_{\text{max}} = 450$ nm was noted (Graph 2.2). An 89% yield, based on extinction coefficient ($1620 \text{ M}^{-1} \text{ cm}^{-1}$), was calculated for $[\text{Fe}^{\text{II}}(\text{OH}_2)(\text{N4Py})]^{2+}$. A clear isobestic point at $\lambda_{\text{max}} = 510$ nm was observed, which indicated the existence of no long-lived intermediates during the decay of the green species (650 nm) and the regeneration of $[\text{Fe}^{\text{II}}(\text{OH}_2)(\text{N4Py})]^{2+}$ (450 nm). Oxidized glutathione (GSSG) was observed as the product by electrospray ionization mass spectrometry. No other oxidation products, such as sulfenic or sulfonic acids, were detected. The yield of GSSG ($90 \pm 20\%$) was determined by monitoring the consumption of GSH using Ellman's reagent. This yield is with respect to the ferryl species (single turnover oxidation) and not GSH.

Graph 2.1 Comparison of $[\text{Fe}^{\text{IV}}(\text{O})(\text{N4Py})]^{2+}$ vs $[\text{Fe}^{\text{III}}(\text{SG})(\text{N4Py})]^{2+}$ for reaction of 1 mM ferryl with 5 mM GSH



Graph 2.2 Decay of $[\text{Fe}^{\text{IV}}(\text{O})(\text{N4Py})]^{2+}$ (650 nm) and regeneration of $[\text{Fe}^{\text{II}}(\text{OH}_2)(\text{N4Py})]^{2+}$ (450 nm)



2.2.1.2 Control Experiments

Control experiments were run to help identify the intermediate responsible for the absorbance maxima at 650 nm. These experiments were meant to determine if the intermediate contained GSH, N4Py and iron. As was mentioned previously, the absorbance at 650 nm is indicative of S→Fe LMCT and control experiments with GSH and either Fe^{II} or Fe^{III} perchlorate salts did not generate this absorption band. This result suggests N4Py is playing a role in the structure of the green intermediate. Likewise, when the aromatic or aliphatic thiols PhSH or EtSH were reacted with the ferryl, no absorption band was detected. Also, rapid formation of an absorption band at 650 nm was not observed when the complex [Fe^{II}(N4Py)(MeCN)](ClO₄)₂ was treated with GSH, suggesting a role for the ferryl in the formation of the green intermediate. However, when the aqueous solution of the complex was allowed to oxidize in air prior to reaction with GSH, rapid generation of the green intermediate was observed which is consistent with our suggested mechanism (*vide infra*), in which a ferric intermediate reacting with GSH is responsible for the formation of the green intermediate. These data taken together suggest GSH, iron and N4Py are involved in the structure of the green intermediate and that the ferryl plays an important role in its formation. The following sections will discuss the characterizations of the green intermediate.

2.2.1.3 Mass Spectrometry Data

Mass spectrometry (MS) was used to follow the reaction of the ferryl with GSH and high-resolution time-of-flight (TOF)-MS was used at early time points during the reaction. The TOF-MS spectrum exhibited a prominent ion cluster centered at m/z 364.5944 whose isotopic distribution fit within 5 ppm for the molecular formula of the dication $[\text{Fe}^{\text{III}}(\text{SG})(\text{N4Py})]^{2+}$ (Figure 2.3). GSH was considered to be a monoanion ($\text{GSH} - \text{H}^+$) where the deprotonated thiolate is bound to the iron center. Another prominent ion cluster was observed at m/z 728.1821 whose isotropic distribution fit within 5 ppm for the molecular formula of the monocation $[\text{Fe}^{\text{II}}(\text{SG})(\text{N4Py})]^+$ (Figure 2.4). For this species, GSH was considered to be a dianion ($\text{GSH} - 2\text{H}^+$) due to protonation of the amine terminus and deprotonation of the two carboxylic acid groups (in addition to deprotonation of the thiol which is bound to the iron center). After allowing the reaction to stand for 1 h at ambient temperature, these two prominent ion clusters dissipated and a cluster at m/z 220.418 became the dominant ion present. The isotropic distribution fit within 5 ppm for the molecular formula $[\text{Fe}^{\text{II}}(\text{OH}_2)(\text{N4Py})]^{2+}$.

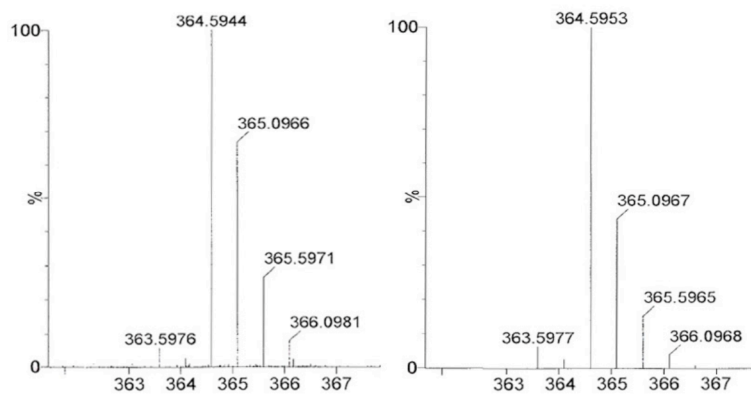


Figure 2.3 High-resolution TOF-MS for $[\text{Fe}^{\text{III}}(\text{SG})(\text{N4Py})]^{2+}$ with m/z 364.5944 (left) and calculated fit (right)

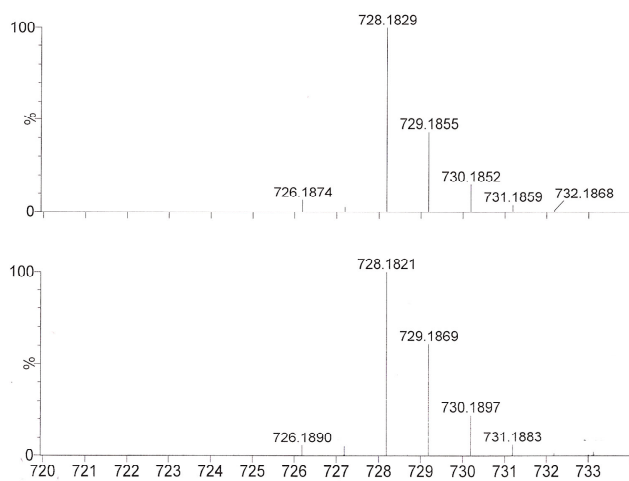
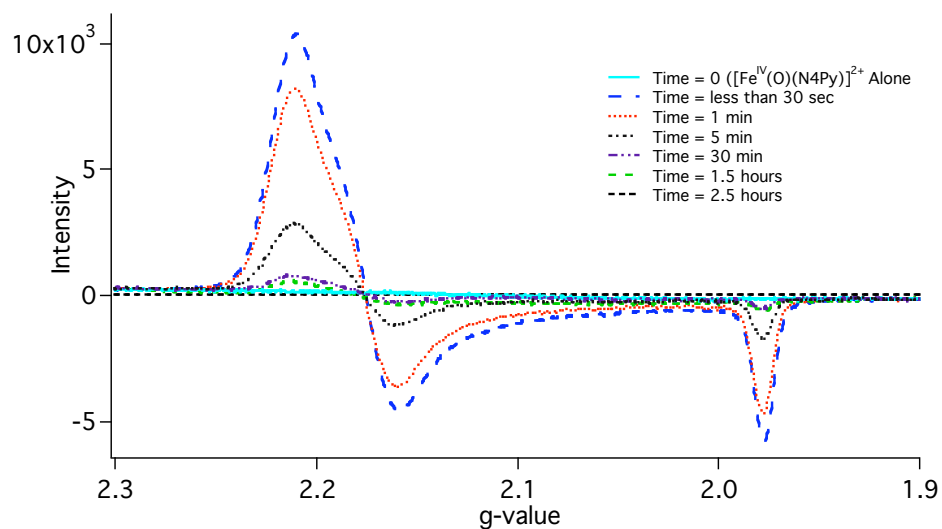
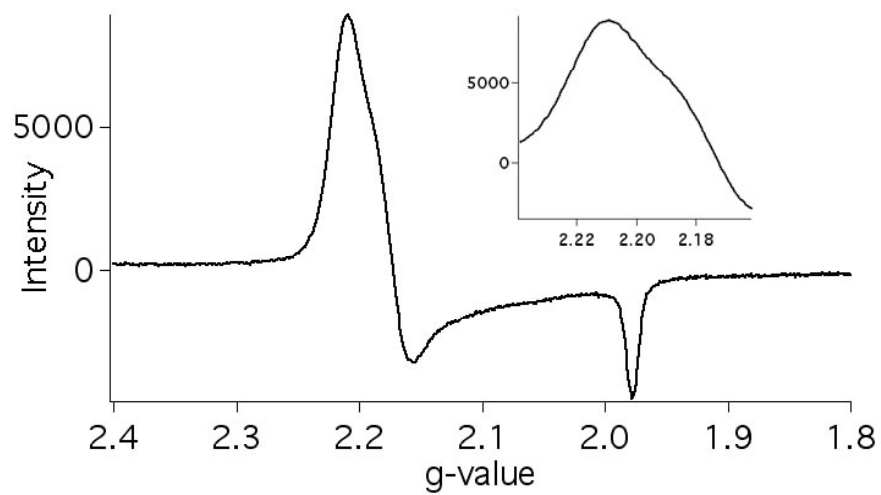


Figure 2.4 High-resolution TOF-MS for $[\text{Fe}^{\text{II}}(\text{SG})(\text{N4Py})]^+$ with m/z 728.1829 (top) and calculated fit (bottom)

2.2.1.4 Electron paramagnetic Resonance Spectroscopy Data

The green species was characterized by electron paramagnetic resonance (EPR) spectroscopy as the suspected intermediate complex, $[\text{Fe}^{\text{III}}(\text{SG})(\text{N4Py})]^{2+}$ is paramagnetic. The reaction between the ferryl and GSH was carried out and portions of the reaction mixture were frozen in liquid nitrogen at various time points. Spectra were acquired to monitor both the formation of $[\text{Fe}^{\text{III}}(\text{SG})(\text{N4Py})]^{2+}$, as well as its decay. [Experimental conditions: temperature, 120 K; microwaves, 1.0 mW at 9.34 GHz; modulation 2.0 G; receiver gain, 14000; GSH (5 mM) and $[\text{Fe}^{\text{IV}}(\text{O})(\text{N4Py})]^{2+}$ (1 mM)] According to Graph 2.3, it can be noted that the paramagnetic species generates and decays within the same time frame as the peak at 650 nm, which supports both data corresponding to the same species. The spectrum of the intermediate, at less than 30 sec, displays two g-values at 2.17 and 1.98 (Graph 2.4), however, an apparent shoulder for the resonance at 2.17 is observed. This shoulder suggests the presence of a third unresolved resonance, indicating rhombic rather than axial symmetry if there were only two g-values. Regardless of the presence of two or three resonances, the data are consistent with a low-spin iron(III) species as they agree with previously reported species, $[\text{Fe}^{\text{III}}(\text{L})(\text{N4Py})]^{2+}$ (L = OOH and OH).⁵⁹

Graph 2.3 EPR spectra over time for the reaction of $[\text{Fe}^{\text{IV}}(\text{O})(\text{N4Py})]^{2+}$ with GSH**Graph 2.4** X-band EPR spectra from reaction of $[\text{Fe}^{\text{IV}}(\text{O})(\text{N4Py})]^{2+}$ (1 mM) with GSH (5 mM)

2.2.1.5 Kinetic Modeling

Variable concentration data were collected, using a stopped-flow equipped UV-vis spectrophotometer, in order to probe the mechanism of the reaction between the ferryl (1 mM) and GSH (5 – 25 mM). The data were fit using *Dynafit*⁶⁰ kinetic modeling software. Even though a stopped-flow apparatus was employed, the decomposition of the ferryl species was too fast to be observed and greater than 50% of the ferryl had decomposed during the deadtime of mixing. This allows for assignment of $1 \times 10^4 \text{ M}^{-1}\text{s}^{-1}$ as a lower limit for the rate constant (k_1) of ferryl quenching by GSH. By our visual observations of a transient yellow color as well as on the basis of previous studies with Ac-Cys-NHtBu, we propose the formation of $[\text{Fe}^{\text{III}}(\text{OH})(\text{N4Py})]^{2+}$ as the first step of the mechanism for the reaction of the ferryl with GSH. *Dynafit* was used to determine the mechanism of the next two steps. Both first- and second-order processes (Scheme 2.10) were evaluated against various mechanistic models. Model 5 was the best fit (Graph 2.5, expansion in Graph 2.6) which involved a second-order reaction between $[\text{Fe}^{\text{III}}(\text{OH})(\text{N4Py})]^{2+}$ and GSH with a rate constant of $14.3(1) \text{ M}^{-1} \text{ s}^{-1}$ (k_2) followed by a second-order decomposition of $[\text{Fe}^{\text{III}}(\text{SG})(\text{N4Py})]^{2+}$ (with zero kinetic order in GSH) with a rate constant of $1.68(1) \text{ M}^{-1} \text{ s}^{-1}$ (k_3) (Scheme 2.11). The response factor that was optimized by *Dynafit* ($1768 \text{ M}^{-1}\text{cm}^{-1}$, Graph 2.5) agreed well with the calculated value of $\epsilon_{650} = 1872 \text{ M}^{-1} \text{ cm}^{-1}$. $1/\text{Abs}$ (at $\lambda_{\text{max}} = 650 \text{ nm}$) was plotted against time and the linear portion of the plot was fit to $y = mx + b$ (Graph 2.7). The extrapolated intercept is equal to $1/\text{Abs}$ (at $\lambda_{\text{max}} = 650 \text{ nm}$) for $t = 0$. The molar absorptivity was calculated to be $1872 \text{ M}^{-1} \text{ cm}^{-1}$ from $A = l\epsilon c$; where $c = 1 \text{ mM}$, $l = 1 \text{ cm}$, and $A = \text{absorbance at } t = 0$.

Scheme 2.10 Theoretical models 1 – 5 considered for *Dynafit***Model 1:**

$A + B \xrightarrow{k_1} C$; bimolecular formation of intermediate

$C + B \xrightarrow{k_2} D + E$; bimolecular decay

Where $A = [\text{Fe}^{\text{IV}}(\text{O})(\text{N4Py})]^{2+}$, $B = \text{GSH}$, $C = [\text{Fe}^{\text{III}}(\text{SG})(\text{N4Py})]^{2+}$, $D = \text{GSSG}$ and
 $E = [\text{Fe}^{\text{II}}(\text{N4Py})]^{2+}$

Model 2:

$A + B \xrightarrow{k_1} C$; bimolecular formation of intermediate

$C \xrightarrow{k_2} D$; formation of second intermediate from first intermediate

$D + B \xrightarrow{k_3} E + F$; bimolecular decomposition of second intermediate

Where $A = [\text{Fe}^{\text{IV}}(\text{O})(\text{N4Py})]^{2+}$, $B = \text{GSH}$, $C = [\text{Fe}^{\text{III}}(\text{SG})(\text{N4Py})]^{2+}$, $D = \text{other}$
intermediate involving GSH and $\text{Fe}(\text{N4Py})$, $E = \text{GSSG}$ and $F = [\text{Fe}^{\text{II}}(\text{N4Py})]^{2+}$

Model 3:

$A + B \xrightarrow{k_1} C$; bimolecular formation of intermediate

$C + B \xrightarrow{k_2} D + E$; bimolecular decomposition of intermediate

$C + C \xrightarrow{k_3} D + 2F$; bimolecular decomposition of intermediate

Where $A = [\text{Fe}^{\text{IV}}(\text{O})(\text{N4Py})]^{2+}$, $B = \text{GSH}$, $C = [\text{Fe}^{\text{III}}(\text{SG})(\text{N4Py})]^{2+}$, $D = \text{GSSG}$ and
 $E \ \& \ F = [\text{Fe}^{\text{II}}(\text{N4Py})]^{2+}$

Model 4:

$A + B \rightarrow C : k_1$; bimolecular formation of intermediate

$C \rightarrow D + E : k_2$; unimolecular decomposition of intermediate

$C + E \rightarrow F + G : k_3$; bimolecular decomposition of intermediate

Where $A = [\text{Fe}^{\text{IV}}(\text{O})(\text{N4Py})]^{2+}$, $B = \text{GSH}$, $C = [\text{Fe}^{\text{III}}(\text{SG})(\text{N4Py})]^{2+}$, $D = \text{GS}\cdot$,

$E \text{ \& } F = [\text{Fe}^{\text{II}}(\text{N4Py})]^{2+}$ and $G = \text{GSSG}$

Model 5:

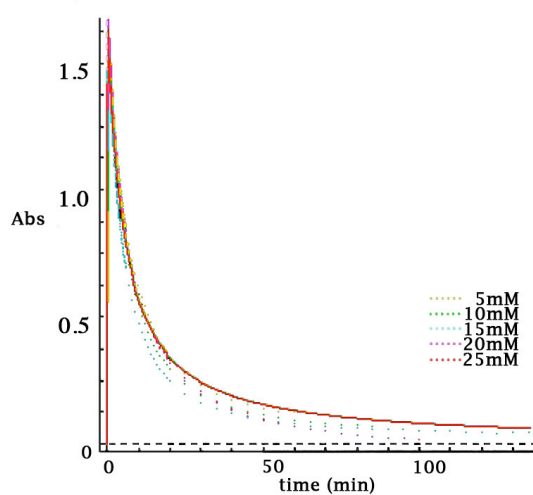
$A + B \rightarrow C : k_1$; bimolecular formation of intermediate

$C + C \rightarrow D + E : k_2$; decay of intermediate

Where $A = [\text{Fe}^{\text{IV}}(\text{O})(\text{N4Py})]^{2+}$, $B = \text{GSH}$, $C = [\text{Fe}^{\text{III}}(\text{SG})(\text{N4Py})]^{2+}$, $D = \text{GSSG}$ and

$E = [\text{Fe}^{\text{II}}(\text{N4Py})]^{2+}$

Graph 2.5 Best-calculated fit for kinetic model 5 for the reaction of $[\text{Fe}^{\text{IV}}(\text{O})(\text{N4Py})]^{2+}$ with varying concentrations of glutathione

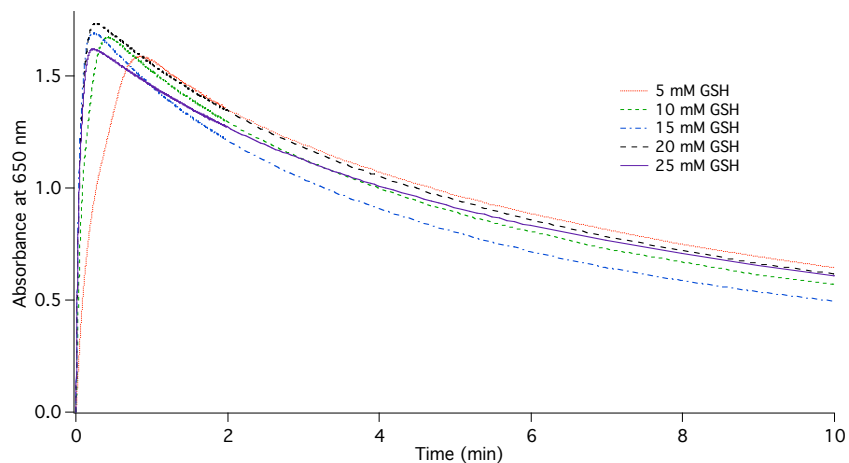


Parameters and Standard Errors for Model 5

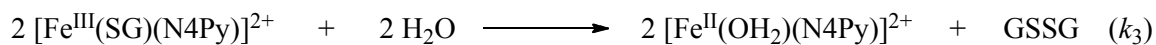
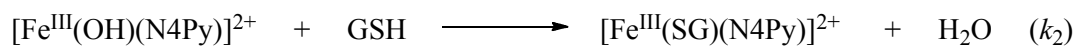
Parameter	Initial ($\text{mM}^{-1}\text{min}^{-1}$)	Unit	Fit	Unit	%Error
k_1	14.2692	$\text{M}^{-1}\text{sec}^{-1}$	14.2692	$\text{M}^{-1}\text{sec}^{-1}$	0.5
k_2	1.6799	$\text{M}^{-1}\text{sec}^{-1}$	1.6799	$\text{M}^{-1}\text{sec}^{-1}$	0.7
r_C	17686.5	$\text{M}^{-1}\text{sec}^{-1}$	17686.5	$\text{M}^{-1}\text{cm}^{-1}$	0.1

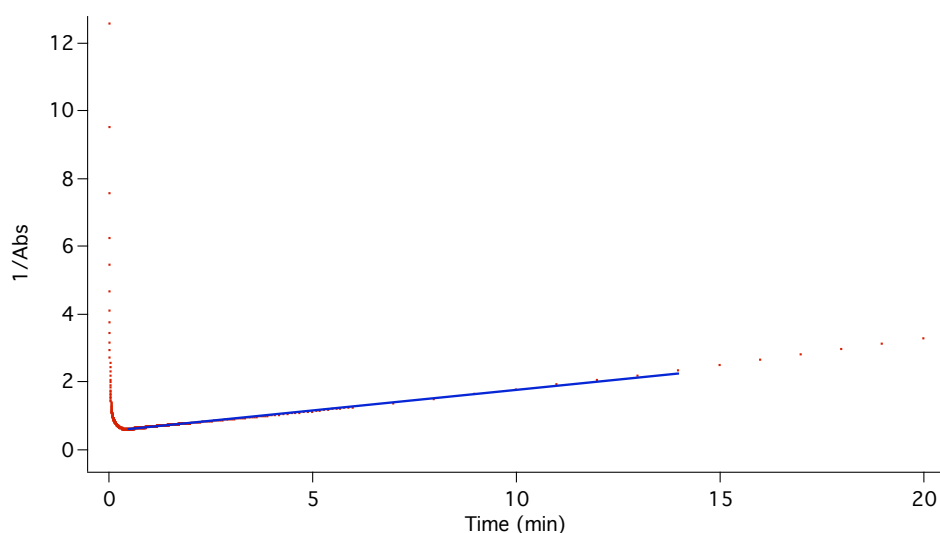
* r_C : Exinction coefficient for C, $[\text{Fe}^{\text{III}}(\text{SG})(\text{N4Py})]^{2+}$

Graph 2.6 Expansion of the first 10 minutes of absorbance vs. time for data used in the kinetic modeling



Scheme 2.11 Proposed mechanism for the reaction of $[\text{Fe}^{\text{IV}}(\text{O})(\text{N4Py})]^{2+}$ with GSH



Graph 2.7 Plot for molar absorptivity at 650 nm

While further work is still needed to determine the structure of the green intermediate, two possible structures are likely based on the observed data (Figure 2.5). These two structures involve iron, N4Py and GSH as determined by the control experiments discussed earlier in this chapter. The first structure is the simple model, where the deprotonated thiolate is bound to the iron center. The second possible structure is a chelated GSH due to participation of the carboxyl group coordinating to the iron center. This chelated structure with a coordination number of seven may be possible due to the fact that coordination numbers greater than six have been observed for complexes of N4Py.⁵⁹

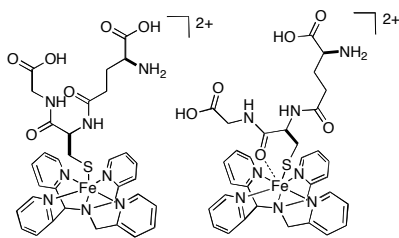
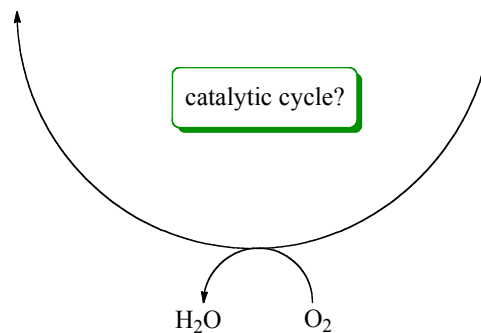
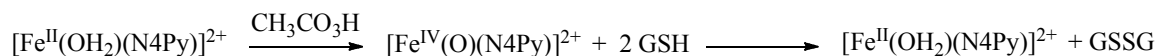


Figure 2.5 Possible structures of $[\text{Fe}^{\text{III}}(\text{SG})(\text{N4Py})]^{2+}$

2.2.2 Catalytic Oxidation of GSH by $[\text{Fe}^{\text{II}}(\text{N4Py})(\text{MeCN})](\text{ClO}_4)_2$

While the previous section covered oxidation of GSH by a pregenerated ferryl species, we were inspired by recent literature proving that non-heme iron-complexes could activate dioxygen in the presence of a reductant,^{61, 62} to attempt the reaction catalytically (Scheme 2.12). A survey of several non-heme complexes was undertaken in which a catalytic amount of iron complexes (1 mM) were treated with GSH (10 mM) in MOPS buffer (pH = 7.9). These reactions were carried out under ambient temperature and atmosphere using Ellman's reagent to determine the consumption of GSH after 6 h. From the data collected in Table 2.1, we notice that several of the complexes display catalytic activity and cause rapid consumption of GSH. Importantly, complexes derived from Bn-TPEN, N4Py, EDTA and TPA cause faster consumption of GSH than the control of GSH alone or GSH with $\text{Fe}^{\text{II}}(\text{ClO}_4)_2$. These data illustrate an important ligand effect during the oxidation of GSH. The complex derived from TPA caused complete consumption of GSH in 6 h. Since these complexes were able to consume an amount of GSH that required catalysis, their mechanism was probed by determining the role of dioxygen.

Scheme 2.12 Possible catalytic cycle for GSH oxidation**Table 2.1** Catalyst screen for oxidation of GSH

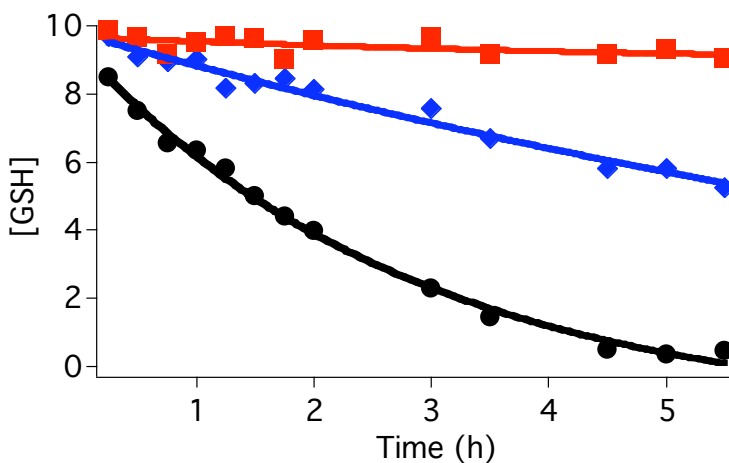
Catalyst	[GSH] ^b
control	10.0 ± 0.2
Fe ^{II} (ClO ₄) ₂	9.8 ± 0.1
[Fe ^{II} (bipy) ₃](ClO ₄) ₂ ^c	10.0 ± 0.5
Fe ^{II} (TPEN)(ClO ₄) ₂ ^c	9.2 ± 0.6
Fe ^{II} (Bn-TPEN)(OTf) ₂	7.4 ± 0.6
[Fe ^{II} (MeCN)(N4Py)](ClO ₄) ₂	4.3 ± 0.2
Fe ^{III} (EDTA)(ClO ₄) ₃ ^c	2.4 ± 0.1
Fe ^{II} (TPA)(OTf) ₂	0.0 ± 0.2

^a Conditions: MOPS buffer (pH = 7.9); [GSH] = 10 mM, [catalyst] = 1 mM; ^b [GSH] determined using Ellman's reagent; data are average of three runs, errors are standard deviations; ^c iron complex formed *in situ* using 1 mM ligand and 1 mM Fe(ClO₄)₂·xH₂O or Fe(ClO₄)₃·xH₂O.

2.2.2.1 Dioxygen Consumption Studies

Consumption of GSH was measured, using Ellman's reagent, during the reaction of $[\text{Fe}^{\text{II}}(\text{MeCN})(\text{N4Py})](\text{ClO}_4)_2$ (1 mM) with GSH (10 mM) under Ar (red), ambient atmosphere (blue, 21% O_2) and under 100% O_2 (black) at ambient temperature (Graph 2.8). From the data collected, a kinetic role for O_2 has been established as the reaction completely consumed GSH under 100% O_2 but under Ar, little consumption was observed. While these reactions were conducted open to light, control experiments in the dark showed oxidation at the same rate. This is important because it excludes the need for light to cause homolysis of the Fe-S bond, even though oxidations through photolysis of $\text{Fe}^{\text{III}}\text{-S}$ bonds are known.⁶³

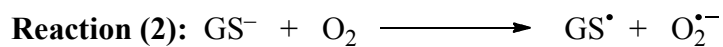
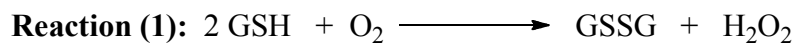
Graph 2.8 Consumption of GSH by $[\text{Fe}^{\text{II}}(\text{MeCN})(\text{N4Py})](\text{ClO}_4)_2$ under Ar (red), ambient O_2 (blue, 21%) and 100% O_2 (black)



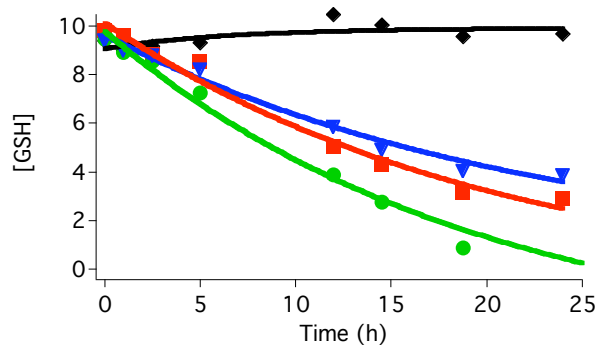
2.2.2.2 Antioxidant Enzyme Inhibition Study

As was discussed earlier in this chapter (2.1.3), the mechanism of the oxidation of GSH has been shown to be complicated involving ROS-, such as superoxide and hydrogen, and pH-dependent pathways.^{48, 64} The auto-oxidation of GSH in the presence of dioxygen can produce hydrogen peroxide and superoxide by either the reaction of GSH, reaction (1), or GS^- , reaction (2), with O_2 (Scheme 2.13). Due to the possibility of oxidation taking place via one of these two reactions, the antioxidant enzymes SOD and catalase were used to determine if the oxidation reactions were dependent on superoxide and hydrogen peroxide, respectively. These control reactions were carried out with the non-heme complexes derived from EDTA and N4Py. While oxidation of GSH with the complex derived from EDTA is completely inhibited by catalase (black, Graph 2.9), suggesting a role of hydrogen peroxide in the oxidation of GSH, catalase has no effect for oxidation of GSH by $[\text{Fe}^{\text{II}}(\text{MeCN})(\text{N4Py})](\text{ClO}_4)_2$ (blue) compared to the reaction without catalase added (red). This is an important result suggesting that the ROS hydrogen peroxide is not contributing to the rate determining step of the oxidation of GSH by $[\text{Fe}^{\text{II}}(\text{N4Py})]^{2+}$. Likewise, SOD does not halt the oxidation of GSH by $[\text{Fe}^{\text{II}}(\text{MeCN})(\text{N4Py})](\text{ClO}_4)_2$, however due to the background reaction where SOD slowly catalyzes the oxidation of GSH in the absence of $[\text{Fe}^{\text{II}}(\text{MeCN})(\text{N4Py})](\text{ClO}_4)_2$, a slight acceleration in the rate of consumption was observed (green). Further studies showed that oxidation of GSH by the complex derived from TPA exhibited the same results as $[\text{Fe}^{\text{II}}(\text{MeCN})(\text{N4Py})](\text{ClO}_4)_2$. These results are important, as they suggest no role for superoxide or hydrogen peroxide before the rate determining steps of the oxidation of GSH for the case of complexes derived from N4Py and TPA.

Scheme 2.13 Reactions of GSH and GS^- with O_2 to yield hydrogen peroxide and superoxide



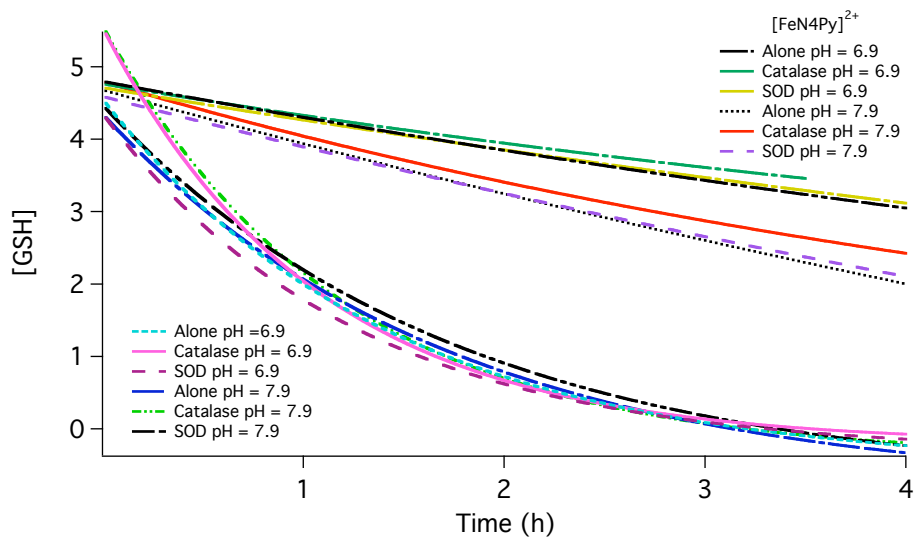
Graph 2.9 Inhibition study with SOD and catalase for the reactions of GSH with the iron complexes derived from EDTA and N4Py



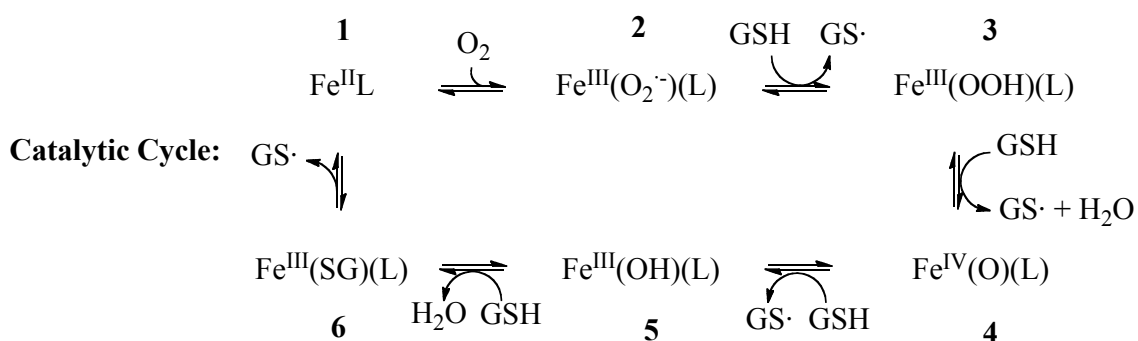
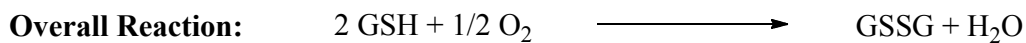
2.2.2.3 pH Dependence Study and Proposed Mechanism

Reactions were carried out at two pH values (6.9 and 7.9) to determine if a dependence on pH existed. Graph 2.10 shows no pH dependence for the oxidation of GSH by the complex derived from TPA and slight pH dependence for the oxidation of GSH by the complex derived from N4Py. These data may suggest that the oxidations by the two complexes have similar pathways but have different mechanisms. Based on the data collected, lack of inhibition by SOD and catalase, a plausible mechanism has been suggested that involves the generation of a ferryl species (**4**, Scheme 2.14, the ligand N4Py has been omitted for clarity). The reaction of dioxygen with $[\text{Fe}^{\text{II}}(\text{N4Py})]^{2+}$ (**1**) leads to the generation of an Fe^{III} -superoxo species **2**. Reduction of **2** followed by protonation by GSH yields the hydroperoxo species **3**. During this step, GS^{\bullet} dimerizes forming GSSG. The O-O bond of **3** homolytically fragments to form ferryl **4** (alternatively after a single electron reduction of **3**), which reacts with GSH leading to the formation of **5**, **6** and then **1** to complete the catalytic cycle. While we have not ruled out other mechanisms, the conversion **1** to **3** and **4** to **1** has been demonstrated.^{62, 65}

Graph 2.10 pH study for the reaction of GSH with the complexes derived from N4Py and TPA in the presence and absence of SOD and catalase



Scheme 2.14 Proposed mechanism for the catalytic oxidation of GSH



2.3 Conclusions and Future Directions

In single turnover experiments with pregenerated $[\text{Fe}^{\text{IV}}(\text{O})(\text{N4Py})]^{2+}$, we have observed and characterized the green intermediate $[\text{Fe}^{\text{III}}(\text{SG})(\text{N4Py})]^{2+}$ by UV-vis spectroscopy, EPR and high-resolution TOF-MS. We have also investigated the kinetics and proposed a plausible mechanism for the reaction of GSH with the ferryl $[\text{Fe}^{\text{IV}}(\text{O})(\text{N4Py})]^{2+}$ based on the best fit model using *DynaFit*. Further studies are needed to elucidate the exact structure of the $[\text{Fe}^{\text{III}}(\text{SG})(\text{N4Py})]^{2+}$.

With respect to catalytic oxidation, we have investigated several non-heme iron complexes in the oxidation of GSH. Results conclude that complexes derived from Bn-TPEN, N4Py, EDTA and TPA cause consumption of GSH faster than the controls, however, the mechanism of the EDTA complex involves the generation of hydrogen peroxide as indicated by experiments with catalase. On the other hand, complexes derived from N4Py show no inhibition by SOD or catalase suggesting a metal-based oxidant being involved in the oxidation of GSH rather than of hydrogen peroxide or superoxide. We have shown dioxygen dependence for the oxidation of GSH with $[\text{Fe}^{\text{IV}}(\text{O})(\text{N4Py})]^{2+}$ and that pH does not play a significant role in the oxidation process. Based on the evidence, we have suggested a plausible mechanism that involves reductive activation of O_2 . Further work is needed in this area such as further studies to elucidate the mechanism of the oxidation, as it is possible the ferryl species may not be generated during the reaction. While we have ruled out generation of hydrogen peroxide and superoxide as being important before the rate-determining step. Experiments will need to be carried out to eliminate or support the possible generation of hydroxyl radical. If the conversion of **3** to **4** in Scheme 2.14 involves homolytic cleavage of the O-O bond, then

hydroxyl radical should be produced and if scavenged, could reduce the quantity of GSH consumed.

Other experiments needed include the examination of other ligands that form iron-complexes, such as tacpyr. Further examination of the reaction of these complexes, as well as the complexes used in the initial catalyst screen, will needed to be looked in further detail. This will include earlier time point determination of GSH. The catalyst screen showed TPA had depleted all GSH by 6 h, however, it is not known yet if this depletion is completed at earlier time points, such as 1 or 2 h. Also, catalyst-loading studies should be preformed to determine the optimal amount of catalyst needed.

An important practical application of the research developed here would be in the field of cancer. It is known that cancer cells contain a higher amount of ROS and therefore are more susceptible to oxidative stress by GSH depletion than normal cells.⁶⁶ Key complexes should be tested *in cellulo* and *in vivo* for anticancer activity via GSH depletion and the mechanism of this depletion should be studied.

2.4 Experimental

2.4.1 Single Turnover Experiments

General Experiment: 2 equiv peracetic acid (100 μ L) in water was added to $[\text{Fe}^{\text{II}}(\text{N4Py})(\text{MeCN})](\text{ClO}_4)_2$ (1 mL, 2 mM) in acetate buffer (pH = 6.02). After complete generation of $[\text{Fe}^{\text{IV}}(\text{O})(\text{N4Py})]^{2+}$, as judged by UV-vis spectroscopy ($\lambda = 680$ nm) on a Varian Cary-50 UV-vis spectrophotometer, 10 equiv reduced glutathione (0.9 mL, 22.2 mM) in acetate buffer (pH = 6.02) was added and mixed for 3 seconds before scanning and monitoring the intermediates generation and decay at $\lambda = 650$ nm. Upon mixing, analyses were conducted using specific instrumentation (see the following descriptions for details). All buffers were prepared using Millipore water and $[\text{Fe}^{\text{II}}(\text{N4Py})(\text{MeCN})](\text{ClO}_4)_2$ solutions were dissolved in the buffer immediately before use.⁶⁵

Stopped-flow Kinetics: Spectra were collected using an Applied Photophysics stopped-flow apparatus and a Varian Cary-50 UV-vis spectrophotometer. Sample experiment is as follows: $[\text{Fe}^{\text{IV}}(\text{O})(\text{N4Py})]^{2+}$ (2 mM in a syringe) was reacted with glutathione (20 mM in a syringe) in acetate buffer (pH = 6.02) via pressure pump that mixed the syringe solutions in a 1 to 1 ratio and the reaction was monitored by UV-vis spectroscopy at $\lambda_{\text{max}} = 650$ nm. Data were collected for five concentrations (5 mM, 10 mM, 15 mM, 20 mM, and 25 mM as final concentrations) of glutathione. The absorbance vs. time data were cut after the residual $[\text{Fe}^{\text{IV}}(\text{O})(\text{N4Py})]^{2+}$ decomposed (< 100 ms) and the minimum at 650 nm was adjusted to $t = 0$ for fitting.⁶⁵

Kinetic Modeling: The kinetic modeling software Dynafit⁶⁰ was used to analyze data collected from stopped-flow equipped UV-vis spectrophotometer. $[\text{Fe}^{\text{IV}}(\text{O})(\text{N4Py})]^{2+}$ (2 mM in a syringe) was reacted with glutathione (20 mM in a syringe) in acetate buffer (pH = 6.02) via pressure pump that mixed the syringe solutions in a 1 to 1 ratio and the reaction was monitored by UV-vis spectroscopy at $\lambda_{\text{max}} = 650$ nm. The absorbance vs. time traces for five concentrations (5 mM, 10 mM, 15 mM, 20 mM, and 25 mM) of glutathione was used for the calculations. The data were evaluated using 5 possible mechanistic models and rate constant values were treated as variables and fit.⁶⁵

Mass Spectroscopy: Data were collected on a high resolution Time-of-Flight Micromass LCT Premier XE Spectrometer. The instrument was set up for routine determinations with water as the liquid carrier: a desolvation temperature of 350.0 °C, source temperature of 120.0 °C, sample cone voltage of 40.0 V, capillary voltage of 3300.0 V, cone gas flow of 200.0 L/hr, and desolvation gas flow of 800.0 L/hr. Mass data were collected on samples of the above reaction mixture with 1 equiv glutathione; the reaction was carried out with water as the solvent.⁶⁵

EPR Spectroscopy: Data were acquired using a Bruker X-band EPR spectrometer for the reaction of $[\text{Fe}^{\text{IV}}(\text{O})(\text{N4Py})]^{2+}$ (1.8 mM, 1 mL) with reduced glutathione (0.9 mL, 22.2 mM) in acetate buffer (pH = 6.02). Upon mixing, reaction mixture samples were frozen at particular time points in liquid N₂. Experimental conditions: temperature, 120 K; microwaves, 1.0 mW at 9.34 GHz; modulation 2.0 G; receiver gain, 14000.⁶⁵

GSH Determination Using Ellman's Reagent: Ellman's reagent (50 μL , 10 mM in Tris buffer pH = 8.0) was added to 4.92 mL Tris buffer (pH = 8.0). To this, 25 μL aliquots of the reaction mixture of $[\text{Fe}^{\text{IV}}(\text{O})(\text{N4Py})]^{2+}$ (1.1 mL, 1.8 mM) with 5 equiv

reduced glutathione (0.9 mL, 11.1 mM) in acetate buffer (pH = 6.02) was added and mixed well. The absorbance at 412 nm was recorded immediately after mixing on a UV-vis spectrometer. By comparing the absorbance at 412 nm to a calibration curve (generated with various concentrations of glutathione), the concentration of reduced glutathione that was unreacted was calculated. Determinations of the quantity of glutathione remaining in solution were performed in triplicates.⁶⁵

2.4.2 Catalytic Oxidation Experiments

General Experiment for Reaction of Iron Complexes with GSH: 300 μL reactions were carried out in 96 well plates using the following conditions. Final [Fe complex] = 1mM, [GSH] = 5 or 10 mM, and where applicable, [SOD/Catalase] = 1 mg/mL. At specific time points during the reaction, 10 μL aliquots were removed and diluted in wells containing 190 μL of the buffer used in the reaction (100 mM MOPS: pH = 6.9 or 7.9). Glutathione concentrations were determined by adding 10 μL from dilution wells into wells containing a solution of Ellman's reagent in Tris buffer (pH = 8.0) (300 μL). The absorption at 412 nm was recorded using a Tecan Infinite 200 microplate reader and converted into concentrations using a calibration curve. All reactions were run in triplicate to obtain averages and standard deviations. All buffers were prepared using Millipore water and all iron complex solutions were dissolved in deoxygenated buffer immediately prior to usage. Fe^{III} EDTA, Fe^{II} Bipy, and Fe^{II} TPEN were generated *in situ* from the ligand (NaEDTA, Bipy or TPEN) and the corresponding iron (II or III) perchlorate salt. $[\text{Fe}(\text{MeCN})(\text{N4Py})](\text{ClO}_4)_2$, $[\text{Fe}(\text{TPA})](\text{OTf})_2$, $[\text{Fe}(\text{Bn-TPEN})(\text{OTf})](\text{OTf})$ and TPEN were synthesized according to literature procedures.⁶⁷⁻⁷⁰ Oxidized glutathione products were detected by mass spectroscopy on a Waters ZQ2000 single quadrupole mass spectrometer using an electrospray ionization source.

2.5 References

- (1) Lu, S. C., *Mol. Aspects. Med.* **2009**, *30*, 42-59.
- (2) Galaris, D.; Cadenas, E.; Hochstein, P., *Free Radic. Biol. Med.* **1989**, *6*, 473.
- (3) D'Agnillo, F.; Alayash, A. I., *Free Radic. Biol. Med.* **2002**, *33*, 1153-1164.
- (4) Abouelatta, A. I.; Campanali, A. A.; Ekkati, A. R.; Shamoun, M.; Kalapugama, S.; Kodanko, J. J., *Inorg. Chem.* **2009**, *48*, 7729-7739.
- (5) Koch, S.; Tang, S. C.; Holm, R. H.; Frankel, R. B.; Ibers, J. A., *J. Am. Chem. Soc.* **1975**, *97*, 916.
- (6) Sies, H., *Free Radic. Biol. Med.* **1999**, *27*, 916-921.
- (7) Kwon, Y.-W.; Masutani, H.; Nakamura, H.; Ishii, Y.; Yodoi, J., *Biol. Chem.* **2003**, *384*, 991-996.
- (8) Peng, Z.; Geh, E.; Chen, L.; Meng, Q.; Fan, Y.; Sartor, M.; Shertzer, H. G.; Liu, Z.-G.; Puga, A.; Xia, Y., *Mol. Pharmacol.* *77*, 784-792.
- (9) Meister, A., *Science* **1983**, *220*, 472-477.
- (10) Circu, M. L.; Yee Aw, T., *Free Rad. Res.* **2008**, *42*, 689-706.
- (11) Shi, Z.-Z.; Osei-Frimpong, J.; Kala, G.; Kala, S. V.; Barrios, R. J.; Habib, G. M.; Lukin, D. J.; Danney, C. M.; Matzuk, M. M.; Lieberman, M. W., *Proc. Natl. Acad. Sci. U. S. A.* **2000**, *97*, 5101-5106.
- (12) Pallardó, F. V.; Markovic, J.; García, J. L.; Viña, J., *Mol. Aspects Med.* *30*, 77-85.
- (13) Bellomo, G.; Vairetti, M.; Stivala, L.; Mirabelli, F.; Richelmi, P.; Orrenius, S., *Proc. Natl. Acad. Sci. U. S. A.* **1992**, *89*, 4412-4416.

- (14) Thomas, M.; Nicklee, T.; Hedley, D. W., *Br. J. Cancer* **1995**, *72*, 45-50.
- (15) Briviba, K., *Biochem. J.* **1993**, *294*, 631.
- (16) Soderdahl, T.; Enoksson, M.; Lundberg, M.; Holmgren, A.; Ottersen, O. P.; Orrenius, S.; Bolcsfoldi, G.; Cotgreave, I. A., *Faseb J.* **2003**, *17*, 124-126.
- (17) Voehringer, D. W.; McConkey, D. J.; McDonnell, T. J.; Brisbay, S.; Meyn, R. E., *Proc. Natl. Acad. Sci. U. S. A.* **1998**, *95*, 2956-2960.
- (18) Hansen, J. M.; Go, Y.-M.; Jones, D. P., *Annu. Rev. Pharmacol. Toxicol.* **2006**, *46*, 215-234.
- (19) Ho, Y., *J. Pharmacol. Toxicol. Methods* **1997**, *38*, 163-168.
- (20) Cotgreave, I. A. A., *BioFactors* **2003**, *17*, 269-277.
- (21) Chen, J., *Toxicol. Sci.* **2003**, *75*, 271-278.
- (22) Holmgren, A., *J. Biol. Chem.* **1989**, *264*, 13963.
- (23) Holmgren, A., *Biochem. Soc. Trans.* **1977**, *5*, 611.
- (24) Lu, S. C., *Faseb J.* **1999**, *13*, 1169-1183.
- (25) Meister, A.; Tate, S. S., *Annu. Rev. Biochem.* **1976**, *45*, 559-604.
- (26) Meister, A., *J. Am. Coll. Nutr.* **1986**, *5*, 137.
- (27) Chen, Z.; Lash, L. H., *J. Pharmacol. Exp. Ther.* **1998**, *285*, 608-618.
- (28) Bass, R.; Ruddock, L. W.; Klappa, P.; Freedman, R. B., *J. Biol. Chem.* **2004**, *279*, 5257-5262.
- (29) Chakravarthi, S., *EMBO J.* **2006**, *7*, 271-275.
- (30) Jessop, C. E.; Bulleid, N. J., *J. Biol. Chem.* **2004**, *279*, 55341-55347.
- (31) Frand, A. R.; Kaiser, C. A., *Mol. Biol. Cell.* **2000**, *11*, 2833-2843.

- (32) Fernandez-Checa, J. C.; Kaplowitz, N.; Garcia-Ruiz, C.; Colell, A.; Miranda, M.; Mari, M.; Ardite, E.; Morales, A., *Am. J. Physiol.-Gastr. L.* **1997**, *273*, G7-17.
- (33) Garcia-Ruiz, C.; Fernandez-Checa, J. C., *J. Gastroenterol. Hepatol.* **2006**, *21*, S3-S6.
- (34) Meister, A., *The Liver: Biology and Pathobiology*. second ed.; Raven Press: New York, 1988; p 401-417.
- (35) Khalife, K. H.; Lupidi, G., *Biochim. Biophys. Acta.* **2008**, *1780*, 627-637.
- (36) Trachootham, D.; Alexandre, J.; Huang, P., *Nat. Rev. Drug Discov.* **2009**, *8*, 579-591.
- (37) Toyokuni, S.; Okamoto, K.; Yodoi, J.; Hiai, H., *FEBS Lett.* **1995**, *358*, 1-3.
- (38) Fridovich, I., *Annu. Rev. Biochem.* **1995**, *64*, 97-112.
- (39) Teixeira, H. D.; Schumacher, R. I.; Meneghini, R., *Proc. Natl. Acad. Sci. U. S. A.* **1998**, *95*, 7872-7875.
- (40) Matés, J.; Pérez-Gómez, C.; Núñez de Castro, I., *Clin. Biochem.* **1999**, *32*, 595-603.
- (41) Stroppolo, M. E.; Sette, M.; O'Neill, P.; Polizio, F.; Cambria, M. T.; Desideri, A., *Biochemistry* **1998**, *37*, 12287-12292.
- (42) Casareno, R. L. B.; Waggoner, D.; Gitlin, J. D., *J. Biol. Chem.* **1998**, *273*, 23625-23628.
- (43) Battistoni, A.; Folcarelli, S.; Cervoni, L.; Polizio, F.; Desideri, A.; Giartosio, A.; Rotilio, G., *J. Biol. Chem.* **1998**, *273*, 5655-5661.

- (44) MacMillan-Crow, L. A.; Crow, J. P.; Thompson, J. A., *Biochemistry* **1998**, *37*, 1613-1622.
- (45) Turrens, J. F. F., *J. Clin. Invest.* **1984**, *73*, 87-95.
- (46) Pavlishchuk, V., *Inorg. Chim. Acta* **1988**, *151*, 261.
- (47) Hamed, M. Y., *Inorg. Chim. Acta* **1983**, *80*, 237.
- (48) Kachur, A. V.; Koch, C. J.; Biaglow, J. E., *Free Radic. Res.* **1998**, *28*, 259-269.
- (49) Albro, P. W.; Corbett, J. T.; Schroeder, J. L., *J. Inorg. Biochem.* **1986**, *27*, 191-203.
- (50) Scarpa, M.; Momo, F.; Viglino, P.; Vianello, F.; Rigo, A., *Biophys. Chem.* **1996**, *60*, 53-61.
- (51) Fels, I. G., *Exp. Eye. Res.* **1971**, *12*, 227-229.
- (52) Biaglow, J. E. E., *Radiat. Res.* **1984**, *100*, 298.
- (53) Winterbourn, C. C., *Arch. Biochem. Biophys.* **1994**, *314*, 284-290.
- (54) Misra, H. P., *J. Biol. Chem.* **1974**, *249*, 2151-2155.
- (55) Albro, P. W., *J. Inorg. Biochem.* **1986**, *27*, 191-203.
- (56) Freedman, J. H., *Biochem. Biophys. Res. Commun.* **1989**, *164*, 134-140.
- (57) Ferreira, A. M.; Ciriolo, M. R.; Marocci, L.; Rotilio, G., *Biochem. J.* **1993**, *292*, 673-676.
- (58) Jouini, M., *J. Inorg. Biochem.* **1986**, *26*, 269-280.
- (59) Roelfes, G.; Vrajmasu, V.; Chen, K.; Ho Raymond, Y. N.; Rohde, J.-U.; Zondervan, C.; La Crois Rene, M.; Schudde Ebe, P.; Lutz, M.; Spek Anthony, L.; Hage, R.; Feringa Ben, L.; Munck, E.; Que, L., Jr., *Inorg. Chem.* **2003**, *42*, 2639-53.

- (60) Kuzmic, P., *Anal. Biochem.* **1996**, *237*, 260-273.
- (61) Thibon, A.; England, J.; Marinho, M.; Young, V. G.; Frisch, J. R.; Guillot, R.; Girerd, J. J.; Muenck, E.; Que, L. J.; Banse, F., *Angew. Chem. Int. Ed.* **2008**, *47*, 7064-7067.
- (62) Hong, S.; Lee, Y. M.; Shin, W.; Fukuzumi, S.; Nam, W., *J. Am. Chem. Soc.* **2009**, *131*, 13910-13911.
- (63) Kunkely, H.; Vogler, A., *Inorg. Chem. Commun.* **2002**, *5*, 730-732.
- (64) Speisky, H.; Gomez, M.; Burgos-Bravo, F.; Lopez-Alarcon, C.; Jullian, C.; Olea-Azar, C.; Aliaga, M. E., *Biorg. Med. Chem.* **2009**, *17*, 1803-1810.
- (65) Campanali, A. A.; Kwiecien, T. D.; Hryhorczuk, L.; Kodanko, J. J., *Inorg. Chem.* **2010**, *49*, 4759-4761.
- (66) Trachootham, D.; Alexandre, J.; Huang, P., *Nat. Rev. Drug Discov.* **2009**, *8*, 579-591.
- (67) Roelfes, G.; Lubben, M.; W. Leppard, S.; Schudde, E. P.; Hermant, R. M.; Hage, R.; Wilkinson, E. C.; Que, L., Jr.; Feringa, B. L., *J. Mol. Catal. A: Chem.* **1997**, *117*, 223-227.
- (68) Diebold, A.; Hagen, K. S., *Inorg. Chem.* **1998**, *37*, 215-223.
- (69) Kaizer, J.; Klinker, E. J.; Oh, N. Y.; Rohde, J.-U.; Song, W. J.; Stubna, A.; Kim, J.; Muenck, E.; Nam, W.; Que, L., Jr., *J. Am. Chem. Soc.* **2004**, *126*, 472-473.
- (70) Chang, H. R.; McCusker, J. K.; Toftlund, H.; Wilson, S. R.; Trautwein, A. X.; Winkler, H.; Hendrickson, D. N., *J. Am. Chem. Soc.* **1990**, *112*, 6814-27.

ABSTRACT**SYNTHESIS OF N-ACETYL AND C-TERT-BUTYL NATURAL AMINO ACID
SUBSTRATES THAT MIMIC RESIDUES OF POLYPEPTIDES AND THEIR
REACTIVITY WITH $[\text{Fe}^{\text{IV}}(\text{O})(\text{N4PY})]^{2+}$: KINETIC AND MECHANISTIC
INVESTIGATIONS
&
OXIDATION OF GLUTATHIONE BY METAL-BASED OXIDANTS**

by

ASHLEY ANN CAMPANALI**May 2011****Advisor:** Jeremy J. Kodanko, Ph.D.**Major:** Chemistry**Degree:** Doctor of Philosophy

This dissertation is divided into two chapters, the first chapter includes an introduction to reactive oxygen species and their reactions with proteins. The introduction also covers metal-based oxidants, including both heme and non-heme enzymes that activate dioxygen as well as complexes that mimic these enzymes. The work discussed in chapter one concerns the synthesis of amino acid substrates that mimic amino acid residues. Substrates synthesized were derived from Gln, Asn, Ile, Cys and Tyr. Once synthesized, these substrates were reacted with $[\text{Fe}^{\text{IV}}(\text{O})(\text{N4Py})]^{2+}$ under pseudo-first order conditions. The mechanisms for the reactions of the most reactive substrates were investigated. Electron-transfer proton-transfer and hydrogen atom transfer mechanisms are suggested for the substrates derived from Cys and Tyr, respectively, for their reaction

with $[\text{Fe}^{\text{IV}}(\text{O})(\text{N4Py})]^{2+}$. An electrophilic aromatic substitution mechanism is suggested for the mechanism of the reaction of the substrate derived from Phe with $[\text{Fe}^{\text{IV}}(\text{O})(\text{N4Py})]^{2+}$.

The second chapter focuses on the oxidation of glutathione by metal-based oxidants, both single turnover and catalytic reactions. The introduction discusses the importance of glutathione in biology and the mechanism of its oxidation by copper ions. The discussion sections cover two related projects. The first is the single turnover oxidation of glutathione by $[\text{Fe}^{\text{IV}}(\text{O})(\text{N4Py})]^{2+}$, which includes the characterization of the intermediate $[\text{Fe}^{\text{III}}(\text{SG})(\text{N4Py})]^{2+}$ by UV-Vis and EPR spectroscopy as well as high resolution time-of-flight mass spectrometry. The kinetics of the reaction were investigated through the use of kinetic modeling software and a mechanism was proposed for this oxidation. The second section is a discussion of the catalytic oxidation of glutathione by metal-based oxidants. Initial catalyst screens were conducted and $[\text{Fe}^{\text{II}}\text{TPA}]^{2+}$ and $[\text{Fe}^{\text{II}}\text{N4Py}]^{2+}$ represent target complexes for further investigations. Antioxidant enzyme studies with catalase and superoxide dismutase show that hydrogen peroxide and superoxide are not involved before the rate-determining step of the oxidation. Also, no pH dependence was observed for the reaction of glutathione with $[\text{Fe}^{\text{II}}\text{TPA}]^{2+}$, however, a slight pH dependence was observed for $[\text{Fe}^{\text{II}}\text{N4Py}]^{2+}$. These results suggest possible differences in mechanisms for the oxidation of GSH by iron complexes of N4Py and TPA, most likely due to denticity differences.

AUTOBIOGRAPHICAL STATEMENT

Education

- 2006-2010 Ph.D. in Chemistry
Wayne State University, Detroit, Michigan
Advisor: Professor Jeremy J. Kodanko
- 2000-2004 B.S. in Chemistry, ACS certification
State University of New York at Brockport
Brockport, New York

Selected Publications

1. Abouelatta, A. I., **Campanali, A. A.**, Ekkati, A. R., Shamoun, M., Kalapugama, Kodanko, J. J. Oxidation of the Twenty Natural Amino Acids by a Ferryl Complex: Kinetic and Mechanistic Studies with Peptide Model Compounds. *Inorg. Chem.* **2009**, *48*, 7729-7739.
2. Ekkati, A. R., **Campanali, A. A.**, Abouelatta, A. I., Shamoun, M., Kalapugama, S., Kelley, M., Kodanko, J. J. Preparation of N-Acetyl, tert-Butyl Amide Derivatives of the Twenty Natural Amino Acids. *Amino Acids* **2010**, *38*, 747-751.
3. **Campanali, A.A.**, Kwiecien, T., Hryhorczuk, L., Kodanko, J.J. Oxidation of Glutathione by $[\text{Fe}^{\text{IV}}(\text{O})(\text{N4Py})]^{2+}$: Characterization of an $[\text{Fe}^{\text{III}}(\text{SG})(\text{N4Py})]^{2+}$ Intermediate. *Inorg. Chem.* **2010**, *49*, 4759-4761.
4. **Campanali, A.A.**, Jackson, C.F. Kwiecien, T., Kodanko, J.J. Catalytic Aerobic Oxidation of Glutathione by Non-Heme Iron Complexes and Associated Toxicity of Ligands *In Cellulo*. *In preparation*.